The Role of Two HtrA/DegP Family Proteases, MamE and MamO, in Protein Sorting and Biomineralization in *Magnetospirillum magneticum* str AMB-1

By

Anna Wiedmann

A dissertation submitted in partial satisfaction of the

requirements for the degree of

Doctor of Philosophy

in

Molecular and Cell Biology

in the

Graduate Division

of the

University of California, Berkeley

Committee in charge:

Professor Arash Komeili, Chair

Professor Kathleen Ryan

Professor Randy Schekman

Professor Karsten Weis

Fall 2010

Abstract
The Role of Two HtrA/DegP Family Proteases, MamE and MamO, in Protein Sorting and Biomineralization in *Magnetospirillum magneticum* str AMB-1
by
Anna Wiedmann
Doctor of Philosophy in Molecular and Cell Biology
University of California, Berkeley
Professor Arash Komeili, Chair

Magnetotactic bacteria (MTB) are a diverse group of bacteria capable of synthesizing magnetosomes, membrane-bound prokaryotic organelles that biomineralize magnetic minerals. Magnetosomes allow cells to align passively with geomagnetic field lines. This is thought to facilitate a bacterium's search for favorable environments, a process referred to as magnetotaxis. To execute biomineralization, a specific set of proteins needs to be localized to the magnetosomes. I have taken both a candidate and a global approach to understanding how these magnetosome proteins (MPs) are sorted to the magnetosome.

In a global approach I attempted to identify magnetosome sorting signals by assaying magnetosome localization of N-terminal truncations of MPs. To carry out this approach I unsuccessfully attempted to optimize magnetosome purification protocols to separate inner membrane proteins from magnetosome membrane proteins.

In the more successful candidate approach, I show that the HtrA/DegP family protease MamE is essential for localization of several soluble, as well as membrane bound MPs. Using site-directed mutagenesis, I show that MamE's role in protein sorting is independent of its protease activity, but that protease activity is essential for a novel 20nm crystal size transition step. Site-directed mutagenesis also revealed that the protease activity of a second HtrA/DegP family protease, MamO, is essential for biomineralization. Furthermore, these studies suggest that MamE and MamO's additional functional domains, not usually found in HtrA/DegP family proteases, are required for magnetosome formation. Lastly, this work highlights the step-wise assembly of magnetosomes, illustrates that several levels of control underlie magnetosome formation, and proposes that by modulating MamE's protease activity, cells could potentially exert control over their degree of magnetism and thus magnetotaxis.

Chapter 1: Introduction to Magnetotactic Bacteria and Magnetosome Formation

The presence of organelles and subcellular organization has traditionally been hailed as one of the defining distinctions between eukaryotic and prokaryotic cells. In the last decades it has become clear that this definition needs to be amended as an ever-increasing number of bacterial subcompartments are identified and characterized (1, 2). From proteinaceous shells that sequester chemical reactions, such as the carboxysome (3) to membrane-bound subcompartments like the thylakoid-like membranes in cyanobacteria (4) and nuclear-like membranes in planctomycetes (5), organelle-like microcompartments are ubiquitous in the prokaryotic world. Whether these compartments are formed, maintained and regulated through mechanisms homologous to ones already characterized in eukaryotes remains to be determined. To add to our understanding of organelle formation in bacteria, my work has focused on the magnetosome of the magnetotactic bacterium *Magnetospirillum magneticum* str AMB-1.

Discovery of Magnetotactic Bacteria and Their Diversity

Magnetotactic bacteria are a diverse group of bacteria that share the ability to align with magnetic field lines. They were first described in 1963 by Salvatore Bellini (Bellini, 1963 unpublished) who termed them “Magnetosensitive Bacteria” and speculated that they must contain a “biomagnetic compass”. He found that some bacteria in drainage water had a tendency to swim towards one edge of a hanging drop. It was possible to isolate these “magnetosensitive” bacteria from other bacteria, by placing a second hanging drop of sterilized spring water north of the sample drop; only magnetosensitve bacteria were found to travel from the sample drop into the spring water drop. Application of external magnetic fields could modify the cells’ behavior. From these observations Bellini concluded that the bacteria must either contain a “biological power generator” or “a magnet inserted in their cellular structure” but correctly predicted that the latter would be more likely, since the bacteria could still respond to external magnetic fields after they were fixed with formaldehyde.

The existence of magnetotactic bacteria did not become widely known until their rediscovery by Richard Blakemore (6), who like Bellini noticed that some cells in hanging drop assays had a tendency to swim towards one edge of the drop and that one could change the direction of their swimming with a magnet placed next to the drop. He was able to use what he called the cells’ “magnetotactic” behavior to enrich for magnetotactic cells and visualize them by transmission electron microscopy (TEM). He described cocci, with two bundles of flagella that all had two chains of 5-10 electron dense crystal-like structures. In thin sections some of these structures looked to be surrounded by a lipid membrane, which led Blakemore to propose that the crystals may grow from these membranes. Observations of these crystals clumping when cells lysed led to the hypothesis that these structures must be made of a material with a permanent magnetic dipole moment such as magnetite. Energy dispersive x-ray microanalysis

confirmed that a major component of these crystals was iron. Blakemore also observed that dead cells did not accumulate at the magnetic north pole of a magnet, but instead only aligned with the magnetic field. As the magnet was moved the cells would rotate to re-align suggesting that alignment with a magnetic field is a passive behavior and that the observed magnetotaxis was a more complex behavior composed of passive alignment with magnetic fields and active swimming once aligned. In total, Blakemore was able to identify 5 morphologically distinct magnetotactic bacteria from marshes around Woods Hole leading him to conclude that magnetotaxis could be a trait acquired by multiple species. Since all of the bacteria he identified seemed either microaerophilic or anaerobic, he in his first description of magnetotactic bacteria proposed what to this date is the prevailing model for the reason for magnetotaxis: that by aligning with the Earth's magnetic field lines, cells are able to more easily find their favored low oxygen environments within the water column.

Since these first descriptions of magnetotactic bacteria (MTB), many more species have been characterized, several can be grown in pure culture and the genomes of six have been at least partially sequenced. As Blakemore predicted the diversity of bacteria capable of magnetotaxis is great. Bacteria of all morphologies, including rods, vibrioid, spirilla, cocci and even multicellular ones have been found capable of magnetotaxis. Their phylogeny and physiology are equally diverse. MTB have been found in several phyla, including the alpha-, the delta- and the gamma-proteobacteria (7) as well as in the Nitrospira phylum (8-10). This diversity also extends to the shape of the crystal-like structures that Blakemore described, which were later shown unequivocally to be the source of the cells' magnetic response and which were therefore termed magnetosomes.

Magnetosomes as the basis of magnetotaxis

The defining trait of MTB, magnetotaxis, is made possible by magnetosomes, nanometer sized membrane-bound organelles in which crystals of magnetite (Fe_3O_4) or greigite (Fe_3S_4) are biomineralized. Organization into a chain is essential for alignment with magnetic field lines, as this generates a fixed net magnetic dipole moment for the cell (11).

(i) Crystals Of Magnetite Or Greigite Confer Magnetic Response

In his first description of MTB, Blakemore observed unusual electron dense crystal-like structures composed of iron and suggested that these structures were responsible for the cells' magnetic response (6). Soon thereafter, as it became possible to grow some MTB in pure culture and to thus chemically characterize their crystals, Frankel *et al* were able to show that these crystals were composed of magnetite and were within the single domain size range (d_{avg}=50nm). Based on the average crystal size and average number of crystals per cell, they calculated that the cells' magnetic moment should be sufficient to support alignment in the geomagnetic field, supporting the idea of magnetite in the cells acting like an internal compass needle (12). They also found that non-magnetic cells no longer formed crystals, further supporting the role of magnetite crystals in magnetotaxis.

Magnetotaxis, however, is not limited to magnetite-producing bacteria; several magnetotactic bacteria have been shown to form crystals of greigite (Fe_3S_4), although very little is known about the mechanisms of greigite magnetosome formation, as no greigite-producing bacteria are available in pure culture. Greigite producers identified to date include multicellular magnetotactic prokaryotes (MMPs) (13) (14) and large rod-shaped prokaryotes (15) (7). While magnetite producing bacteria are found at the oxic-anoxic interface (OAI) of both marine and freshwater environments, greigite producing magnetotactic bacteria have only been found in marine environments and are primarily found below the OAI where S^{2-} is readily available.

(ii) Basis of magnetite vs greigite formation

It has been suggested that the habitat of magnetotactic bacteria in the water column may play a determining factor in whether magnetite or greigite crystals are formed. In support of this hypothesis an organism was identified that forms both crystals of magnetite and greigite and whose ratio of magnetite to greigite crystals is modulated by environmental conditions. Cells of this species collected from more oxidized regions of the OAI had a higher percentage of magnetite crystals than those collected from more reduced regions. Cells of this species collected from anoxic region of the water column formed almost exclusively greigite crystals (16, 17). Environmental factors, however, do not seem to be the sole determinant of crystal type, as magnetite and greigite crystals found in this organism retained distinct crystal properties and morphologies, which suggests that separate biomineralization processes are responsible for the two crystal types. In support of the hypothesis that environmental factors alone do not determine crystal type, growing magnetite-forming species, such as MV-1, MC-1 and MV-2 in the presence of hydrogen sulfide does not result in biomineralization of greigite (18, 19) and *Desulfovibrio magneticus* str RS-1, an anaerobic sulfate reducer, nonetheless biomineralizes magnetite not greigite. Bazylinski *et al* concluded that the unusual magnetotactic bacterium capable of magnetite and greigite biomineralization must contain both the gene set required for greigite formation as well as that, which allows magnetite biomineralization. Since surprisingly, both crystals are found within the same magnetosome chain, they propose that chain formation of greigite and magnetite crystals may be under common genetic control. If these crystals are formed within magnetosome membranes, as is believed to be true for most magnetotactic bacteria with the possible exception of RS-1 (20), the co-existence of crystals of different shape and chemical composition within one chain poses many exciting questions about magnetosome formation. How is one magnetosome designated as a greigite- and another as a magnetite-containing magnetosome, as based on our current understanding of magnetosome formation one would expect different sets of proteins to be responsible for the formation of the two. What, if any, is the advantage of forming both types of magnetic crystals? Unfortunately, species that produce both greigite and magnetite or even species that only form greigite are currently not available in pure culture, hampering efforts to answer these types of questions.

(iii) Magnetite and Greigite Crystals Are Membrane-Bound

The term magnetosome, describing the magnetite crystal as well as their "associated bounding layers" was first coined in 1980 by Balkwill *et al*. (21). Their study of the *Magnetospirillum magnetotacticum* MS-1 supported Blakemore's observation of membrane-bound crystals and his hypothesis that crystals may be formed within membranes. Balkwill *et al* found that MS-1's crystals seemed to be surrounded by what could be a true lipid membrane layer. In addition, the chain seemed to always be located near the inner surface of the cytoplasmic membrane, suggesting some control of chain positioning and organization. This observation led Balkwill to entertain the possibility that the particle chains could be somehow connected to the inner membrane (21), a prediction that has proven to be true for at least some MTB (22).

Further evidence for the presence of a magnetosome membrane came from a study by Gorby *et al.* (23), where thin sections of cells grown under iron-limiting conditions showed chains of empty magnetosomes, magnetosomes with smaller inclusions of amorphous iron and membranes that were completely filled with magnetite. EM analysis of freeze-etched cells confirmed the presence of a lipid bilayer around the magnetite crystal. Many subsequent studies (22, 24, 25) have confirmed the existence of a lipid membrane surrounding the magnetite crystal, and its existence is now widely accepted and incorporated into all models of magnetosome formation. Greigite crystals seem to be formed in a membrane compartment like their magnetite counterpart (26). Interestingly, a recent study by Byrne, *et al.* of the magnetite forming delta-proteobacterium RS-1 suggests that a magnetosome membrane may not be involved in crystal formation in all species of magnetotactic bacteria (20).

(iv.) The Magnetosome Membrane Contains Magnetosome-Specific Proteins

Species-dependent differences in crystal shape, size, number and organization led to the proposal that genetic control must underlie biomineralization of magnetite and greigite crystals. This was supported by early studies of Gorby *et al*, which identified two magnetosome-specific proteins in MS-1, leading them to propose that these proteins may be directly involved in magnetite synthesis (23). Several subsequent studies (27, 28) similarly found magnetosomes to be enriched for certain proteins. Extensive proteomic analyses of magnetosomes isolated from *Magnetospirillum gryphiswaldense* MSR-1 (29)(Table 1) and *Magnetospirillum magneticum* AMB-1 (30)(Table 2) confirmed the existence of a magnetosome-specific set of proteins, termed magnetosome proteins. Surprisingly, magnetosome fractions from AMB-1 and MSR-1 showed strikingly different banding patterns even when the same purification protocol was used (29). These differences can most likely be attributed to fact that mature magnetosomes are invaginations in AMB-1 (Fig. 1), but free-floating vesicles in MSR-1, and thus to the difficulty of purifying magnetosomes in AMB-1. But this may also be representative of true differences in magnetosome protein composition and/or formation as is discussed below.

Many of the proteins identified at the magnetosome are encoded by a conserved genomic island, the magnetosome island (MAI), which is essential for

magnetosome formation. This further solidified the belief that these proteins were responsible for various aspects of magnetosome formation. This hypothesis was verified by a recent genetic dissection of the AMB-1 MAI, discussed further below and presented in Chapter 2 of this dissertation, which found many of the genes encoding magnetosome proteins to be essential for various aspects of magnetosome formation such as magnetosome membrane formation, crystal formation and chain organization (Fig. 2).

Chain organization

One of the striking features of magnetosomes is that they are organized into one or multiple chains per cell. This alignment maximizes the net magnetic dipole moment of the cell, as all of the dipoles of the single crystals are aligned, and thus contribute in an additive fashion to the cell's magnetic moment (11). Balkwill *et al.* (21) found in their early studies of magnetotactic bacteria that the crystal chains were stable structures, as crystals remained in chains upon severe cell shape deformation as cultures aged and cells formed coccoid bodies. Crystals even remained in chains when they were isolated, a phenomenon that has been supported by several subsequent studies (29, 31-33) The chain's resistance to deformation led Balkwill to suggest that there may be protein or membrane structures that organize and stabilize the chains.

A candidate for such an organizing protein structure was identified in the MAI as part of the conserved *mamAB* operon by Schuebbe *et al.* (34), who suggested that an MreB homolog, which they termed MamK may contribute to chain organization. This hypothesis was confirmed when cytoskeletal filaments running parallel to the magnetosomes were observed in AMB-1 by cryoelectron tomography and found to most likely be composed of MamK (22, 35). In the absence of *mamK*, these filaments were no longer observed, and magnetosome invaginations were scattered throughout the cytoplasm, suggesting that MamK was essential for chain organization. Intriguingly, the cells were still magnetic and could turn in a magnetic field, and magnetosomes were not completely randomly distributed throughout the cell, as may be expected if MamK were the only factor contributing to chain organization.

Another magnetosome protein, MamJ was implicated in chain formation in MSR-1 (35, 36) as in its absence, magnetosomes were found to form clusters within the cell. Since MSR-1 MamK and MamJ interacted in a yeast two-hybrid screen, MamJ was proposed to act as an adaptor protein, attaching magnetosomes to the adjacent MamK filament. This of course posed the obvious question of why the AMB-1 Δ*mamK* and MSR-1 Δ*mamJ* phenotypes were not more similar. One explanation for this difference could be that since MSR-1 magnetosomes seem not to be attached to the inner membrane, as in AMB-1, they may be more prone to clustering due to the attractive forces of the individual crystals; inner membrane attachment in AMB-1 may pose a more significant barrier to diffusion of magnetosomes towards each and thus prevent clustering. Another explanation based on the recent work of Rioux *et al*. (37) is that a *mamK* homolog *mamK-like*, which is found in AMB-1 but not MSR-1, could prevent magnetosome clustering in

the absence of *mamK* in AMB-1. A *mamK*/*mamK-like* double mutant in AMB-1 could address this latter hypothesis.

The role of MamK as the sole chain-imposing element has come into question in recent years. It had been hoped that a *mamK* deletion strain in MSR-1 would reconcile differences in the *mamK* and *mamJ* deletion phenotypes between AMB-1 and MSR-1, and that the difference in the Δ*mamJ* and Δ*mamK* strains was due to additional functions performed by *mamJ*. This, however, was not the case. In the absence of *mamK*, no cytoskeletal filaments are seen near the magnetosomes, yet MSR-1 is still able to organize magnetosomes into chains. Unlike the AMB-1 Δ*mamK* strain, MSR-1 Δ*mamK* was less magnetic than the wild type strain, and a chain placement and magnetosome number defect was observed rather than disorganization of the chain. This is a truly puzzling finding as it calls into question MamK's role in chain organization in MSR-1, as well as the proposed role of MamJ, as it is difficult to explain MamJ's role as an adaptor protein if its phenotype is much more severe than that of Δ*mamK*. The true extent of MamK's role thus remains to be determined, and differences between the two strains have yet to be reconciled. Interestingly, MC-1 and MV-1 do not have genes encoding MamJ (38) suggesting that these MTB may have different means of attaching magnetosomes to MamK, if this is MamJ's role.

Genetics of magnetosome formation

i. Discovery of the Magnetosome Island

The study of magnetotactic bacteria began with ultra-structural and biochemical analyses. As genetic tools were developed for some species, random mutagenesis approaches were added to the available tools, and slowly a list of magnetosome-associated proteins emerged, some of which were tentatively assigned specific functions in magnetosome formation based on their homology to known proteins and/or their deletion phenotypes (28)((39). The central focus of most research of magnetosome formation today, the MAI, eluded identification for many decades. First clues came from a low-resolution physical map of the MS-1 chromosome constructed by Bertani *et al.* (40), which suggested that at least some genes involved in magnetosome formation are clustered similarly in MS-1 and AMB-1. This hypothesis was confirmed by Grünberg *et al.* in 2001 (41). Their analysis of the magnetosome membrane in MSR-1 in combination with partial sequencing of the MC-1 and MS-1 genomes paved the way for the identification of what became known as the MAI. Comparing N-terminal sequences of proteins that co-purified with the magnetosome membrane to genes found in the available MC-1 and MS-1 genome sequences, Grünberg *et al* (41) found that several of the magnetosome-specific proteins in MSR-1 are conserved in MC-1 and MS-1 and that the genes encoding these proteins are clustered in what was termed the *mamAB* operon. This operon contained several other open reading frames whose content and organization were conserved in MC-1 and MS-1. Two of the Mam (magnetosome membrane) proteins identified in this early study, MamC and MamD were encoded by genes outside of the *mamAB* cluster, suggesting the presence of a region responsible for magnetosome formation much larger than the *mamAB* operon. The true extent of the magnetosome-

associated genome and its organization into a single genomic island were discovered when a spontaneous non-magnetic mutant of MSR-1 was characterized (42). This strain had lost an 80kb region of its chromosome, which included the genes encoding all of the magnetosome-associated proteins identified at that point in time. This included the previously identified *mamAB* and *mamCD* operons as well as a new gene cluster comprising the previously identified *mms6* gene, termed the *mms6* cluster. These operons could be placed in a 35kb continuous fragment of DNA. The conservation of the sequences in MS-1 and MC-1, the organization of these three operons and the presence of many insertion elements led to the suggestion that these operons may comprise a genomic island, which was termed the magnetosome island (MAI). The boundaries of this island, defined by Ullrich *et al.* in 2005 (43), led to what is now considered the MSR-1 MAI, a 130kb region of the chromosome. This region encodes almost all magnetosome-associated proteins with the exceptions of MagA, MpsA and Mms16, but also contains many genes with no obvious connection to magnetosome formation. The genome sequence of AMB-1, together with analysis of a spontaneous non-magnetic mutant, revealed that AMB-1's MAI is much smaller, comprising only 98kb (44). This region, like the MSR-1 island contains many additional genes and only the *mamAB*, *mamGFDC* operons and the *mms6* gene cluster genes are conserved. It was hypothesized that some of the species-specific genes may confer species-specific magnetosome and chain characteristics.

ii. Conservation of the Magnetosome Island

As alluded to in the previous section, the MAI is a highly conserved genomic island that is common to all magnetotactic bacteria sequenced to date, and evidence has been presented (42, 43, 45) that the MAI has been transferred horizontally between different species of MTB.

Although *mam* genes are conserved in AMB-1, MSR-1, MS-1, MC-1, and MV-1, their genomic order is not. Many examples of inversions as well as transpositions are found. For example, magnetospirilla as well as MC-1 have a *mamGFDC* operon with the four *mam* genes in the respective order. MV-1, however, has *mamD* and *mamF* clustered with a *mamK-like* gene as well as with *mamH*, which is found in the *mamAB* operon of the other four MTB. Similarly *mamC*, which is found in the *mamAB* operon in most MTB is clustered with *mamX*, *mamZ* and *mamY* instead (45). How such diversity has evolved and whether differences in gene order can potentially account for some of the diversity of crystal shape, size and number observed amongst MTB remains unclear. This latter hypothesis has gained attention in light of a recent dissection of the AMB-1 MAI (1 and Chapter 2), which found that almost all of the non-conserved genes can be deleted without severe defects in magnetosome and magnetite formation, at least under laboratory conditions. This has re-ignited keen interest in the source of species-specific magnetosome characteristics, as they had previously been attributed to these non-conserved MAI genes.

Comparing the MAI gene content of MV-1, MC-1, MSR-1, AMB-1 and MS-1 led to the proposal of a minimal set of genes for magnetosome formation: *mamH, I, E,*

K, M, O, P, A, Q, B, S, T, C, D, Z, and *X* and *mms6* and *mmsF* (45). However, a comparative genome approach to identify a minimal MTB genome may be faulted, as *mamL* and *mamN*, which are absent from this list, have been shown to be essential for magnetosome formation in AMB-1 ((1), Chapter 2 of dissertation). It is, however, possible that *mamL* eluded identification in MC-1 and MV-1, as it encodes a very small protein. It is also possible that the primary structure of MamL is not as important as secondary structure, and that another protein can perform MamL's function in these two species.

Even more striking differences were observed when the genome of the delta-proteobacterium *Desulfovibrio magneticus* str RS-1 was published (46). RS-1 was found to have a highly reduced MAI lacking many of the *mam* genes that were found to be essential for magnetosome formation in MSR-1 and AMB-1. The implications of this observation for magnetosome formation in RS-1 remain to be uncovered although first clues have emerged that magnetosome formation, at least its end product, is quite different in this organism; RS-1 magnetosomes seem to be membrane-less crystals of magnetite (20). Whether this means that these crystals do not require a membrane for formation remains to be determined. Another outstanding question is how conserved MAI genes are in greigite-producing MTB and in MTB from the Nitrospira and gamma proteobacteria. Given the large divergence of the delta-proteobacterium RS-1's MAI from that of the alpha-proteobacteria discussed above, similar or even greater divergence could be expected amongst these organisms.

Molecular Basis of Magnetosome Formation

Since its discovery the MAI has been the focus of many attempts to understand magnetosome formation. Many of its genes are highly conserved amongst MTB, and some were shown to be essential for magnetosome formation. Therefore, it was hypothesized that elucidating the function of these conserved gene products would lead to a mechanistic understanding of magnetosome formation. Several factors involved in magnetosome formation were identified through transposon mutagenesis and others were implicated in magnetosome formation through their presence at the magnetosome membrane. In addition, a recent systematic dissection of the AMB-1 MAI by Murat *et al.* (1) presented in Chapter 2 of this dissertation identified factors required for several aspects of magnetosome formation, including magnetosome membrane formation, magnetosome protein sorting and crystal formation (Table 1). Whether the factors identified to date play a role in the formation of greigite-containing magnetosomes remains to be determined.

It had previously been observed that in the absence of the MAI, cells not only were no longer magnetic but also no longer formed magnetosome membranes, suggesting that factors involved in forming these membranes were encoded by the MAI (1, 22). This was confirmed when four factors encoded by the *mamAB* operon were found to be essential for membrane formation. In the absence of *mamI*, *mamL*, *mamQ* or *mamB*, AMB-1 cells were no longer magnetic and did not form magnetosome membranes, implicating these factors in the process of membrane invagination and/or stabilization. These factors are not sufficient for

magnetosome formation in the absence of the *mamAB* operon, indicating that other magnetosome proteins play a role in membrane formation.
The GTPase Mms16 was implicated in magnetosome membrane formation by Okamura *et al.* (47), but subsequently found to be a PHB granule-associated protein, and a function in magnetosome formation was thus deemed unlikely (48).
Lastly, a study by Tanaka *et al.* suggested MamY may have a role in constricting the magnetosome membrane (49).
One gene product, MamE, has been implicated in the process of magnetosome protein sorting. How magnetosome proteins are targeted to and maintained at the magnetosome remains a mystery, but in the absence of the putative DegP/HtrA family protease MamE, at least some magnetosome proteins are no longer correctly localized. ((1), Chapters 2 and 3,).
Two *mamAB* operon genes, *mamK* and *mamJ* have been implicated in magnetosome chain formation (22, 35). Their exact role is unclear, and the recent generation of a Δ*mamK* mutant in MSR-1 has called into question whether this MreB homolog is essential for chain formation in all MTB (50).
Whereas identification of chain and membrane formation defects require time-consuming and technically difficult techniques such cryo-ultramicrotomy or cryo-electron tomography, defects in crystal formation are more easily identifiable by measuring the cells' magnetic response and by more accessible techniques such as whole cell TEM. Several gene products have thus been implicated in crystal formation, although their exact mechanisms of action remain largely unknown. As greigite-producing MTB are not available in pure culture, factors involved in greigite biomineralization remain to be identified.
Early studies identified *magA* in a transposon screen for non-magnetic mutants. *magA* is found outside of the MAI and encodes a putative iron transport protein with high homology to the *E.coli* KefC sodium efflux transporter. When deleted, cells are no longer magnetic, and *magA* expressed in *E.coli* allows for the influx of iron into inverted *E.coli* membrane vesicles in an ATP-dependent manner. This led to the suggestion that MagA may mediate iron import into magnetosomes.
Several MAI gene products, *mms5*, *mms6*, *mms7* (*mamD*) and *mms13* (*mamC*), were implicated in biomineralization because of their tight association with the magnetite crystal (51). Mms6 was directly implicated in biomineralization as it was found to bind iron and to allow for the formation of more shape- and size-uniform magnetite crystals *in vitro* (51, 52). Intriguingly all four proteins share a common LGLGLGLGAWGPXXLGXXGXAGA amino acid sequence whose importance and function in biomineralization remains to be determined.
The MAI of magnetosprilla, but not MC-1 and MS-1, encodes a second copy of the tubulin homolog *ftsZ* in addition to the one encoded outside of the MAI. This gene, named *ftsZ-like*, may have a role in biomineralization. When this gene is deleted, MSR-1 forms fewer and smaller magnetite crystals. FtsZ-like shows GTPase activity *in vitro* and polymerizes into filaments posing the question of how a cytoskeletal protein can affect biomineralization (53). The deletion of the MreB-homolog *mamK* in MSR-1 also results in a biomineralization defect, although cells form fewer crystals rather than smaller ones. Although not identical, the Δ*ftsZ-like* and Δ*mamK* phenotypes surprisingly implicate the magnetosome cytoskeleton in

magnetosome crystal formation rather than in magnetosome alignment, at least in MSR-1.

The *mamCDFG* operon in MSR-1 is required for the generation of wild type-sized crystals, as a deletion of the entire operon led 25% reduction in crystal size (54). These genes show some level of redundancy, as single deletions of *mamC*, *mamD*, *mamF* and *mamG* do not show biomineralization defects. The importance of this operon and of the *mms6* gene cluster were confirmed by a large deletion, R3, of the AMB-1 MAI that encompasses both gene clusters and shows severe crystal defects (1).

A second large deletion of the AMB-1 MAI, the deletion of R2, which encompasses genes not conserved in other MTB, led to a biomineralization defect as well (1).

In addition, the deletions of *mamS*, *mamT*, *mamP* and *mamR* in AMB-1 show varying defects in crystal size and/or shape and number. In the absence of *mamS*, cells form small, amorphous electron-dense particles that are unevenly spaced and at times clustered within the cells, suggesting MamS acts to control crystal morphology and size. MamT was implicated in crystal growth, as the Δ*mamT* strain forms significantly smaller crystals than wild type cells do. MamR and MamP were implicated in the control of crystal size and number, although the *mamR* deletion phenotype is significantly different from that of the *mamP* deletion. Whereas in the absence of *mamP*, cells form 1-4 crystals per cell that are larger than wild type crystals, the Δ*mamR* strain forms one to seven small crystals. These phenotypes are further discussed in Murat *et al.* (1) and in Chapter 2 of this dissertation.

Lastly, single deletions of four genes (*mamM*, *mamN*, *mamE* and *mamO*) in AMB-1 resulted in cells that were able to form magnetosome membranes, but were not able to biomineralize crystals within them (1). My work described in this dissertation has focused on two of these gene products, *mamE* and *mamO*, and their roles in magnetosome protein sorting and biomineralization.

Models of magnetosome formation

Based on the work summarized in this chapter, several models for magnetosome formation have been proposed. All include four general steps: magnetosome membrane formation, iron import into the magnetosome, biomineralization of magnetite crystals, and chain organization. As data suggested that the trait of magnetosome formation was likely attained via horizontal gene transfer from a common ancestor, it was assumed that magnetosome formation would follow a similar general mechanism in all magnetotactic bacteria. Because evermore irreconcilable differences in magnetosome formation are discovered in different MTB, the idea has to be entertained that different MTB, although sharing a common core MTB genome, may have evolved slightly different mechanisms of magnetosome formation.

One striking discrepancy can be observed in MSR-1 and AMB-1 grown in low Fe containing media. While both strains make small crystals empty magnetosomes and those contained small crystals are scattered throughout the cell in MSR-1 (35). By contrast, magnetosomes in AMB-1 are found aligned into a chain in

these conditions. Even in the complete absence of iron, when cells make no crystals, AMB-1 can organize its empty magnetosomes into chains (1, 22). This has led to two different models for chain organization. In AMB-1 it is believed that magnetosomes are organized into a chain independently of crystal formation and that there must be factors that either direct formation of new magnetosomes only adjacent to existing ones or factors that can move and integrate new magnetosomes formed randomly within the cell into the existing chain. The model for MSR-1 takes into account that chain organization is only observed when crystals are large enough to carry a fixed magnetic dipole moment. This led to the hypothesis that magnetosomes form throughout the cell and are integrated into existing chains based on interactions between the magnetic dipole moments of different crystals.

A second mechanistic difference between AMB-1 and MSR-1 is that mature magnetosomes remain attached to the inner membrane in AMB-1 (22), wheras mature, large crystal-containing magnetosomes in MSR-1 appear to be free-floating vesicles within the cytoplasm of MSR-1 cells (50). This implies that MSR-1 magnetosome formation contains a step in which magnetosomes bud off of the membrane, a step that is not present in AMB-1. This difference also has obvious implications for magnetosome protein dynamics and targeting, and for the chemical environment inside the magnetosome; whereas MSR-1 magnetosomes are autonomous vesicles, the AMB-1 magnetosome membrane is continuous with the inner membrane, and the magnetosome lumen is continuous with the periplasm. Whether diffusion of magnetosome contents into the periplasm or the inner membrane is restricted in AMB-1 remains unknown, although it seems likely that there must be diffusion barriers in AMB-1 that may not be required in MSR-1 magnetosome formation.

Another reason to believe that there is no single mechanism for magnetosome formation is that mature magnetosome crystals of RS-1 are not surrounded by a lipid bilayer (20). Thus, the definition of a magnetosome as a crystal of iron oxide or sulfide surrounded by a lipid bilayer may not apply to the magnetosomes of all MTB. This poses many questions about magnetosome formation in RS-1. Are RS-1's magnetite crystals initially formed as invaginations but the crystal somehow escapes the magnetosome membrane as it matures? Or are RS-1's crystals nucleated at the inner membrane without the formation of a true magnetosome membrane? The presence of genes in the RS-1 MAI that encode proteins identified as magnetosome membrane proteins in magnetospirilla suggest that a membrane phase may be involved in magnetosome formation in RS-1 as well. How the reduced set of MAI genes found in RS-1 mediates magnetosome formation remains to be determined.

Conclusion

Much has been added to our understanding of magnetosome formation in the past decade as genetic tools have become available. We now possess the tools to genetically dissect the MAI of different species and thus link function to specific gene products and to piece together the molecular mechanisms underlying magnetosome formation in different MTB. Such approaches are beginning to

suggest that although the trait of magnetotaxis seems to have been obtained by MTB via horizontal gene transfer, slight variations in the mechanism of magnetosome formation are found in different species. Gaining an understanding of the molecular basis of magnetosome formation and how gene products that are conserved in all MTB contribute to magnetosome formation in different magnetotactic bacteria will not only further our understanding of bacterial organelle formation but will also allow us to address the question of conservation of mechanisms of magnetosome formation amongst different MTB.

My work has focused on how magnetosome proteins are localized to the magnetosome. Magnetosomes are invaginations of the inner membrane in AMB-1 (Fig. 1), which poses the interesting question of how magnetosome proteins are concentrated at the magnetosome membrane and kept from being equally distributed across the magnetosome and general inner membrane. To answer this question I took two approaches. In one approach, summarized in Chapter 4, I attempted to identify sorting signals; amino acid sequences of magnetosome membrane proteins that are necessary and sufficient for magnetosome localization. As this approach proved unsuccessful, I focused my work on elucidating how two conserved DegP/HtrA family proteases, MamE and MamO, encoded by the MAI and found at the magnetosome, contribute to the process of magnetosome formation. As mentioned above and illustrated in Chapter 2 of this dissertation, in the absence of either *mamE* or *mamO*, AMB-1 can still form magnetosome membranes but no longer forms magnetite crystals. In addition, in the absence of *mamE*, several magnetosome proteins are mislocalized (Chapter 2 and Chapter 3), posing the intriguing question of how MamE contributes to magnetosome protein sorting (Chapter 3). Protease activity of MamE and MamO is essential for biomineralization of large single-domain crystals of magnetite but MamE protease activity is not essential for biomineralization of small 20 nm magnetite crystals. This suggests that MamE's protease activity is not required for initiation of biomineralization but for continued growth of crystals after they have reached 20 nm in size. MamE's protease activity is not required for restoration of magnetosome protein localization, suggesting that MamE is a bifunctional protein with a protease-independent role in sorting of magnetosome proteins and a protease dependent one in crystal size maturation (Chapter 3). Lastly, the results presented in this dissertation suggest that additional functional domains of MamE and MamO, which are not usually found in DegP/HtrA family proteases, are required for their activity (Chapter 3).

References:

Bellini S. 1963. Su di un particolare comportamento di batteri d'acqua dolce (About a particular behavior of freshwater bacteria) and Ulteriori studi sui “batteri magnetosensibili” (Further studies on “Magnetosensitive Bacteria.”) *J. Inst. Microbiol.*, Univ. Pavia, Italy. http://www.calpoly.edu/~rfrankel/SBellini1.pdf

1. Murat D, Quinlan A, Vali H, & Komeili A (2010) Comprehensive genetic dissection of the magnetosome gene island reveals the step-wise assembly of a prokaryotic organelle. *Proc Natl Acad Sci U S A* 107(12):5593-5598.
2. Murat D, Byrne M, & Komeili A (2010) Cell biology of prokaryotic organelles. *Cold Spring Harb Perspect Biol* 2(10):a000422.
3. Yeates TO, Kerfeld CA, Heinhorst S, Cannon GC, & Shively JM (2008) Protein-based organelles in bacteria: carboxysomes and related microcompartments. *Nat Rev Microbiol* 6(9):681-691.
4. Vothknecht UC & Westhoff P (2001) Biogenesis and origin of thylakoid membranes. *Biochim Biophys Acta* 1541(1-2):91-101.
5. Fuerst JA (2005) Intracellular compartmentation in planctomycetes. *Annu Rev Microbiol* 59:299-328.
6. Blakemore R (1975) Magnetotactic bacteria. *Science* 190(4212):377-379.
7. Simmons SL, Sievert SM, Frankel RB, Bazylinski DA, & Edwards KJ (2004) Spatiotemporal distribution of marine magnetotactic bacteria in a seasonally stratified coastal salt pond. *Appl Environ Microbiol* 70(10):6230-6239.
8. Spring S*, et al.* (1993) Dominating role of an unusual magnetotactic bacterium in the microaerobic zone of a freshwater sediment. *Appl Environ Microbiol* 59(8):2397-2403.
9. Lin W, Jogler C, Schuler D, & Pan Y (2010) Metagenomic analysis reveals unexpected subgenomic diversity of magnetotactic bacteria within the Nitrospirae phylum. *Appl Environ Microbiol*.
10. Lefevre CT, Frankel RB, Abreu F, Lins U, & Bazylinski DA (2010) Culture-independent characterization of a novel, uncultivated magnetotactic member of the Nitrospirae phylum. *Environ Microbiol* .
11. Frankel RB & Bazylinski DA (2006) How magnetotactic bacteria make magnetosomes queue up. *Trends Microbiol* 14(8):329-331.
12. Frankel RB, Blakemore RP, & Wolfe RS (1979) Magnetite in freshwater magnetotactic bacteria. *Science* 203(4387):1355-1356.
13. Farina M, Debarros HL, Esquivel DMS, & Danon J (1983) Ultrastructure of a Magnetotactic Microorganism. *Biol Cell* 48(1):85-88.
14. Mann S, Sparks NHC, Frankel RB, Bazylinski DA, & Jannasch HW (1990) Biomineralization of Ferrimagnetic Greigite (Fe3s4) and Iron Pyrite (Fes2) in a Magnetotactic Bacterium. *Nature* 343(6255):258-261.

15. Heywood BR, Rajam S, & Mann S (1991) Oriented Crystallization of Caco3 under Compressed Monolayers .2. Morphology, Structure and Growth of Immature Crystals. *J Chem Soc Faraday T* 87(5):735-743.
16. Bazylinski DA, Heywood BR, Mann S, & Frankel RB (1993) Fe3o4 and Fe3s4 in a Bacterium. *Nature* 366(6452):218-218.
17. Bazylinski DA*, et al.* (1995) Controlled Biomineralization of Magnetite (Fe(inf3)O(inf4)) and Greigite (Fe(inf3)S(inf4)) in a Magnetotactic Bacterium. *Appl Environ Microbiol* 61(9):3232-3239.
18. Meldrum FC, Mann S, Heywood BR, Frankel RB, & Bazylinski DA (1993) Electron-Microscopy Study of Magnetosomes in a Cultured Coccoid Magnetotactic Bacterium. *P Roy Soc Lond B Bio* 251(1332):231-236.
19. Meldrum FC, Mann S, Heywood BR, Frankel RB, & Bazylinski DA (1993) Electron-Microscopy Study of Magnetosomes in 2 Cultured Vibrioid Magnetotactic Bacteria. *P Roy Soc Lond B Bio* 251(1332):237-242.
20. Byrne ME*, et al.* (2010) Desulfovibrio magneticus RS-1 contains an iron- and phosphorus-rich organelle distinct from its bullet-shaped magnetosomes. *Proc Natl Acad Sci U S A* 107(27):12263-12268.
21. Balkwill DL, Maratea D, & Blakemore RP (1980) Ultrastructure of a Magnetotactic Spirillum. *Journal of Bacteriology* 141(3):1399-1408.
22. Komeili A, Li Z, Newman DK, & Jensen GJ (2006) Magnetosomes are cell membrane invaginations organized by the actin-like protein MamK. *Science* 311(5758):242-245.
23. Gorby YA, Beveridge TJ, & Blakemore RP (1988) Characterization of the bacterial magnetosome membrane. *J Bacteriol* 170(2):834-841.
24. Komeili A, Vali H, Beveridge TJ, & Newman DK (2004) Magnetosome vesicles are present before magnetite formation, and MamA is required for their activation. *Proc Natl Acad Sci U S A* 101(11):3839-3844.
25. Katzmann E, Scheffel A, Gruska M, Plitzko JM, & Schuler D (2010) Loss of the actin-like protein MamK has pleiotropic effects on magnetosome formation and chain assembly in Magnetospirillum gryphiswaldense. *Mol Microbiol* 77(1):208-224.
26. Silva KT, Abreu F, Keim CN, Farina M, & Lins U (2008) Ultrastructure and cytochemistry of lipid granules in the many-celled magnetotactic prokaryote, 'Candidatus Magnetoglobus multicellularis'. *Micron* 39(8):1387-1392.
27. Okamura Y, Takeyama H, & Matsunaga T (2000) Two-dimensional analysis of proteins specific to the bacterial magnetic particle membrane from Magnetospirillum sp AMB-1. *Appl Biochem Biotech* 84-6:441-446.
28. Okuda Y, Denda K, & Fukumori Y (1996) Cloning and sequencing of a gene encoding a new member of the tetratricopeptide protein family from magnetosomes of Magnetospirillum magnetotacticum *Gene.* 171(1):99-102.
29. Grunberg K*, et al.* (2004) Biochemical and proteomic analysis of the magnetosome membrane in Magnetospirillum gryphiswaldense. *Appl Environ Microbiol* 70(2):1040-1050.

30. Tanaka M*, et al.* (2006) Origin of magnetosome membrane: Proteomic analysis of magnetosome membrane and comparison with cytoplasmic membrane. *Proteomics* 6(19):5234-5247.
31. Kobayashi A*, et al.* (2006) Experimental observation of magnetosome chain collapse in magnetotactic bacteria: Sedimentological, paleomagnetic, and evolutionary implications. *Earth Planet Sc Lett* 245(3-4):538-550.
32. Scheffel A*, et al.* (2006) An acidic protein aligns magnetosomes along a filamentous structure in magnetotactic bacteria. *Nature* 440(7080):110-114.
33. Taoka A, Asada R, Wu LF, & Fukumori Y (2007) Polymerization of the actin-like protein MamK, which is associated with magnetosomes. *Journal of Bacteriology* 189(23):8737-8740.
34. Schubbe S*, et al.* (2003) Characterization of a spontaneous nonmagnetic mutant of Magnetospirillum gryphiswaldense reveals a large deletion comprising a putative magnetosome island. *Journal of Bacteriology* 185(19):5779-5790.
35. Scheffel A*, et al.* (2006) An acidic protein aligns magnetosomes along a filamentous structure in magnetotactic bacteria. *Nature* 441(7090):248-248.
36. Scheffel A & Schuler D (2007) The acidic repetitive domain of the Magnetospirillum gryphiswaldense MamJ protein displays hypervariability but is not required for magnetosome chain assembly. *J Bacteriol* 189(17):6437-6446.
37. Rioux JB*, et al.* (2010) A Second Actin-Like MamK Protein in Magnetospirillum magneticum AMB-1 Encoded Outside the Genomic Magnetosome Island. *Plos One* 5(2).
38. Jogler C*, et al.* (2009) Toward cloning of the magnetotactic metagenome: identification of magnetosome island gene clusters in uncultivated magnetotactic bacteria from different aquatic sediments. *Appl Environ Microbiol* 75(12):3972-3979.
39. Okuda Y & Fukumori Y (2001) Expression and characterization of a magnetosome-associated protein, TPR-containing MAM22, in Escherichia coli. *FEBS Lett* 491(3):169-173.
40. Bertani LE, Weko J, Phillips KV, Gray RF, & Kirschvink JL (2001) Physical and genetic characterization of the genome of Magnetospirillum magnetotacticum, strain MS-1. *Gene* 264(2):257-263.
41. Grunberg K, Wawer C, Tebo BM, & Schuler D (2001) A large gene cluster encoding several magnetosome proteins is conserved in different species of magnetotactic bacteria. *Appl Environ Microbiol* 67(10):4573-4582.
42. Schubbe S*, et al.* (2003) Characterization of a spontaneous nonmagnetic mutant of Magnetospirillum gryphiswaldense reveals a large deletion comprising a putative magnetosome island. *J Bacteriol* 185(19):5779-5790.
43. Ullrich S, Kube M, Schubbe S, Reinhardt R, & Schuler D (2005) A hypervariable 130-kilobase genomic region of Magnetospirillum

gryphiswaldense comprises a magnetosome island which undergoes frequent rearrangements during stationary growth. *J Bacteriol* 187(21):7176-7184.
44. Fukuda Y, Okamura Y, Takeyama H, & Matsunaga T (2006) Dynamic analysis of a genomic island in Magnetospirillum sp. strain AMB-1 reveals how magnetosome synthesis developed. *FEBS Lett* 580(3):801-812.
45. Jogler C*, et al.* (2009) Comparative analysis of magnetosome gene clusters in magnetotactic bacteria provides further evidence for horizontal gene transfer. *Environ Microbiol* 11(5):1267-1277.
46. Nakazawa H*, et al.* (2009) Whole genome sequence of Desulfovibrio magneticus strain RS-1 revealed common gene clusters in magnetotactic bacteria. *Genome Res* 19(10):1801-1808.
47. Okamura Y, Takeyama H, & Matsunaga T (2001) A magnetosome-specific GTPase from the magnetic bacterium Magnetospirillum magneticum AMB-1. *J Biol Chem* 276(51):48183-48188.
48. Schultheiss D, Handrick R, Jendrossek D, Hanzlik M, & Schuler D (2005) The presumptive magnetosome protein Mms16 is a poly(3-hydroxybutyrate) granule-bound protein (phasin) in Magnetospirillum gryphiswaldense. *J Bacteriol* 187(7):2416-2425.
49. Tanaka M, Arakaki A, & Matsunaga T (2010) Identification and functional characterization of liposome tubulation protein from magnetotactic bacteria. *Mol Microbiol* 76(2):480-488.
50. Katzmann E, Scheffel A, Gruska M, Plitzko JM, & Schuler D (2010) Loss of the actin-like protein MamK has pleiotropic effects on magnetosome formation and chain assembly in Magnetospirillum gryphiswaldense. *Mol Microbiol* 77(1):208-224.
51. Arakaki A, Webb J, & Matsunaga T (2003) A novel protein tightly bound to bacterial magnetic particles in Magnetospirillum magneticum strain AMB-1. *J Biol Chem* 278(10):8745-8750.
52. Arakaki A, Masuda F, Amemiya Y, Tanaka T, & Matsunaga T (2010) Control of the morphology and size of magnetite particles with peptides mimicking the Mms6 protein from magnetotactic bacteria. *J Colloid Interface Sci* 343(1):65-70.
53. Ding Y*, et al.* (2010) Deletion of the ftsZ-Like Gene Results in the Production of Superparamagnetic Magnetite Magnetosomes in Magnetospirillum gryphiswaldense. *Journal of Bacteriology* 192(4):1097-1105.
54. Scheffel A, Gardes A, Grunberg K, Wanner G, & Schuler D (2008) The major magnetosome proteins MamGFDC are not essential for magnetite biomineralization in Magnetospirillum gryphiswaldense but regulate the size of magnetosome crystals. *J Bacteriol* 190(1):377-386.

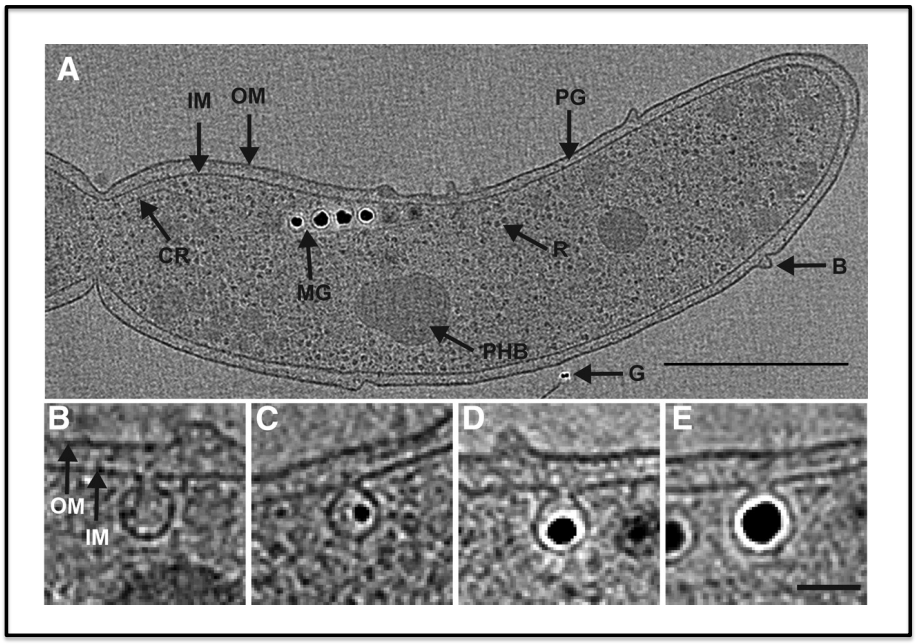

Figure 1: Electron cryotomography (ECT) of AMB-1 shows that magnetosomes are invaginations of the inner membrane and that magnetite crystals grow within mature-sized magnetosome membranes. (A) 12nm section of an ECT reconstruction highlighting features of AMB-1. Outer membrane, OM; inner membrane IM; peptidoglycan layer, PG; ribosomes, R; outer membrane bleb, B; chemoreceptor bundle, CR; poly-β-hydroxybuterate granule, PHB; gold fiduciary marker, G; magnetosome chain, MG. Scale bar represents 500nm. Magnetosome membrane containing (B) no magnetite, (C) and (D) growing magnetite crystals, and (E) a mature magnetite crystal. Scale bar represents 50nm. Image and figure legend adapted from A. Komeili *et al.* (22).

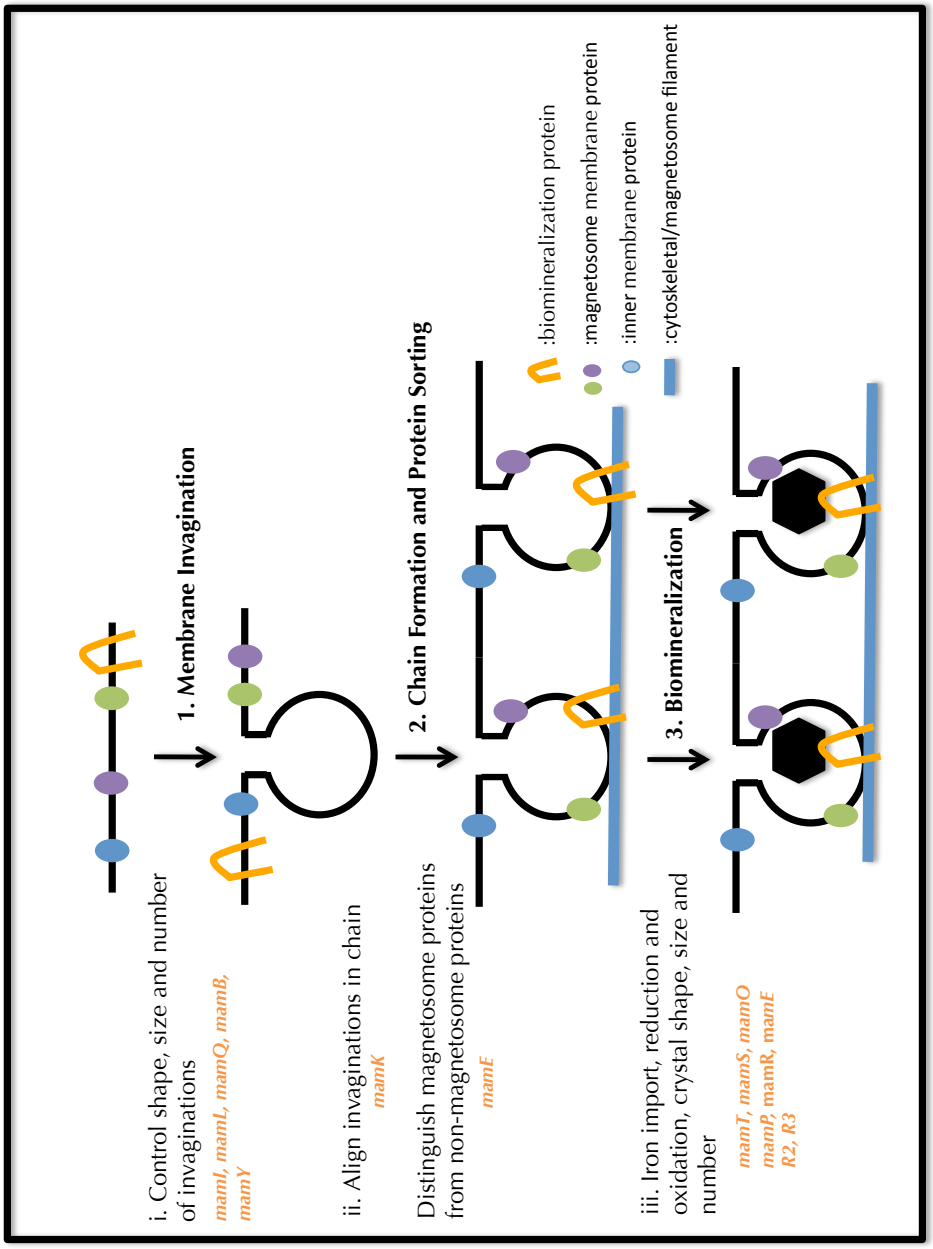

Figure 2: Model for magnetosome formation in AMB-1. Magnetosomes are thought to form in a step-wise process (1.-3.) where magnetosome membrane invagination is followed by magnetosome protein sorting and initiation of crystal formation. Whether new invaginations only form adjacent to existing invaginations or whether integration of new Invaginations into the existing chain is an active process is unknown but unlike in MSR-1 empty magnetosomes are always found integrated into the existing magnetosome chain. Levels of control required for proper magnetosome formation are indicated in i.-iii. and genes that have been implicated in these process are listed in orange below.

Protein	At Magnetosome	Characteristic features	Proposed function
MamA	Y (AMB-1, MSR-1)	TPR motifs	Activation of magnetosomes. Forms matrix around magnetosome (AMB-1)
MamB	Y (AMB-1, MSR-1)	Cation (CDF) transporter	Magnetosome membrane formation (AMB-1)
MamC	Y (AMB-1, MSR-1)	Most abundant magnetosome protein	Biomineralization (AMB-1, MSR-1)
MamD	Y (AMB-1, MSR-1)	Leu/Gly rich motif	Biomineralization (AMB-1, MSR-1)
MamE	Y (AMB-1, MSR-1)	HtrA/DegP family protease; CXXCH heme-binding domains	Biomineralization and Protein sorting (AMB-1, MSR-1)
MamF	Y (AMB-1, MSR-1)	none	Biomineralization (AMB-1, MSR-1)
MamG	Y (MSR-1)	Leu/Gly rich motif	Biomineralization (AMB-1, MSR-1)
MamH	N	none	Unknown
MamI	N	none	Magnetosome membrane ormation (AMB-1)
MamJ	Y (AMB-1, MSR-1)	Acidic repeats	Attaches magnetosomes to MamK filament (MSR-1)
MamK	Y (AMB-1)	MreB homolog	Magnetosome chain formation (AMB-1, MSR-1)
MamL	N	none	Magnetosome membrane formation (AMB-1)
MamM	Y (AMB-1, MSR-1)	Cation (CDF) transporter	Biomineralization (AMB-1)
MamN	Y (MSR-1)		Biomineralization (AMB-1)
MamO	Y (AMB-1, MSR-1)	HtrA/DegP family protease; DUF81 domain	Biomineralization (AMB-1, MSR-1)
MamP	N	CXXCH heme-binding and PDZ domains	Biomineralization (AMB-1)
MamQ	Y (MSR-1)	Homology to LemA protein	Magnetosome membrane formation (AMB-1)
MamR	Y (AMB-1, MSR-1)	none	Biomineralization (AMB-1)
MamS	Y (AMB-1, MSR-1)	none	Biomineralization (AMB-1)
MamT	Y (MSR-1)	CXXCH heme-binding domains	Biomineralization (AMB-1)
MamU	N	none	Unknown
MamV	N	none	Unknown
MamW	N	none	Unknown
MamX	N	none	Unknown
MamY	N	none	Magnetosome membrane shaping factor (AMB-1)
MamZ	N		Unknown
Mms6	Y (AMB-1, MSR-1)	Leu/Gly rich motif	Biomineralization
MagA	N	Homology to KefC sodium efflux pump	Iron transport into magnetosome

Table 1: List of magnetosome proteins including their characteristic features and proposed function. Proposed functions are based on experimental results, not homology.

Chapter 2: Comprehensive Genetic Dissection of the Magnetosome Gene Island Reveals the Stepwise Assembly of a Prokaryotic Organelle

Dorothée Murat, Anna (Wiedmann) Quinlan, H. Vali and Arash Komeili

ABSTRACT

Although membrane-bounded compartments are commonly known as a unique eukaryotic characteristic, many species of bacteria have organelles. While compartmentalization is well studied in eukaryotes, the molecular factors and processes leading to organelle formation in bacteria are poorly understood. We use the non-essential magnetosome of magnetotactic bacteria as a model system to investigate organelle biogenesis in bacteria. The magnetosome is an invagination of the cell membrane that contains a specific set of proteins able to direct the synthesis of a nanometer-sized magnetite crystal. A well-conserved region called the magnetosome island (MAI) is known to be essential for magnetosome formation and contains most of the genes previously implicated in magnetosome formation. Here, we present the first complete functional analysis of the MAI genes in a magnetotactic bacterium, *Magnetospirillum magneticum* AMB-1. By characterizing MAI deletion mutants, we show that parts of its conserved core are not essential for magnetosome biogenesis and that non-conserved genes are important for crystal formation. Most importantly, we show that one gene cluster is essential for magnetosome biogenesis and encodes for factors important for cell membrane invagination, targeting of proteins to this compartment and for several steps during magnetite formation. Altogether, this genetic analysis defines the function of more than a dozen factors participating in magnetosome formation and shows that magnetosomes are assembled in a step-wise manner where membrane biogenesis, magnetosome protein localization and biomineralization are placed under discrete genetic control.

INTRODUCTION

The ability to form organelles and organize the cytoplasm in several compartments is often considered a unique eukaryotic trait, one that is absent from simpler prokaryotic cells. However, microscopic studies have led to the identification of an increasing number of prokaryotic membrane-bounded organelles suggesting that sub-cellular compartmentalization in eukaryotes and prokaryotes may share a common evolutionary origin, as reviewed elsewhere (1, 2). Although some prokaryotic organelles, such as the photosynthetic membranes of heterotrophic photosynthetic bacteria and the nucleus-like compartments found in some *Planctomycete* species, have been studied at the ultrastructural level, little is known about the molecular mechanisms of their assembly and maintenance. A thorough molecular understanding of intracellular compartmentalization in prokaryotes is necessary in order to draw meaningful mechanistic and evolutionary connections to the well-studied processes of organelle assembly in eukaryotes.

A particularly attractive system to characterize the cell biology of bacterial organelles is the magnetosome compartment of magnetotactic bacteria (MTB). The magnetosome organelle is a lipid-bounded invagination of the cytoplasmic membrane that directs the biomineralization of a single, highly ordered magnetic crystal of magnetite (Fe_3O_4) or greigite (Fe_3S_4). Individual magnetosomes are aligned in one or more chains that allow MTB to orient in geomagnetic field lines, which in turn facilitates their search for low oxygen environments (3, 4). Magnetosomes have been largely used as a model to study biomineralization, the process by which living organisms build highly ordered three-dimensional structures out of inorganic molecules. MTB produce membrane-bounded magnetite crystals with a narrow and species-specific size and shape distribution under ambient conditions, unique properties that have made them a target for applications in biotechnology, nanotechnology and medical sciences (5). In recent years, magnetosomes have also proven to be an excellent model to study the cell biology of bacterial organelle formation. To build a magnetosome, a cell must create and maintain a highly curved membrane compartment, sort the proper set of proteins to it and organize individual magnetosomes into chains with the use of a dedicated cytoskeletal system (6-7). Many of these processes resemble those implicated in the formation and maintenance of eukaryotic organelles, but at the moment, the molecular factors implicated in each one of these steps, or their chronology, remain for the most part unknown.

To date, the strategies to identify molecular factors important for magnetosome formation have been based on genetic screens for non-magnetic mutants, comparative genomics of MTB, and proteomic analyses of purified magnetosome (8-13). These independent approaches have revealed that the majority of the genes potentially participating in magnetosome formation are grouped in four conserved gene clusters present within a large unstable genomic region called the Magnetosome Island (MAI) (8, 10, 14). This region appears to be conserved in all MTB analyzed thus far, although the size and gene content of the MAI vary significantly between species. Interestingly, the spontaneous loss of the MAI leads to a non-magnetic phenotype, demonstrating its central role in magnetosome biogenesis (15-16). In the magnetite-producing α-proteobacterium *Magnetospirillum magneticum* strain AMB-1 (AMB-1), MAI loss prevents both crystal and magnetosome compartment formation, indicating that at least some factors essential for magnetosome membrane biogenesis are present in that region (6).

This study presents the first directed functional analysis of MAI genes in a magnetotactic bacterium with the goal of defining the molecular factors involved in magnetosome membrane biogenesis. The term magnetosome refers to both the magnetite crystal and its surrounding lipid bilayer. Accordingly, throughout the manuscript, “magnetosome membrane” is used to describe only the lipid bilayer portion of the compartment. We show that two regions of the MAI play a crucial role in magnetite crystal formation and that the highly conserved *mamAB* gene cluster is essential for magnetosome membrane biogenesis in AMB-1. By independently disrupting each gene in this cluster, we demonstrate that this organelle is assembled in a stepwise manner such that magnetosome membrane

biogenesis, magnetosome protein localization and biomineralization are placed under discrete genetic control.

RESULTS

The *mamAB* gene cluster is essential for magnetosome formation

In *Magnetospirillum magneticum* strain AMB-1 (AMB-1), the Magnetosome Island (MAI) contains 106 annotated open reading frames (ORFs) which represent approximately 2% of AMB-1's gene content. To determine parts of the MAI important for magnetosome formation, it was divided into fourteen independent regions (named R1 to R14) based on predicted operon structure and potential gene function (Fig.1A and Table S1). In order to assess the importance of each region in the process of magnetosome formation, the magnetic properties of the mutants were quantified by measuring their ability to turn in an applied magnetic field in a spectrophotometric assay (9, 17) and by visualizing the magnetosome chains by transmission electron microscopy (TEM) (detail about the mutant characterization is provided in SI and Table S1A). This analysis shows that the majority of MAI subdeletions retain a wild-type phenotype. However, deletions of regions R2 and R3 lead to severe defects in the size and morphology of the crystals and the magnetic properties of the cells (Fig. S1A). Most importantly, the deletion of region R5 is the only mutation that prevents the formation of magnetic minerals, as indicated by a null magnetic response and the lack of magnetite in the bacteria imaged by TEM.

Because magnetosome membrane formation precedes magnetite formation (9), the non-magnetic phenotype of the ΔR5 mutant could be explained either by the lack of magnetite or the complete absence of magnetosome membranes. To determine the presence of magnetosome compartments in this strain, ultrathin cell sections obtained by cryo-ultramicrotomy were investigated by TEM (9). As shown in Fig.2A, empty magnetosome compartments were observed in wild-type cells grown in the absence of iron. In contrast, no structures resembling magnetosomes were observed in the ΔMAI (6 and Fig. S1B) or the ΔR5 mutants (Fig. 2A), suggesting that no magnetosomes are made in these mutants. It is also likely that in the absence of magnetosome membranes, magnetosome-associated proteins should be mislocalized. Thus, as an independent measure of magnetosome membrane formation, the localization of two magnetosome proteins, MamA and MamJ tagged with the Green Fluorescent Protein (GFP), was characterized in AMB-1 wild-type, ΔMAI and ΔR5 cells. In wild-type cells (Fig. 2B), both tagged proteins localize as a line running along the inner curvature of the cell in a manner reminiscent of the subcellular position of the magnetosome chain. However, in the spontaneous ΔMAI and ΔR5 strains, MamA-GFP and MamJ-GFP are mislocalized; their fluorescent signals are mostly diffuse throughout the cytoplasm with some enhanced accumulation around the cell membrane in a fraction of the population (Fig.S1C, Fig. 2B). The defects observed by combination of electron microcopy and localization study of GFP-tagged magnetosome proteins suggest that the region R5 encodes for one or several factors essential for magnetosome membrane invagination.

Comprehensive analysis of the *mamAB* genes

ΔR5 carries an 18-kilobase deletion that encompasses the highly-conserved *mamAB* gene cluster (Fig. 1B), a region that contains several of the magnetosome formation factors found through genetic and proteomic studies (6-7, 9, 11, 13, 18). Most of these genes are shared between AMB-1, *Magnetospirillum gryphiswaldense* MSR-1, *Magnetospirillum magnetotacticum* MS-1, *Magnetococcus* sp. MC-1 and the magnetotactic marine vibrio strain MV-1, and a subset have recently been found in the distantly related *Desulfovibrio magneticus* RS-1 (10, 19). Despite the apparent importance of this cluster, only three of its genes have been studied through direct genetic analysis. MamA is important for magnetosome activation (9) and MamK and MamJ are required for proper magnetosome chain organization (6-7) leading us to hypothesize that these genes would not be necessary for the biogenesis of the magnetosome membrane. Thus, fourteen single non-polar deletions of the remaining genes of this cluster were generated while the last gene of the region, *mamV,* was disrupted by insertional mutagenesis. One potential complication in analyzing the function of *mamAB* genes is that three of its ORFs, *mamQ*, *mamR* and *mamB*, are perfectly duplicated (100% identity at the nucleotide level) in the R9 gene cluster of the MAI (Fig. 1A). Therefore, these three genes were deleted in wild-type AMB-1 (leading to strains Δ*mamQ*, Δ*mamR* and Δ*mamB*) and in the ΔR9 deletion strain (leading to strains ΔR9Δ*mamQ*, ΔR9Δ*mamR* and ΔR9Δ*mamB*), a strain which synthesizes magnetosomes of wild-type appearance and is missing the repeat. Three mutants were indistinguishable from wild-type cells (Δ*mamH*, Δ*mamU* and Δ*mamV*) while the rest fell into two large classes of mutants: non-magnetic mutants and mutants with altered magnetic phenotypes as a result of biomineralization defects (Table 1). The mutants that had severely decreased magnetic properties were systematically complemented (Table S2). And, as described in the following sections, they were subjected to a series of secondary screens in order to determine their specific role in magnetosome formation.

Four conserved genes in the *mamAB* cluster are essential, but not sufficient, for biogenesis of the magnetosome membrane

As evidenced by a null magnetic response, eight of the mutants generated above are unable to synthesize magnetic particles. This phenotype could be due to the absence of magnetite crystals or by a complete block in magnetosome membrane formation. To distinguish between these two possibilities, the presence of empty magnetosome compartments in these mutants was investigated by cryo-ultramicrotomy followed by TEM (Table 1). This analysis revealed that four of the mutants, bearing deletions in *mamE*, *mamM*, *mamN* or *mamO*, had chains of empty magnetosomes. In contrast the imaging of the Δ*mamI* and Δ*mamL* mutants showed that these strains do not form structures resembling empty magnetosome compartments. Additionally, while Δ*mamQ* and Δ*mamB* mutants are magnetic, the ΔR9Δ*mamQ* and ΔR9Δ*mamB* double mutants fail to form magnetosome compartments. The phenotypes of the ΔR9Δ*mamQ* and ΔR9Δ*mamB* double deletion strains could be complemented in *trans* by the

expression of *mamQ* or *mamB* respectively indicating that the two copies of these genes are functionally redundant.
mamI, *mamL*, *mamQ* and *mamB* were the only genes found to be essential for magnetosome compartment formation in R5, suggesting that they may also be sufficient for inner membrane invagination in AMB-1. To test this, the ability of these four genes to restore membrane formation in the ΔR5 mutant strain was investigated. Using reverse transcription followed by PCR, it was first shown that under normal growth conditions *amb1005* and *amb1007,* the duplicated versions of *mamQ* and *mamB* respectively*,* are expressed from the R9 region of the MAI in the ΔR5 deletion strain. To provide *mamI* and *mamL in trans*, an integrational plasmid allowing for the expression of both genes (pAK*397*-IL) from a neutral chromosomal locus was constructed (Material and Methods and SI Text). This plasmid allows for complementation in the single deletion strains Δ*mamI* and Δ*mamL* as well as in a strain where both genes were deleted (Δ*mamL*Δ*mamI*), indicating that the construct can provide a sufficient amount of each gene product. When pAK*397*-IL was integrated in the ΔR5 strain, however, no structures resembling empty magnetosome membranes could be observed by TEM, indicating that *mamI, mamL, mamQ*, and *mamB* are not sufficient for magnetosome membrane formation. As no other single gene deletions within R5 led to the absence of magnetosome membranes, it is likely that a combination of additional factors located within the *mamAB* cluster is also required for magnetosome membrane biogenesis.

MamI has a magnetosome-dependent localization in AMB-1
In contrast to MamQ and MamB, MamI and MamL have not previously been shown to be physically associated with magnetosomes in cell fractionation analyses of either AMB-1 or MSR-1 (11, 13, 20). Since the genetic analysis indicates that they play a role in magnetosome membrane invagination, it might be expected that MamI and MamL would be, at least transiently, associated with the magnetosomes. To investigate the localization of these two small proteins, GFP fusions to MamI and MamL were visualized in AMB-1. These fusion proteins allow for partial complementation in the Δ*mamI* and $\Delta\mu\alpha\mu\Lambda$ mutants respectively (Table S2). MamL-GFP mostly localizes around the cell membrane (SI Text and Fig. S2A) but can localize as aligned dots or very short lines running tangential to the inner curvature in about 10% of the cells suggesting that MamL-GFP may associate transiently with the magnetosomes (Fig. S2B and C). In contrast, GFP-MamI localizes as a continuous straight line extending from pole to pole, running tangential to the inner curvature of the cell (Fig. 3), consistent with localization to the magnetosome chain. GFP-MamI is mislocalized in both the ΔMAI and ΔR5 mutants, where it appears all around the cell membrane (localization of GFP-MamI in the ΔMAI strain is shown in Fig. 3) also suggesting that it specifically associates with the magnetosomes *in vivo*. As a further proof of the association of GFP-MamI to with the magnetosome chain, its localization was investigated in a Δ*mamK* strain. MamK is a bacterial actin-like cytoskeletal protein required for proper alignment of the magnetosomes in a chain in AMB-1. In a Δ*mamK* mutant, the magnetosome chain is disorganized and individual

magnetosomes can localize around the cell periphery (6). As illustrated in Fig. 3, a rough linear pattern for GFP-MamI can still be observed in the Δ*mamK* mutant, however the fluorescence is not homogeneously distributed and intense foci of fluorescence outside the chain are present adjacent to the membrane, which is reminiscent of the clustering and uneven spacing of magnetosomes seen in the Δ*mamK* strain (6). The localization of GFP-MamI strongly suggests that MamI associates with the magnetosomes and that GFP-MamI can be used as a marker for the presence and positioning of magnetosome compartments.

MamE is important for the localization of a subset of proteins to the magnetosome membrane

As described above, four non-magnetic mutants carrying deletions of *mamE, mamO, mamM* or *mamN* are able to form a chain of empty magnetosome membranes, but cannot synthesize magnetite within these compartments (Fig. 4A). The absence of magnetite suggests that MamE, MamO, MamM and MamN are potentially important for biomineralization and could be involved in iron transport, magnetite nucleation or the establishment of the proper chemical environment for magnetite synthesis in the magnetosome. However, this phenotype could also be a consequence of the inability of the mutant to properly localize magnetosome proteins. To test this possibility, the localization of the GFP-tagged magnetosome proteins MamA and MamJ was determined in these four mutants. Both MamA-GFP and MamJ-GFP are correctly localized in the Δ*mamM*, Δ*mamN* and Δ*mamO* mutants, suggesting a potential role for MamM, MamN and MamO in biomineralization. In the Δ*mamE* mutant however, MamA-GFP is mislocalized and found at or in close proximity to the cell membrane as small foci that are randomly positioned as opposed to being organized as a line in wild-type AMB-1 cells (Fig. 4B). MamJ-GFP is also mislocalized in the Δ*mamE* mutant, although the defect is subtle (Fig. S3). These observations suggest that in the Δ*mamE* mutant, the absence of magnetite crystals could be a consequence of the mislocalization of at least a subset of magnetosome proteins.

Biomineralization is placed under discrete genetic control in AMB-1

Finally, the deletion strains Δ*mamP*, Δ*mamT,* Δ*mamR*, and Δ*mamS* display drastically decreased magnetic properties and TEM shows that they each harbor a different biomineralization defect (Fig. 5). First, the Δ*mamP* mutant synthesizes fewer inclusions (up to four per cell compared to fifteen to twenty-five per cell in AMB-1 wild-type) that resemble wild-type crystals in shape but are overall larger than those synthesized in wild-type AMB-1. All the particles measured were above 35 nm in length and more than 70 % are above 50 nm in length as compared to less than 30% in wild-type cells. This suggests that MamP could play a role in controlling crystal size and number in AMB-1. In the Δ*mamT* mutant, the chain of magnetosomes contains significantly smaller particles (15.9 ± 4.2 nm in width and 24.4 ± 8.3 nm in length comparing to 32.3 ± 13.9 nm in width and 39.1 ± 16.1 nm in length for wild-type crystals). This phenotype suggests a role for MamT in magnetite crystal growth. *mamR* is the third gene,

besides *mamQ* and *mamB*, present in the perfect 1957 base-pair direct repeat and it is identical to *amb1006* (Fig. 1). Although the magnetic properties of the Δ*mamR* mutant are slightly lower than wild-type (Table 1), no obvious defect in the magnetosome chain could be detected by TEM. In contrast, when both *mamR* and *amb1006* are deleted (ΔR9Δ*mamR*) the cells retain the ability to produce magnetosomes, as indicated by the ability of cell pellets to be attracted to a bar magnet. However, the magnetic response could not be detected in the quantitative spectrophotometric assay. Electron microscopy shows that the ΔR9Δ*mamR* strain forms shorter chains (one to seven particles per cell) of significantly smaller sized particles. More than 50 % are between 10 and 20 nm in width with an average size of 18.6 ± 7.3 nm in width and 21.2 ± 7.7 nm in length. Their morphology is similar to that of wild-type, indicating that MamR plays a role in controlling both particle number and size but does not participate in the control of crystal morphology. Finally, the Δ*mamS* mutant synthesizes a large majority of amorphous-looking particles (Fig. 5, white arrowheads) with few rounder crystals of wild-type appearance. They are significantly smaller than wild-type crystals (19.1 ± 5.7 nm in length), their spacing is irregular, and small clusters can be observed within the chain (Fig. 5B). This phenotype suggests that MamS plays a major role in controlling crystal morphology and size. However, the morphology defect in this mutant is different from that observed in the Δ*mamT* strain, suggesting that MamS and MamT participate in different steps during magnetite synthesis. It should be noted that the nature of the minerals observed in these mutants has not been determined and will require further investigation. These observations demonstrate that the number, size and morphology of the magnetite crystals are placed under discrete genetic control in AMB-1.

DISCUSSION

In this work, a comprehensive genetic approach was undertaken to characterize the steps and molecular factors controlling the biogenesis of a bacterial organelle, the magnetosomes of magnetotactic bacteria. The magnetosome island, a conserved genomic region in MTB, was known to be essential for magnetosome biogenesis. However, the results of this study show that most of its genes are not essential for the assembly of a functional chain of magnetosomes. It is possible that some deletion strains would have a magnetosome defect under different growth conditions, or that the combination of several deletions would affect magnetosome formation in case of functional redundancy among the MAI genes. Interestingly, the degree of conservation of a region is not sufficient to predict its role in magnetosome formation. Indeed, at least one of the gene clusters conserved in MTB is not essential for magnetosome synthesis (*mamXY* gene cluster) (10) and, conversely, regions that are specific to AMB-1 are important for biomineralization and magnetosome membrane invagination (R2 and R9). Finally, the role in biomineralization of the *mamCDF* and *mms6* gene clusters previously reported (11, 18, 21) was confirmed since the ΔR3 mutant, a strain containing a deletion of both gene clusters, has a severe magnetite formation defect. Taken together, the deletion

analysis of the MAI suggests that its size could be significantly reduced, facilitating further genetic manipulations to synthesize magnetosome-like compartments in heterologous systems. It should be emphasized, however, that genes outside of the MAI could also play important roles in the formation of this organelle.

This global analysis reveals that magnetosome biogenesis relies on four major steps that can be genetically decoupled: inner membrane invagination, localization of the magnetosome proteins, positioning of the magnetosomes in the cell, and biomineralization. Interestingly, factors involved in each one of these steps are clustered within the conserved *mamAB* region (Fig. 6). First, the formation of a highly curved membrane-bound compartment seems to rely on four conserved putative membrane proteins, MamB, MamQ, MamI and MamL. With the possible exception of MamQ (discussed below), bioinformatic analysis of these proteins at the primary and secondary structure levels does not reveal any significant homology to eukaryotic proteins known to be involved in deformation of cellular membranes, such as the BAR domain-containing proteins and the Dynamin superfamily of GTPases (22) (SI Text). MamB is the only one of these four proteins that has a domain of known function. It is predicted to belong to the cation-diffusion facilitator superfamily, which includes a ferrous iron transport system (23). The homology of MamB with transporters suggests it could have an indirect role in magnetosome membrane invagination or that it could potentially have a role in both magnetosome membrane invagination and biomineralization that would allow the cells to couple compartment and crystal formation. MamQ shares homology with the LemA protein, the function of which remains unknown (24). In addition, using its predicted secondary structure as a query, we discovered weak hits for MamQ to a number of eukaryotic proteins including Tropomyosin, Spectrin, and the EFC/BAR domain of the Formin Binding Protein 17. We believe that this is mainly due to the high alpha-helical content of LemA-like proteins, which includes MamQ, and does not represent a true homology to BAR domains. All four genes were identified in the genomes of the magnetotactic a-proteobacteria, but *mamL* was not found in MC-1 (10). However, the protein encoded by the MC-1 gene *Mmc1_2257* shares 32% identity with MamL of AMB-1 and its position downstream of *mamK* is conserved. Interestingly, *mamQ* and *mamB,* but not *mamI* and *mamL,* were found in the recently sequenced and distantly related *Desulfovibrio magneticus* RS-1, which belongs to the d-proteobacteria (19). This suggests that magnetosome formation in RS-1 may rely on a different mechanism. Surprisingly, these four proteins do not seem to be sufficient to trigger magnetosome compartment formation in the absence of the *mamAB* gene cluster. Assuming that their expression in the engineered strain is optimal, this result would suggest that in addition to MamB, MamQ, MamI and MamL a combination of other MamAB proteins, which are not independently essential for inner membrane invagination, are required for formation or maintenance of magnetosome membranes. Further genetic and biochemical studies are needed in order to elucidate the specific role of these proteins in membrane dynamics.

Another key finding of this work is that magnetosome membrane biogenesis can happen independently and prior to the targeting of at least a subset of proteins to this compartment. MamE, a putative membrane-bound serine protease, is required for magnetite formation. In its absence, MamA and MamJ, which are not essential for biomineralization, are mislocalized, suggesting that MamE may also control the localization of other magnetosome proteins. Alternatively, MamE could play a direct role in biomineralization independent of its function in magnetosome protein localization.
After the magnetosome compartments are formed and positioned, the final step in magnetosome biogenesis is the biomineralization of magnetite. Three factors that are essential for crystal formation, as well as four factors that control the size, number, and morphology of the magnetite crystals, were also identified through this genetic analysis. The wide range of biomineralization phenotypes suggests a complex regulation of magnetite synthesis in AMB-1. A more thorough analysis of the crystals formed in these mutants may help reveal intermediate minerals synthesized during magnetite formation.
In conclusion, the comprehensive genetic analysis of the conserved magnetosome island reveals a step-wise assembly of the magnetosome organelle in which membrane invagination, magnetosome protein localization, organelle positioning, and magnetite formation are independently regulated. This genetic study allowed definition of the role of two large genomic regions and twelve conserved factors in the major steps of magnetosome formation. The fact that most factors investigated in this study do not share homology with proteins known to participate in organelle biogenesis in other systems may suggest a unique pathway for intracellular compartmentalization in MTB. However, it may be possible that even in the absence of primary sequence conservation, the general mechanisms of compartmentalization are conserved across the various of domains of life. Finally, beyond the fundamental new insights into potentially conserved processes in organelle-containing organisms, these results will also have an impact on efforts to manipulate and engineer magnetosome compartments for applications in nanotechnology and medical sciences.

Material and methods

General Microbiology and Molecular biology

Magnetospirillum magneticum strain AMB-1 was grown in microaerobic conditions in a slightly modified version of the media described previously (9) using 0.1 g of sodium thiosulfate per liter (see (9) and SI). Cmag measurements, conjugations, gene inactivations and complementations were done as described previously ((6) and SI).

mamI-mamL two-gene operon

A plasmid allowing for the expression of genes under the control of the *tac* promoter on the chromosome of AMB-1 was generated (pAK397, details in SI). An 1106 bp fragment amplified from an intergenic region located between *amb0397* and *amb0398* was amplified and cloned in pAK0 (6). *mamI* and *mamL* were cloned in several steps as a two-gene operon in pAK22 (6) and then sub-

cloned in the pAK*397* vector leading to pAK397-*IL*. A ribosome binding site was provided for *mamL*.

TEM and cryo-ultramicrotomy

TEM characterization and cryo-ultramicrotomy were performed using standard methods and as described previously (9) with slight modifications (see SI). At least 200 sections of bacteria were analyzed for each strain and in strains where present, 30-50% of the sections contained magnetosome chains. Mutants were designated as deficient in magnetosome membrane formation if none of the sections contained magnetosome-like structures.

Fluorescence microscopy

The GFP fusions were derived from the pAK22 plasmid and analyzed as described previously ((6) and SI). For each construct, more than 200 cells were photographed and analyzed.

References

1. Shively, JM (ed) (2006) in *Microbiology Monographs* Vol. 2., *Complex Intracellular Structures in Prokaryotes* (Springer, Heidelberg).
2. Fuerst JA (2005) Intracellular compartmentation in planctomycetes. *Annu Rev Microbiol* 59:299-328.
3. Komeili A (2007) Molecular mechanisms of magnetosome formation. *Annu Rev Biochem* 76:351-366.
4. Smith MJ, et al. (2006) Quantifying the magnetic advantage in magnetotaxis. *Biophys J* 91(3):1098-1107.
5. Faivre D & Schuler D (2008) Magnetotactic bacteria and magnetosomes. *Chem Rev* 108(11):4875-4898.
6. Komeili A, Li Z, Newman DK, and Jensen GJ (2006) Magnetosomes are cell membrane invaginations organized by the actin-like protein MamK. *Science* 311(5758):242-245.
7. Scheffel A, et al. (2006) An acidic protein aligns magnetosomes along a filamentous structure in magnetotactic bacteria. *Nature* 440(7080):110-114.
8. Fukuda Y, Okamura Y, Takeyama H, and Matsunaga T (2006) Dynamic analysis of a genomic island in *Magnetospirillum* sp. strain AMB-1 reveals how magnetosome synthesis developed. *Febs Lett* 580(3):801-812.
9. Komeili A, Vali H, Beveridge TJ, and Newman DK (2004) Magnetosome vesicles are present before magnetite formation, and MamA is required for their activation. *Proc Natl Acad Sci U S A* 101(11):3839-3844.
10. Richter M, et al. (2007) Comparative genome analysis of four magnetotactic bacteria reveals a complex set of group-specific genes implicated in magnetosome biomineralization and function. *J Bacteriol* 189(13):4899-4910.
11. Grunberg K, et al. (2004) Biochemical and proteomic analysis of the magnetosome membrane in *Magnetospirillum gryphiswaldense*. *Appl Environ Microbiol* 70(2):1040-1050.

12. Okuda Y, Denda K, and Fukumori Y (1996) Cloning and sequencing of a gene encoding a new member of the tetratricopeptide protein family from magnetosomes of *Magnetospirillum magnetotacticum*. *Gene* 171(1):99-102.
13. Tanaka M, et al. (2006) Origin of magnetosome membrane: proteomic analysis of magnetosome membrane and comparison with cytoplasmic membrane. *Proteomics* 6(19):5234-5247.
14. Grunberg K, Wawer C, Tebo BM, and Schuler D (2001) A large gene cluster encoding several magnetosome proteins is conserved in different species of magnetotactic bacteria. *Appl Environ Microbiol* 67(10):4573-4582.
15. Matsunaga T, et al. (2005) Complete genome sequence of the facultative anaerobic magnetotactic bacterium *Magnetospirillum* sp. strain AMB-1. *DNA Res* 12(3):157-166.
16. Ullrich S, Kube M, Schubbe S, Reinhardt R, and Schuler D (2005) A hypervariable 130-kilobase genomic region of *Magnetospirillum gryphiswaldense* comprises a magnetosome island which undergoes frequent rearrangements during stationary growth. *J Bacteriol* 187(21):7176-7184.
17. Schuler DU, R. Bauerlein, E (1995) A simple light scattering method to assay magnetism in *Magnetospirillum gryphiswaldense*. *FEMS Microbiol Letters* 132:139-145.
18. Scheffel A, Gardes A, Grunberg K, Wanner G, and Schuler D (2008) The major magnetosome proteins MamGFDC are not essential for magnetite biomineralization in *Magnetospirillum gryphiswaldense* but regulate the size of magnetosome crystals. *J Bacteriol* 190(1):377-386.
19. Nakazawa H, et al. (2009) Whole genome sequence of *Desulfovibrio magneticus* strain RS-1 revealed common gene clusters in magnetotactic bacteria. *Genome Res* 19(10):1801-1808.
20. Schuler D (2004) Molecular analysis of a subcellular compartment: the magnetosome membrane in *Magnetospirillum gryphiswaldense*. *Arch Microbiol* 181(1):1-7.
21. Amemiya Y, Arakaki A, Staniland SS, Tanaka T, and Matsunaga T (2007) Controlled formation of magnetite crystal by partial oxidation of ferrous hydroxide in the presence of recombinant magnetotactic bacterial protein Mms6. *Biomaterials* 28(35):5381-5389.
22. McMahon HT and Gallop JL (2005) Membrane curvature and mechanisms of dynamic cell membrane remodeling. *Nature* 438(7068):590-6.
23. Grass G, et al. (2005) FieF (YiiP) from *Escherichia coli* mediates decreased cellular accumulation of iron and relieves iron stress. *Arch Microbiol* 183(1):9-18.
24. D'Orazio SE, Velasquez M, Roan NR, Naveiras-Torres O, and Starnbach MN (2003) The *Listeria monocytogenes lemA* gene product is not required for intracellular infection or to activate fMIGWII-specific T cells. *Infect Immun* 71(12):6721-6727.

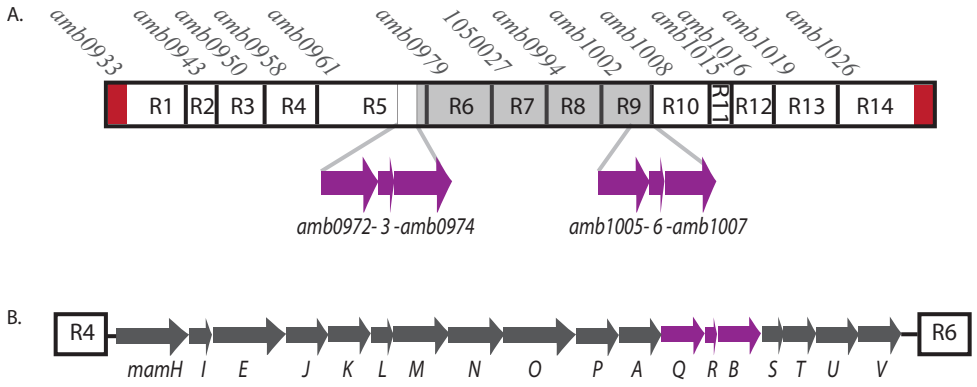

Figure 1 : Genomic organization of the MAI and the *mamAB* gene cluster in *Magnetospirillum magneticum* AMB-1. (A): Schematic representation of the 14 regions of the Magnetosome Island (MAI) (labelled R1 to R14) that were independently deleted in AMB-1. The number corresponding to the first gene of each region is indicated. Above R7, the genomic coordinate of the beginning of the region is indicated. The 1137-bp direct repeats flanking the MAI are represented by red rectangles. In purple are represented the three ORFs that constitute the perfect 1957-bp duplication in the MAI of AMB-1 (*amb0972-3-4* and *amb1005-6-7* respectively). The grey rectangle represents the region spontaneously deleted in SID25. (B): Organization of the *mamAB* gene cluster (R5). *mamQ*, *mamR* and *mamB*, corresponding to *amb0972, amb0973 and amb0974* respectively, are shown in purple.

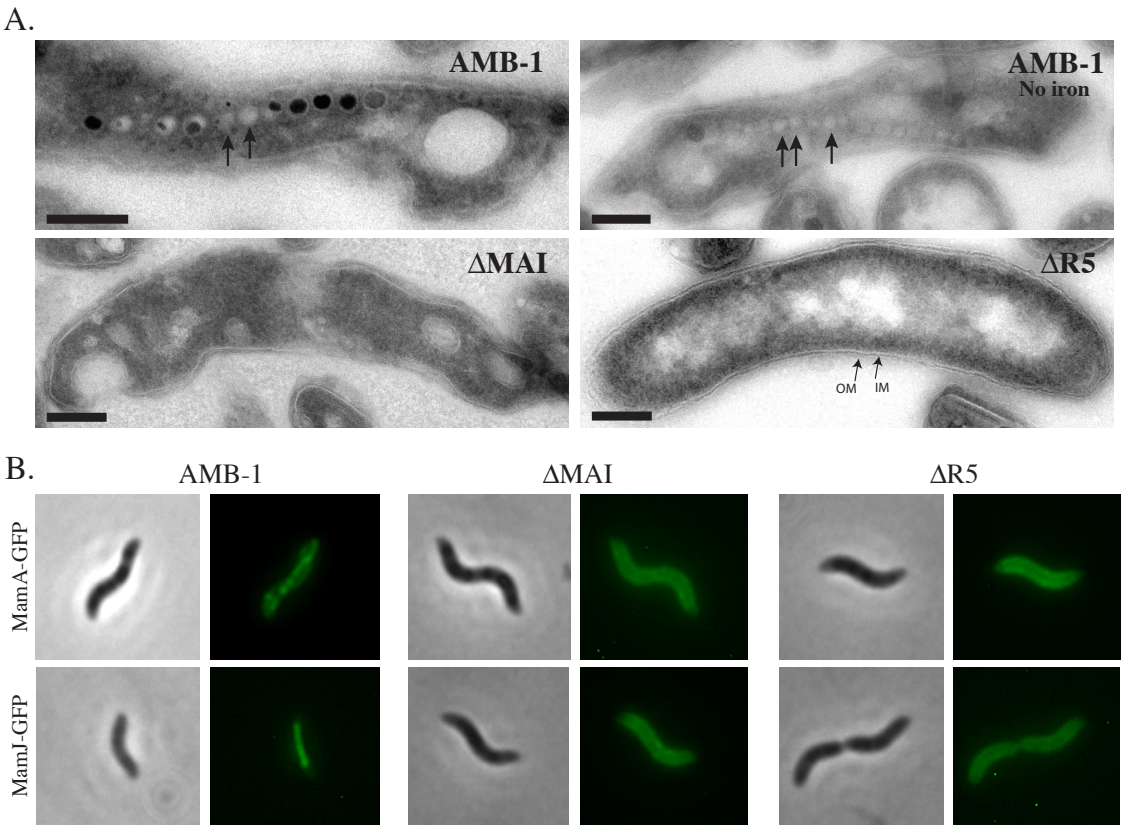

Figure 2 : The *mamAB* gene cluster (R5) is essential for magnetosome membrane formation. (A): The ΔR5 mutant does not synthesize magnetosome compartments. Electron micrographs of thin cryo-sections of AMB-1 wild-type grown in the presence or absence of iron, ΔMAI and ΔR5 mutants. The black arrows indicate the position of empty magnetosome compartments in wild type cells. The electron dense structures within the magnetosome compartments are magnetite crystals. Scale bar: 100 nm. IM: Inner membrane; OM: outer membrane. (B): Magnetosome-associated proteins are mislocalized in the ΔMAI and ΔR5 mutants. Upper panel: Localization of MamA-GFP in AMB-1 wild-type, ΔMAI and ΔR5 cells. Lower panel: Localization of MamJ-GFP in AMB-1 wild-type, ΔMAI and ΔR5 cells. Left: phase contrast image, right: fluorescence image.

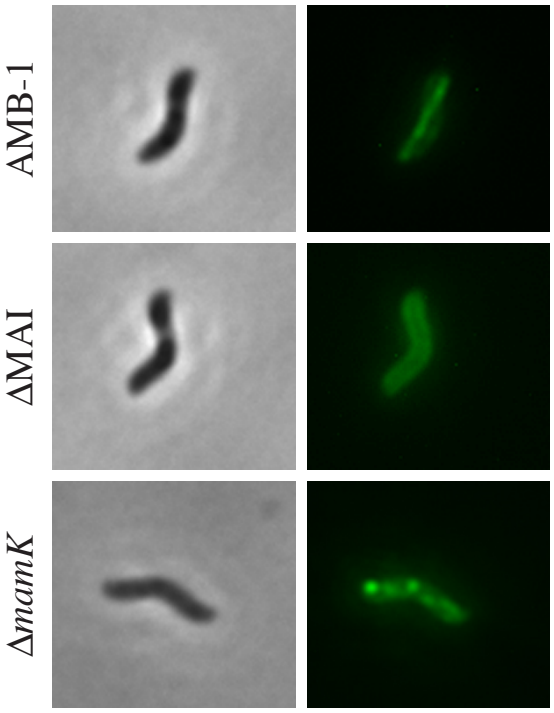

Figure 3 :GFP-MamI has a magnetosome-dependent localization in AMB-1. Phase contrast and fluorescence images of GFP-MamI in AMB-1 wild type, ΔMAI, ΔR5 and Δ*mamK* mutants (100X objective).

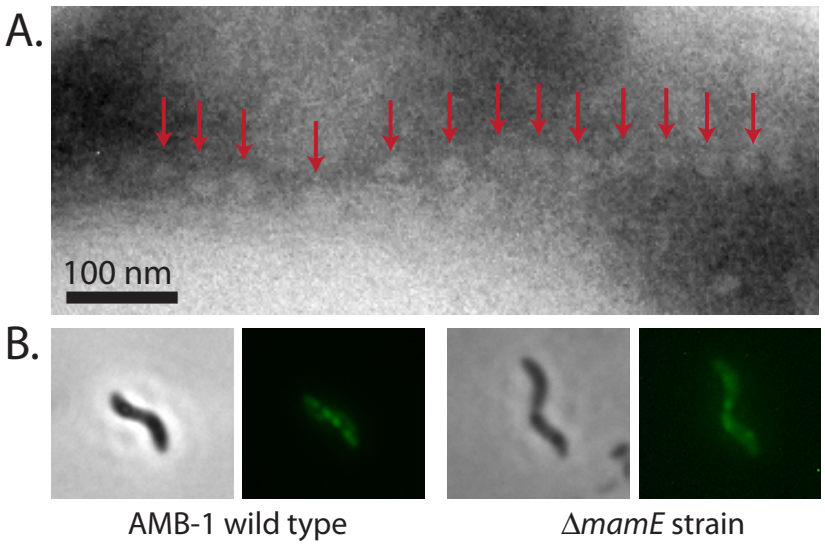

Figure 4 : The Δ*mamE* mutant forms empty magnetosome compartments and has a defect in magnetosome protein localization. (A): The Δ*mamE* strain synthesizes a chain of empty magnetosome compartments. Electron micrograph of a thin cryo-section of a Δ*mamE* mutant cell. Empty magnetosomes are indicated by the red arrows. (B): MamA-GFP is mislocalized in the Δ*mamE* strain. Phase contrast (left) and fluorescence images (right) of MamA-GFP in AMB-1 wild type and Δ*mamE* cells (100X objective).

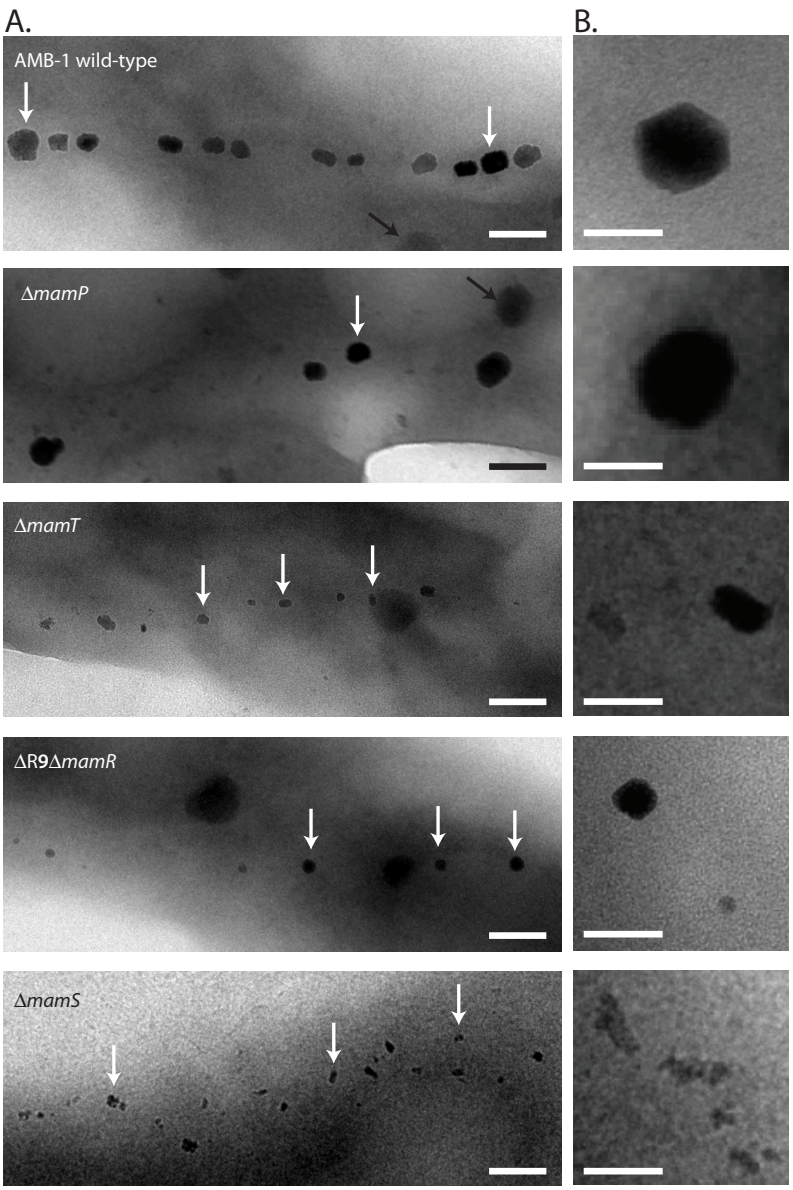

Figure 5 : Biomineralization is placed under discrete genetic control in AMB-1. A. Transmission electron micrographs obtained on whole cells of (top to bottom) AMB-1 wild type, Δ*mamP*, Δ*mamT*, ΔR9Δ*mamR* and Δ*mamS* mutants. The white arrows indicate the position of magnetite crystals; the black arrows indicate unidentified storage granules. Scale bar: 100 nm. B. Close ups of crystals in the mutant strains shown in A. Scale bar: 50 nm.

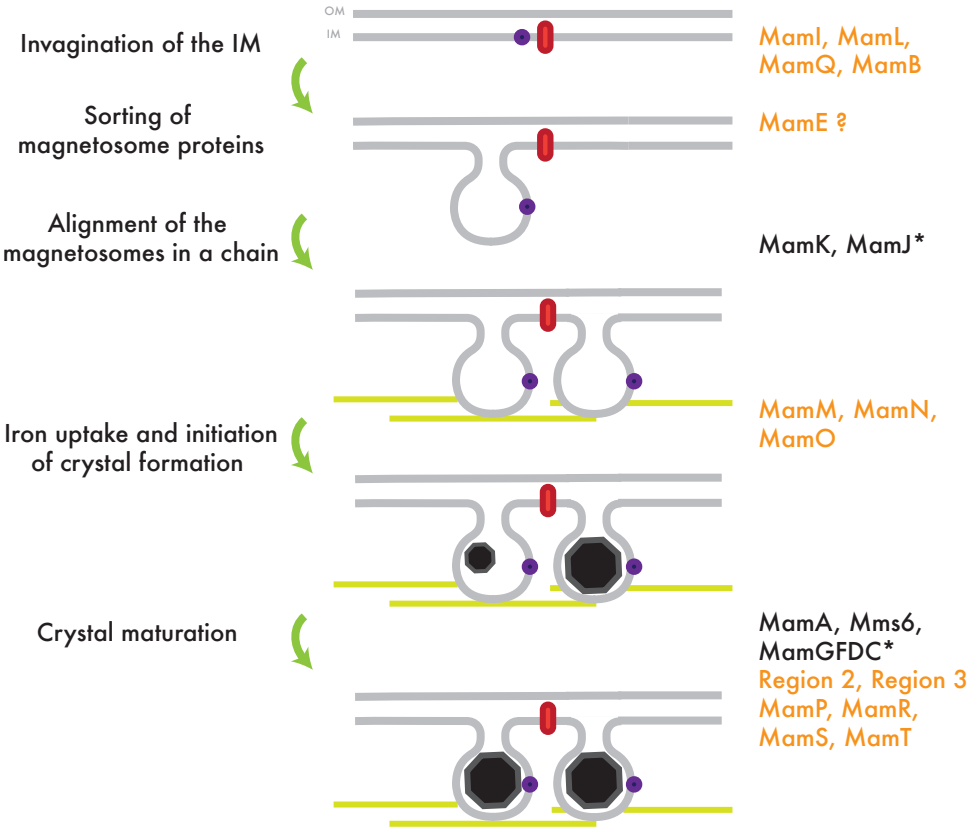

Figure 6 : Model for magnetosome stepwise assembly in AMB-1. The steps leading to magnetosome formation are indicated on the left side of the model and the factors known to play a role in each of these steps are indicated on the right side. The gene names in black indicate factors discovered in previous studies in AMB-1, in orange, the genes whose possible functions were defined in the present study. The asterisk indicates genes characterized in MSR-1. The black octagons represent growing and mature magnetite crystals. The red symbol indicate inner membrane proteins, the purple dot indicate magnetosome-associated protein. The yellow lines represent the MamK cytoskeletal filaments. IM: inner membrane; OM: outer membrane.

Mutant	Magnetic response (Cmag)	Presence of magnetosome membranes
Δ*mamU*	Wt	+
Δ*mamV*	Wt	+
Δ*mamH*	Intermediate	+
Δ*mamQ*	Intermediate	+
Δ*mamR*	Intermediate	+
Δ*mamB*	Intermediate	+
Δ*mamP*	Weak	+
ΔR9Δ*mamR*	Weak	+
Δ*mamS*	Weak	+
Δ*mamT*	Weak	+
Δ*mamE*	Null	+
Δ*mamM*	Null	+
Δ*mamN*	Null	+
Δ*mamO*	Null	+
Δ*mamI*	Null	-
Δ*mamL*	Null	-
ΔR9Δ*mamQ*	Null	-
ΔR9Δ*mamB*	Null	-

Table 1: Phenotypic characterization of the *mamAB* mutants.
Wild Type: not significantly different from wild type; Intermediate: 60-80% of wild type magnetic response; Weak: below 40% of wild type magnetic response. The presence of magnetosome membranes was assessed by visualizing of uranyl acetate stained thin sections of cells by TEM.

Appendix : Supplemental Information

Growth conditions

The MG media was completed by adding 1/100 volume of Wolfe's mineral solution (where the iron was omitted) and 1/100 volume of 3 mM ferric malate 9mM. For iron-limited conditions, the cells were grown in the absence of iron and diluted in iron-free media twice after they reached exponential phase. AMB-1 was grown in conical tubes (15 or 50 mL) filled with media to the top and incubated in a 30°C incubator. For fluorescence microscopy, Cmag measurements (8) and mutant screens, the cells were grown in 10 mL of MG media in 20 mL culture tubes and incubated at 30°C in a microaerobic chamber where the oxygen concentration was maintained below 10%. In AMB-1, the antibiotics were used as follow: kanamycin was used at a concentration of 7-10 µg per mL in liquid cultures, 15 µg per mL in solid media, carbenicillin was used at a concentration of 20 mg per mL in both liquid and solid media and chloramphenicol was used at a concentration of 35 to 45 µg per mL in liquid and solid media.
All clonings were performed in the DH5alpir strain of *E. coli*. In *E. coli*, the antibiotics were used as follows: kanamycin 50 mg per mL, chloramphenicol 25 mg per mL and carbenicillin 100 mg per mL. The WM3064 strain of *E.coli* was used as a donor strain in the conjugations and grown in the presence of diaminopimelic acid (DAP) at a final concentration of 300 mM.

Gene deletion and complementation

All PCR were performed using the Promega GoTaq® Green Master Mix according to supplier using a Biorad **My**Cycler™ thermocycler. Enzymes (restriction enzymes, T4 DNA ligase) were purchased from New England Biolabs, Inc. A two-step recombination method previously described (8) was used to delete the 12 regions in the MAI as well as to generate non-polar single deletions of *mamH, mamI, mamE, mamL, mamM, mamN, mamO, mamP, mamQ, mamR, mamB, mamS, mamT and mamU*. Regions ranging from 750 to 1250 bp located upstream and downstream of the region to be deleted were amplified by PCR so that they would overlap by a 21-nucleotide linker including a SwaI restriction site (8). A 1,5–2,5 kb fusion PCR fragment generated and cloned between the SpeI sites of the pAK0 suicide plasmid carrying a kanamycin resistance cassette and the *sacB* gene. The plasmids used to delete R3, R5 and R6 were generated in two steps. After the product of the fusion PCR was cloned into pAK0, the CAT cassette conferring resistance to chloramphenicol was amplified and cloned in the SwaI site of the linker. The plasmids were transferred into AMB-1 cells by conjugation and the transconjugants were selected on MG media plates containing kanamycin. The deletion mutants were screened on media containing sucrose or sucrose and chloramphenicol in the case of ΔR3, ΔR5 and ΔR6. The sucrose resistant colonies were screened by PCR for the product of the deletion and the absence of the plasmid markers (*kan* and *sacB* primers are listed in Fig. S6). The double deletions ΔR9Δ*mamQ* and ΔR9Δ*mamB* were obtained by generating the *mamQ* and the *mamB* deletions respectively in

the ΔR9 mutant strain. The double deletion strain Δ*mamI*Δ*mamL* was generated by deleting *mamI* in the Δ*mamL* strain. To generate a polar insertion in *mamV*, a ~750 bp fragment corresponding to the middle of *mamV* was amplified by PCR and cloned between the SpeI sites of the pAK0 plasmid. The plasmid was integrated on the chromosome of AMB-1 by conjugation selecting for kanamycin resistant transconjugants.

The genes of interest were cloned between the EcoRI and SpeI sites downstream of the *tac* promoter in the pAK22 plasmid (5). The complementation plasmids were introduced in the AMB-1 mutants by conjugation. In the case of *mamB,* the gene conferring resistance to ampicillin (*bla*) placed downstream of the *tac* promoter, was introduced in the pAK22-derived complementation vector. The Cmag of the complemented ΔR9Δ*mamB* strain was higher when the cells were grown in media containing carbenicillin compared to media containing kanamycin suggesting that the latter antibiotic is not always optimal for plasmid maintenance in AMB-1. Similar improvement in complementation efficiency were observed using chloramphenicol as a selection marker.

A plasmid allowing for the systematic expression of genes on the chromosome of AMB-1 was designed. A 1106 bp fragment selected in the intergenic region located between *amb0397* and *amb0398* (named *397*) was amplified from genomic DNA by PCR using 5Xho-intergen397 and 3-intergen397tac, carrying a 22-nucleotide tail homologous to the beginning of the *tac* promoter (see Fig. S6). The *tac* promoter was amplified from the pAK22 plasmid using 5tac-Pm and 3tacPm. A fragment containing *397* directly followed by the *tac* promoter was obtained by fusion PCR and cloned between the XhoI and SpeI sites of pAK0 leading to pAK*397*. We verified that the integration of pAK*397* in wild type AMB-1 did not have an effect on magnetosome formation. The genes of interest were cloned between the SpeI and NotI sites of pAK*397*.

GFP localization

The C-terminal GFP fusions were derivatives of pAK22 (5). To generate a N-terminal GFP fusion, *gfp* was amplified from pAK22 using a forward primer including a 5' EcoRI site and a reverse primer including the alpha helical HL4 linker (LA(EAAAK)$_4$AAA) described in (23) followed by a BamHI site. *mamI* was amplified by PCR and cloned between the BamHI and SpeI sites.

***mamI-mamL* two gene operon**

mamI and *mamL* were cloned in several steps in pAK22 and then subcloned in pAK*397*. First, *mamI* was cloned in the pET28a vector (Stratagene) between NcoI and BamHI sites using the primers 5NcoI and 3BamI to generate the plasmid pET-I (primers are listed in table S3). *mamL* was amplified by PCR using a forward primer comprising a ribosome binding site gaaggagatatacc (5RBS-BamL) and cloned downstream of *mamI* using BamHI and XhoI to generate pET-*IL*.

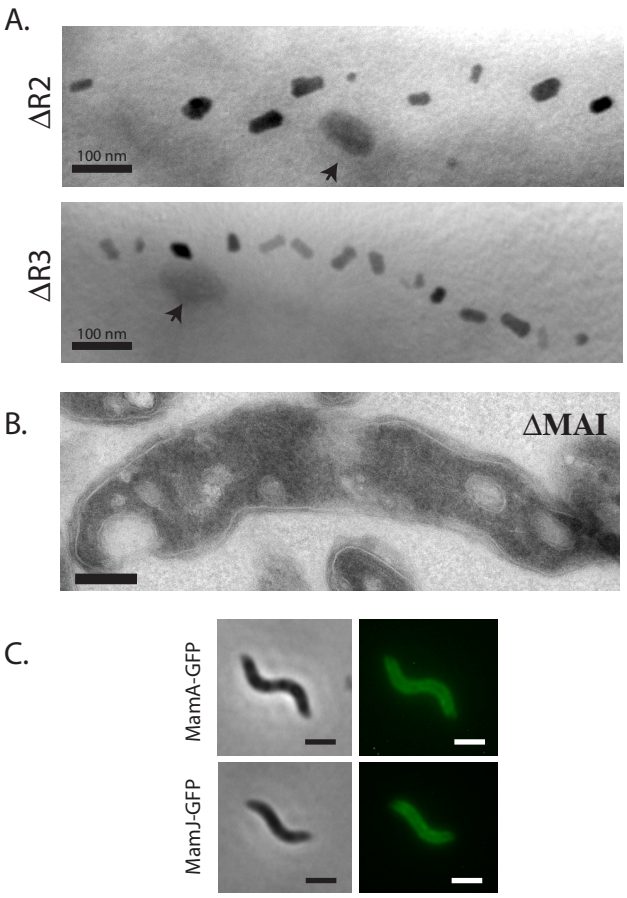

Figure S1: (A) The ΔR2 and ΔR3 mutants present a defect in magnetite formation. TEM images of the ΔR2 and ΔR3 AMB-1 mutants showing irregular shaped magnetite crystals. Black arrowheads indicate uncharacterized granules. (B) TEM on ultra-thin sections reveals the absence of magnetosome membranes in the ΔMAI mutant. (Scale bar, 100nm) (C) MamA-GFP and MamJ-GFP are mislocalized in the ΔMAI mutant. Phase contrast image (Left) and fluorescence image (Right) are shown. (Scale bar, 2μm)

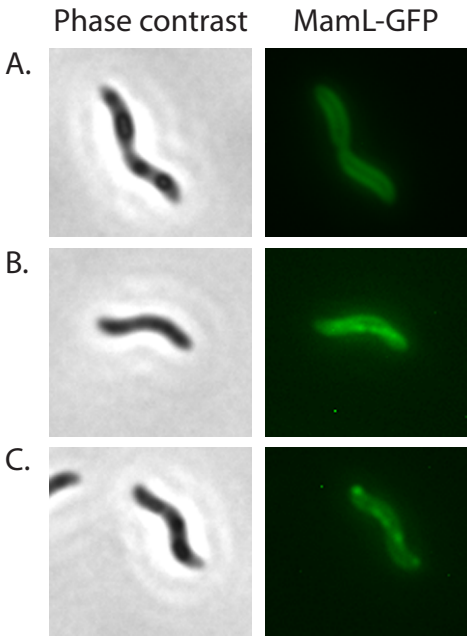

Figure S2: MamL-GFP mostly localizes around the cell membrane in AMB-1. A: MamL-GFP localization in 90 % of the population in AMB-1 wild type cells. B and C: MamL-GFP localizes as aligned dots or short lines in 10 % of the population in AMB-1 wild type cells. Left: Phase contrast image; Right: Fluorescence image. (100X objective).

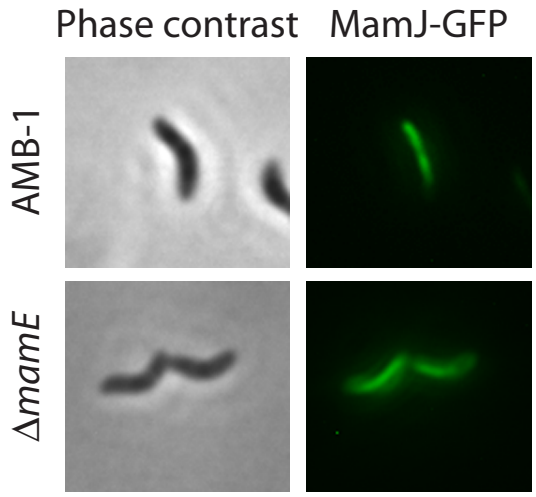

Figure S3: MamJ-GFP is mislocalized in the Δ*mamE* mutant strain. Phase contrast and fluorescence images of MamJ-GFP in wild type (upper panel) and ΔmamE strains (lower panel).

Name of the region	Genes included in the deletion	Coordinates	Magnetic phenotype
R1	*amb0933* to *amb0941*	996982 to 1006971	Wt
R2	*amb0943* to *amb0949*	1007720 to 1012672	Weak
R3	*amb0950* to *amb0957*	1013510 to 1017469	Weak
R4	*amb0958* to *amb0960*	1018350 to 1021417	Wt
R5	*amb0961* to *amb0978*	1022198 to 1039149	NO
R6	*amb0997* to *amb0993*	1039864 to 1050469	Intermediate
R9	*amb1002* to *amb1007*	106413 to 1069299	Wt
R10	*amb1008* to *amb1014*	1069399 to 1074622	Wt
R11	*amb1015*	1074679 to 1075614	Wt
R12	*amb1016* to *amb1018*	1075660 to 1079676	Intermediate
R13	*amb1019* to *amb1025*	1079914 to 1086548	Intermediate
R14	*amb1026* to *amb1031*	1086668 to 1096635	Wt
SID25	*amb0975* to *amb1007*	1036078 to 1069379	Weak

Table S1 : Coordinates and magnetic phenotype of the MAI mutants.
The magnetic phenotypes were determined by Cmag measurement; Intermediate: 80% of wild-type values; NO: cells are nonmagnetic; weak, 20% of wild-type values; Wt, indistinguishable from wild-type.

Strain	% of wild type	Complemented with	% of wild type
MAI mutants			
AMB-1	100	100	
ΔMAI	0	ND	
ΔR1	100	ND	
ΔR10	100	ND	
ΔR4	80-100	ND	
ΔR6	80-100	ND	
ΔR9	80-100	ND	
ΔR11 *amb1015*			
ΔR13	80-100	ND	
ΔR14	80-100	ND	
ΔR12	60-80	ND	
ΔR2	0-20	ND	
ΔR3	0-20	ND	
ΔR5	0	ND	
mamAB single mutants			
Δ*mamU*	80-100	ND	
mamV-	80-100	ND	
Δ*mamH*	60-80	ND	
Δ*mamQ*	60-80	ND	
Δ*mamR*	60-80	ND	
Δ*mamB*	60-80	ND	
Δ*mamP*	0-20	pAK-*mamP*	60-80
Δ*mamS*	0-20	pAK-*mamS*	60-80
Δ*mamT*	0-20	ND	
ΔR9Δ*mamR*	0-20	ND	
SID25	0-20	ND	
Δ*mamE*	0	pAK-*mamE*	40-60
Δ*mamM*	0	pAK-*mamM*	60-80
Δ*mamN*	0	pAK-*mamN*	40-60
Δ*mamO*	0	pAK-*mamO*	80-100
Δ*mamI*	0	pAK-*mamI*	60-80
		pAK-GFP-*mamI*	60-80
		pAK397-mamI	100
Δ*mamL*	0	pAK-*mamL*	100
		pAK397-mamL	100
		pAK-*mamL*-GFP	0-20
ΔR9Δ*mamQ*	0	pAK-*mamQ*	100
ΔR9Δ*mamB*	0	pAK-*mamB*	100

Table S2 : Magnetic properties of AMB-1 mutants, represented as percentage of wild type, before and after complementation. Note that the ΔR2, ΔR3 and ΔR5 MAI mutants were not complemented due to the large size of the region deleted (5.7; 4.8 and 17.7 kilobases respectively). The magnetic properties are represented as percentage of wild type values. The maximum Cmag values are different for AMB-1 and AMB-1 containing a kanamycin resistant plasmid, also the values for the mutants were compared to two different wild type Cmag values. The mutants which magnetic properties were above 60% of wild type's were not systematically complemented.

Name	Sequence	Target	In Plasmid
LD1a.up	GG**ACTAGT**TTCATCACCGTGCTGCATAC	Region R1	pAK229
LD1b	CCCATCCACTAAATTTAAATAggcgccatccgatcccactga	Region R1	pAK229
LD1c	TATTTAAATTTAGTGGATGGGcggaccgcgataaagttctaa	Region R1	pAK229
LD1d_do	GG**ACTAGT**CGCTCCTCTTTCTGTGCATT	Region R1	pAK229
LD2a	GG**ACTAGT**cggaccgcgataaagttctaa	Region R2	pAK230
LD2b	CCCATCCACTAAATTTAAATAgccgagcgggtctcattgcag	Region R2	pAK230
LD2c	TATTTAAATTTAGTGGATGGGccggcagcacaggccgcctga	Region R2	pAK230
LD2d	GG**ACTAGT**cccaattcccctgcgaatttg	Region R2	pAK230
LD3a	GG**ACTAGT**ccggcagcacaggccgcctga	Region R3	pAK231
LD3b	CCCATCCACTAAATTTAAATAcccaattcccctgcgaatttg	Region R3	pAK231
LD3c	TATTTAAATTTAGTGGATGGGtgggtcgcccaccggatctga	Region R3	pAK231
LD3d	GG**ACTAGT**cgccgcccttctcggccagag	Region R3	pAK231
LD4a.1	GG**ACTAGT**cgttgggatgtttcgtttct	Region R4	pAK232
LD4b	CCCATCCACTAAATTTAAATAcgccgcccttctcggccagag	Region R4	pAK232
LD4c	TATTTAAATTTAGTGGATGGGttctggtgaagagagcatctg	Region R4	pAK232
LD4d.1	GG**ACTAGT**tcatgaacgcggtattggaca	Region R4	pAK232
LD5a	GG**ACTAGT**ttctggtgaagagagcatctg	Region R5	pAK233
LD5b	CCCATCCACTAAATTTAAATAgccagccaagcaccggccaggg	Region R5	pAK233
LD5c.1	TATTTAAATTTAGTGGATGGGtcgcctatttggttgagg	Region R5	pAK233
LD5d.1	GG**ACTAGT**cgtccaggttgtccaagag	Region R5	pAK233
LD6a.1	GG**ACTAGT**tcgcctatttggttgagg	Region R6	pAK234
LD6b.1	CCCATCCACTAAATTTAAATAcgtccaggttgtccaagag	Region R6	pAK234
LD6c	TATTTAAATTTAGTGGATGGGaagcccaaatcagccacctga	Region R6	pAK234
LD6d	GG**ACTAGT**cttcaaggctgacgatgttgg	Region R6	pAK234
LD9a.up	GG**ACTAGT**CGGTGATCTCGTCGTCTTCT	Region R9	pAK235
LD9b	CCCATCCACTAAATTTAAATAgtgccgatattttccaccgtgg	Region R9	pAK235
LD9c	TATTTAAATTTAGTGGATGGGgccgccgcggcacgggcctga	Region R9	pAK235
LD9d_do	GG**ACTAGT**GCTTTTCCATCGATTCCATC	Region R9	pAK235
LD10a.1	GG**ACTAGT**gacccagctcagcttgaaga	Region R10	pAK236
LD10b	CCCATCCACTAAATTTAAATAgcccgtcaccgtcgggtctga	Region R10	pAK236
LD10c	TATTTAAATTTAGTGGATGGGttcgccccccgcggcgagtga	Region R10	pAK236
LD10d.1	GG**ACTAGT**gacgcccatatggtgttcat	Region R10	pAK236
1015KO1	GG**ACTAGT**aaagcggcggctattatttcga	Region R11	pAK331*
1015KO2	CCCATCCACTAAATTTAAATAtctcggacggactatcgtcat	Region R11	pAK331*
1015KO3	TATTTAAATTTAGTGGATGGGgtagccaccggaatcgcctga	Region R11	pAK331*
1015KO4	GG**ACTAGT**atcacagcgacgaccgggagctg	Region R11	pAK331*
1016a	GG**ACTAGT**cctatggcggcatctacatt	Region R12	pAK237
1016b	CCCATCCACTAAATTTAAATAcgcgccctgcggatcggctga	Region R12	pAK237
LD11c	TATTTAAATTTAGTGGATGGGcatgatggccgcaatcgccatcc	Region R12	pAK237
LD11d_do	GG**ACTAGT**ttcttccagcacgaaggaat	Region R12	pAK237
LD12a.1	GG**ACTAGT**caaggtcatggcctcgtc	Region R13	pAK238
LD12b	CCCATCCACTAAATTTAAATAcctgatttcgggcgatagcataatg	Region R13	pAK238
LD12c	TATTTAAATTTAGTGGATGGGgattggtggcgccggatgtga	Region R13	pAK238
LD12d.1	GG**ACTAGT**gcacggttggtagcactgtc	Region R13	pAK238
LD13a.up	GG**ACTAGT**GGAGCTTTCTTCGCCGATA	Region R14	pAK297
LD13b.1	CCCATCCACTAAATTTAAATAtatatcgccgaccgtatctga	Region R14	pAK297
LD13	TATTTAAATTTAGTGGATGGGatggggatcagcaagcgcgg	Region R14	pAK297
LD13d_do	GG**ACTAGT**AGCCGCAGCCCTAATTATCT	Region R14	pAK297
CAT1Swa	g**ATTTAAAT**cattaatgaatcggccaacg	CAT	
CAT2Swa	g**ATTTAAAT**gttgataccgggaagccctg	CAT	

*: Joyce Cueto

Table S3: Primers used for the genetic dissection of the Magnetosome Island.

Primer name	Primer sequence	Used to amplify
5kan	caggatgaggatcgtttcgc	Kanamycin cassette
3kan	GAAGAACTCGTCAAGAAGGCG	Kanamycin cassette
5sacB	GGAAGAAGCAGACCGCTAAC	*sacB* gene
sacBrev	TTAGCCATTTGCCTGCTTTT	*sacB* gene

Table S4: Primers for the verification of the mutant strains

Primer Name	Sequence	Target	In plasmid
Ha-del	GG**ACTAGT**cagccgttgaccgatctc	*mamH*	pAK239
Hb	CCCATCCACTAAATTTAAATAagccgcttccactcgagacac	*mamH*	pAK239
Hc	TATTTAAATTTAGTGGATGGGccaggggacgacggggtggcgtag	*mamH*	pAK239
Id	gg**ACTAGT**aatcagatcgtggcaggtg	*mamH*	pAK239
Ha	GG**ACTAGT**cacaacgccctttatttgct	*mamI*	pAK240
IbNS	CCCATCCACTAAATTTAAATAaaacgttactccagtcttgat	*mamI*	pAK240
IcNS2	TATTTAAATTTAGTGGATGGGatggccatgttcaatggtgac	*mamI*	pAK240
Id	gg**ACTAGT**aatcagatcgtggcaggtg	*mamI*	pAK240
Ea	GG**ACTAGT**cggtcgtttatcgagcattt	*mamE*	pAK241
Eb	CCCATCCACTAAATTTAAATAgccgtcttctacgtcaccat	*mamE*	pAK241
Ec	TATTTAAATTTAGTGGATGGGggccaagagttctggattgt	*mamE*	pAK241
Ed	gg**ACTAGT**caccgtgatatccgaagtga	*mamE*	pAK241
La	GG**ACTAGT**ctttcgagatgcgctcctac	*mamL*	pAK242
Lb.3	CCCATCCACTAAATTTAAATAcatgccactgtcctagac	*mamL*	pAK242
Lc.2	TATTTAAATTTAGTGGATGGGtgaatcccttcgcttggg	*mamL*	pAK242
Ld	GG**ACTAGT**atgtcggcccagatgtctt	*mamL*	pAK242
La	GG**ACTAGT**ctttcgagatgcgctcctac	*mamM*	pAK279
Mb	CCCATCCACTAAATTTAAATAcgtgcaaccgctcttcctcat	*mamM*	pAK279
Mc	TATTTAAATTTAGTGGATGGGttgtcgaaggtggataactag	*mamM*	pAK279
Md	GG**ACTAGT**gccatccacatcaaaaggat	*mamM*	pAK279
5Lspe	GG**ACTAGT**aagattgatcggatcgttgg	*mamN*	pAK280
Nb	CCCATCCACTAAATTTAAATAaagggtgagaagtccgatcat	*mamN*	pAK280
Nc	TATTTAAATTTAGTGGATGGGatcgcggttctcgtgggatga	*mamN*	pAK280
Nd	GG**ACTAGT**acaccaccacattggtcaga	*mamN*	pAK280
Oa	GG**ACTAGT**gaccgtcggcttttgagtta	*mamO*	pAK243
Ob	CCCATCCACTAAATTTAAATAatcttgttggtgggcaattc	*mamO*	pAK243
Oc	TATTTAAATTTAGTGGATGGGcgctctcaagatgctgacct	*mamO*	pAK243
Od	GG**ACTAGT**ggcaggcttatcaaatctgg	*mamO*	pAK243
5OSpe	GG**ACTAGT**gaattgcccaccaacaagat	*mamP*	pAK244
mamPKO2	CCCATCCACTAAATTTAAATAagcgccaccttgctattcatg	*mamP*	pAK244
mamPKO3	TATTTAAATTTAGTGGATGGGgcctgccacgtcataaagtga	*mamP*	pAK244
R_in_rev	CGG**ACTAGT**atcttgtccaccagcaccat	*mamP*	pAK244
5P2	GG**ACTAGT**ctttccccagcccctgtat	*mamQ*	pAK245
Qb	CCCATCCACTAAATTTAAATAattcgcgtcgcctaatgccat	*mamQ*	pAK245
Qc	TATTTAAATTTAGTGGATGGGgcgcaggacatcaagaaatga	*mamQ*	pAK245
Rd	GG**ACTAGT**gccgttgtcgatccagata	*mamQ*	pAK245
5Qspe	GG**ACTAGT**cgttctcggcctgacctat	*mamR*	pAK246
Rb	CCCATCCACTAAATTTAAATAgatcaccgccgtccagatcat	*mamR*	pAK246
Rc	TATTTAAATTTAGTGGATGGGgtggattacatgaaccgatga	*mamR*	pAK246
Rd	GG**ACTAGT**gccgttgtcgatccagata	*mamR*	pAK246
Ba	GG**ACTAGT**catcgacagcttcaagatcg	*mamB*	pAK333
Bb	CCCATCCACTAAATTTAAATAgacccccttgaacagggtcat	*mamB*	pAK333
Bc	TATTTAAATTTAGTGGATGGGgccgccgcggcacgggcctga	*mamB*	pAK333
3speT†	GG**ACTAGT**tcataattgccatctcatgcc	*mamB*	pAK333
5upQspe	gg**ACTAGT**cttagagaggcggatatg	*mamS*	pAK247
Sb	CCCATCCACTAAATTTAAATAacgctctggccggatgtccat	*mamS*	pAK247
Sc	TATTTAAATTTAGTGGATGGGctgtggatggtggtgcagtga	*mamS*	pAK247
3speU†	GG**ACTAGT**ttatttgggcaccagcatgggt	*mamS*	pAK247
Ta	GG**ACTAGT**atctgcgcatcaaggacagt	*mamT*	pAK334
Tb	CCCATCCACTAAATTTAAATAgccgcgccgcggcgcctccat	*mamT*	pAK334
Tc	TATTTAAATTTAGTGGATGGGggcatgagatggcaattatga	*mamT*	pAK334
3speU†	GG**ACTAGT**ttatttgggcaccagcatgggt	*mamT*	pAK334
5SSpe	GG**ACTAGT**gccagagcgtatgttgagc	*mamU*	pAK248
Ub	CCCATCCACTAAATTTAAATAgatgatcgccgcgatgcgcat	*mamU*	pAK248
Uc	TATTTAAATTTAGTGGATGGGcccatgctggtgcccaaataa	*mamU*	pAK248
3Vspe†	GG**ACTAGT**ggatgcggatgtgacagg	*mamU*	pAK248
5VSpe	GG**ACTAGT**ttctgaccaagggcatcaat	*mamV*	pAK276
3VSpe†	GG**ACTAGT**ggatgcggatgtgacagg	*mamV*	pAK276

Table S5: Primers used for the characterization of the *mamAB* gene cluster: Single-gene deletions. † indicates primers described earlier in the table.

Name	Sequences	Plasmid	In plasmid
5Xho intergen397	gg**CTCGAG**aactagccgcttctgtgcat	pAK*397*	pAK253
3intergen 397tac	GATGATTAATTGTCAACAGCTCGGAT CCcgccgtctttaaaagcagat	pAK*397*	pAK253
5tacPm	GAGCTGTTGACAATTAATCATC	pAK*397*	pAK253
3tacPmSpe	gg**ACTAGT**TGTTTCCTGTGTGAAATTG	pAK*397*	pAK253
5speI	ggc**ACTAGT**atgccaagcgtgattttcgg	pAK*397maml*	
3NotI	ggc**GCGGCCGC**tcaaccatcgatgtcaggg	pAK*397maml*	
5SpeI†	ggc**ACTAGT**atgccaagcgtgattttcgg	pAK*397-IL*	pAK314
3NotL	gg**GCGGCCGC**tcagcgcttgatgacgatg	pAK*397-IL*	pAK314
5EcoL	ggc**GAATTC**atggtaagattgatcggatc	pAK*mamL*	pAK265
3SpeL	gg**ACTAGT**tcagcgcttgatgacgatg	pAK*mamL*	pAK265
5a†	GG**ACTAGT**ttctggtgaagagagcatctg	pAK5a3E	pAK250
3SpeE	gg**ACTAGT**tcaaaggacaatccagaac	pAK5a3E	pAK250
5MfeM	CGC**CAATTG**atgaggaagagcggttgcacg	pAK*mamM*	pAK261
3SpeM	GG**ACTAGT**ctagttatccaccttcgacaa	pAK*mamM*	pAK261
5EcoN	ggc**GAATTC**atgatcggacttctcaccctt	pAK*mamN*	pAK258
3SpeN	GG**ACTAGT**tcatcccacgagaaccgcgat	pAK*mamN*	pAK258
5EcoO	ggc**GAATTC**atgattgaagtcggcgag	pAK*mamO*	pAK263
3SpeO	ggc**ACTAGT**tcacaccgaggtcagcatc	pAK*mamO*	pAK263
5EcoP	gg**GAATTC**atgaatagcaaggtggcg	pAK*mamP*	pAK262
3SpeP	gg**ACTAGT**tcactttatgacgtggcag	pAK*mamP*	pAK262
ORF10-GFP1	GGC**GAATTC**ATGGCATTAGGCGACGCGAATGT	pAK*mamQ*	pAK259
3SpeQ	gg**ACTAGT**tcatttcttgatgtcctg	pAK*mamQ*	pAK259
5EcoR	GG**GAATTC**ATGATCTGGACGGCGGTG	pAK*mamR*	pAK257
3SpeR	GG**ACTAGT**TCATCGGTTCATGTAATC	pAK*mamR*	pAK257
ORF11-GFP1	GGC**GAATTC**ATGAAGTTCGAAAATTGCAGGGA	pAK*mamB*	pAK260
3SpeB	gg**ACTAGT**tcaggcccgtgccgcggc	pAK*mamB*	pAK260
5EcoS	GG**GAATTC**ATGGACATCCGGCCAGAG	pAK*mamS*	pAK256
3SpeS	GG**ACTAGT**TCACTGCACCACCATCCAC	pAK*mamS*	pAK256
5MfeT.2	CGC**CAATTG**atggaggcgccgcggcgcggccgtc	pAK*mamT*	pAK254
3SpeT	GG**ACTAGT**tcataattgccatctcatgcc	pAK*mamT*	pAK254
5NcoI	ggc**CCATGG**atgccaagcgtgattttcgg	pET-I	pAK275
3BamI	CGC**GGATCC**accatcgatgtcaggg	pET-I	pAK275
5BamRBS-L	CGC**GGATCC**gaaggagatataccatggtaagattgatcggatc	pET-*IL*	pAK337
3XhoL	CGC**CTCGAG**gcgcttgatgacgatgc	pET-*IL*	pAK337
GFP Fusion			
ORF2-GFP1	GGC**GAATTC**ATGGCGAATAACCGGCGAGATC	pAKmamJ-GFP	pAK212*
ORF2-GFP2	GGC**GGATCC**TTTTTTCTTGCCCACCGTATCGCATTGAGACG TGG	pAKmamJ-GFP	pAK212*
3BamL	CGC**GGATCC**gcgcttgatgacgatgc	pAK-mamL-GFP	pAK301
5EcoL†	ggc**GAATTC**atggtaagattgatcggatc	pAK-mamL-GFP	pAK301
NGFP-F	gcc**GAATTC**atgagtaaaggagaagaacttttcactcg	pAK-GFP-maml	pAK266
NGFPHL4-R	ccg**GGATTC**cgctgctgctttggccgccgcttccttagccgct ggctcctttggggccgcttctttagccgccgcggcctcggcca gtttgtatagttcatccatgccat	pAK-GFP-maml	pAK266
5BamI	ggc**GGATCC**atgccaagcgtgattttcgg	pAK-GFP-maml	pAK266
3SpeI	ggc**ACTAGT**tcaaccatcgatgtcaggg	pAK-GFP-maml	pAK266

*: Joyce Cueto

Table S6: Primers used to generate complementation plasmids and fusions to GFP.

Plasmid name	Plasmid of origin	Experiment
		Deletions
pAK229	pAK0-derived	Deletion plasmid for R1
pAK230	pAK0-derived	Deletion plasmid for R2
pAK231	pAK0-derived	Deletion plasmid for R3
pAK232	pAK0-derived	Deletion plasmid for R4
pAK233	pAK0-derived	Deletion plasmid for R5
pAK234	pAK0-derived	Deletion plasmid for R6
pAK235	pAK0-derived	Deletion plasmid for R9
pAK236	pAK0-derived	Deletion plasmid for R10
pAK331	pAK0-derived	Deletion plasmid for R11
pAK237	pAK0-derived	Deletion plasmid for R12
pAK238	pAK0-derived	Deletion plasmid for R13
pAK297	pAK0-derived	Deletion plasmid for R14
pAK276	pAK0-derived	Insertion plasmid in *mamV*
pAK241	pAK0-derived	Deletion plasmid for *mamE*
pAK243	pAK0-derived	Deletion plasmid for *mamO*
pAK242	pAK0-derived	Deletion plasmid for *mamL*
pAK279	pAK0-derived	Deletion plasmid for *mamM*
pAK248	pAK0-derived	Deletion plasmid for *mamU*
pAK245	pAK0-derived	Deletion plasmid for *mamQ*
pAK333	pAK0-derived	Deletion plasmid for *mamB*
pAK280	pAK0-derived	Deletion plasmid for *mamN*
pAK239	pAK0-derived	Deletion plasmid for *mamH*
pAK246	pAK0-derived	Deletion plasmid for *mamR*
pAK244	pAK0-derived	Deletion plasmid for *mamP*
pAK245	pAK0-derived	Deletion plasmid for *mamQ*
pAK334	pAK0-derived	Deletion plasmid for *mamT*
pAK240	pAK0-derived	Deletion plasmid for *mamI*
pAK247	pAK0-derived	Deletion plasmid for *mamS*
		Complementation vectors
pAK263	pAK22-derived	Complementation plasmid for Δ*mamO*
pAK265	pAK22-derived	Complementation plasmid for Δ*mamL*
pAK258	pAK22-derived	Complementation plasmid for Δ*mamN*
pAK261	pAK22-derived	Complementation plasmid for Δ*mamM*
pAK254	pAK22-derived	Complementation plasmid for Δ*mamT*
pAK250	pAK0-derived	Complementation plasmid for Δ*mamE*
pAK267	pAK22-derived	Complementation plasmid for Δ*mamU*
pAK309	pAK22-derived	Complementation plasmid for Δ*mamI*
pAK259	pAK22-derived	Complementation plasmid for ΔR9Δ*mamQ*
pAK256	pAK22-derived	Complementation plasmid for Δ*mamS*
pAK260	pAK22-derived	Complementation plasmid for ΔR9Δ*mamB.* Amp^R
pAK257	pAK22-derived	Complementation plasmid for ΔR9Δ*mamR*
pAK262	pAK22-derived	Complementation plasmid for Δ*mamP*
pAK253	pAK0-derived	Systematic complementation plasmid pAK397
pAK275	pET28-derived	*mamI* cloned in pET28
pAK337	pET28-derived	*mamI* and *mamL* cloned in pET28
pAK314	pAK0-derived	*mamI* and *mamL* cloned in pAK397
		GFP fusions
pAK301	pAK22-derived	C-terminal GFP fusion to *mamL*
pAK266	pAK22-derived	N-terminal GFP fusion to *mamI*
pAK212	pAK22-derived	C-terminal GFP fusion to mamJ (J. Cueto)

Table S7: Plasmids generated for this work.

Strain number	Name and description
AK30	AMB-1 wild type
AK31	ΔMAI (Spontaneous Magnetosome Island deletion)
AK51	ΔR1
AK35	ΔR2
AK36	ΔR3, chloramphenicol resistant
AK38	ΔR4
AK32	ΔR5, chloramphenicol resistant
AK39	ΔR6, chloramphenicol resistant
AK57	ΔR9
AK40	ΔR10
AK71	ΔR11
AK52	ΔR12
AK41	ΔR13
AK54	ΔR14
AK67	Δ*mamH*
AK64	Δ*mamI*
AK42	Δ*mamE*
AK78*	*Δmam*J
AK33	Δ*mamL*
AK44	Δ*mamM*
AK55	Δ*mamN*
AK34	Δ*mamO*
AK69	Δ*mamP*
AK72	Δ*mamQ*
AK46	ΔR9Δ*mamQ*
AK70	Δ*mamR*
AK74	ΔR9Δ*mamR*
AK53	Δ*mamB*
AK45	ΔR9Δ*mamB*
AK73	Δ*mamS*
AK60	Δ*mamT*
AK43	Δ*mamU*
AK75	*mamV-*
AK76	SID25, spontaneous deletion of *amb0975* to *amb1007*
AK77	Δ*mamI*Δ*mamL*

Table S8: Strains of AMB-1 generated in this work.

Chapter 3: The HtrA/DegP family protease MamE is a bifunctional protein with roles in magnetosome protein sorting and magnetite biomineralization.

Introduction

Organelles have long been hailed as a defining feature of eukaryotic cells, a definition that is changing as we gain more insight into the membrane- and protein-bound compartments found in bacteria and archaea (1-3). The existence of organelles in bacteria presents interesting evolutionary questions about the conservation of mechanisms of organelle formation, maintenance and organization. Bacterial organelles have also received attention because they often compartmentalize otherwise inefficient or toxic processes, a feature which may be exploited to carry out useful, but potentially cytotoxic, reactions.

One such organelle is the magnetosome of magnetotactic bacteria, which facilitates biomineralization processes that *in vitro* require harsh cytotoxic conditions. The magnetosome is a membrane-bound compartment that directs biomineralization of nanometer-sized, fixed single domain crystals of iron oxide (magnetite, Fe_3O_4) or iron sulfide (greigite, Fe_3S_4). In a species-dependent manner, cells contain anywhere from ten to hundreds of magnetosomes, which are organized into one or several chains, allowing the cells to align with the earth's magnetic field lines. This passive alignment is thought to facilitate the bacterium's search for favored low oxygen environments, a process referred to as magnetoaerotaxis (4-6). The magnetosome membrane is enriched for a specific set of proteins termed magnetosome proteins (7, 8). Many of these proteins, as well as other factors implicated in magnetosome formation, are encoded by a genomic island, the magnetosome island (MAI), which is a region essential for magnetosome formation conserved in all magnetotactic bacteria studied to date. The proteins found at the magnetosome are thought to facilitate magnetosome membrane formation, crystal formation, and chain formation and it is hypothesized that they impart the species-specific size and shape of the magnetic mineral.

In *Magnetospirillum magneticum* AMB-1 (AMB-1), magnetosomes are invaginations of the inner membrane formed in a step-wise fashion, where membrane invagination is followed by sorting of magnetosome proteins and then magnetite biomineralization (6). Of particular interest is the question of how magnetotactic bacteria generate such uniformly sized and shaped crystals of magnetite, since traditional recapitulation of magnetite synthesis *in vitro* yields a heterogeneous mixture of crystals. How bacteria can exercise such tight control over the process of magnetite formation is of interest for many proposed applications in medicine and biotechnology (9) and has driven much of the research of magnetotactic bacteria. In addition, understanding the steps and proteins involved in magnetite biomineralization may also inform how other processes of biomineralization, such as those of teeth or bone, are accomplished.

Although little is known about the molecular mechanisms underlying magnetite biomineralization, recent biochemical and genetic studies have implicated several factors in this process. For instance, addition of the magnetosome protein Mms6 to *in vitro* magnetite synthesis reactions confers more shape and size homogeneity, thus illustrating both the ability of magnetosome proteins to impart shape to magnetite crystals and the potential that specific proteins present for future applications (10, 11). In *Magnetospirillum gryphiswaldense* MSR-1 (MSR-1), the absence of the *mamCDFG* operon results in cells that form crystals approximately 75% of the size of wild type crystals, and it was suggested that the activity of these four genes in concert may exercise regulatory or accessory functions in crystal formation (12). Several factors important for magnetite biomineralization were also recently identified in a genetic dissection of the MAI in AMB-1. Confirming the importance of the *mamCDFG* and *mms6* gene clusters, the loss of a large region of the MAI, R3, which contains both of these gene clusters, resulted in a severe defect in crystal size. In addition, other genes, including *mamP, mamR, mamS and mamT,* were implicated in control of crystal size, number and/or shape. Lastly, four genes, *mamM*, *mamN*, *mamE* and *mamO*, were shown to be essential for the early steps of biomineralization, as the loss of any of the four genes individually led to a complete absence of minerals within magnetosomes (13).

Two of these genes, *mamE* and *mamO* encode putative DegP/HtrA family proteases. The members of this family of serine proteases are found in bacteria, archaea and eukaryotes and are known for their involvement in essential housekeeping functions such as the degradative removal of unfolded proteins during the periplasmic stress response, the initiation of the σ^E stress response and the removal of peroxisomal targeting signals (14-16). In AMB-1, several HtrA/DegP family proteases are encoded outside of the MAI. MamE and MamO, however, are encoded by the MAI suggesting a specific connection to magnetosome formation and not a general role in cellular homeostasis. Accordingly, in the absence of *mamE* or *mamO*, cells are viable and form magnetosome membranes, but fail to produce minerals within these membranes (13). This phenotype could be due to a specific defect in mineral formation or result from a more general defect in the sorting of biomineralization proteins to the magnetosome. The latter was suggested for MamE since two cytoplasmic magnetosome-associated proteins are mislocalized in the *mamE* deletion strain (13). Also suggestive of less canonical functions for MamE and MamO is the presence of additional functional domains not usually found in DegP/HtrA family proteases (15). MamE contains two putative *c*-type cytochrome CXXCH heme-binding motifs, and MamO contains a domain of unknown function (DUF81) predicted to code for seven transmembrane domains. Whether the putative protease activities of MamE and MamO are required for magnetosome formation and whether the unusual additional domains are of importance to their function was unknown. We thus undertook a mechanistic dissection of MamE and MamO to further define their roles in magnetosome biogenesis and to begin to develop an understanding of magnetosome formation at the molecular level.

Using a mutagenesis approach, we show that MamE and MamO are likely to act as proteases *in vivo* and that the additional domains, uncommon for DegP/HtrA family proteases, are important for their functions. By dissecting MamE's functional domains, we find that MamE is a bifunctional protein with a previously unidentified role in biomineralization that can be decoupled from its role in protein sorting. Based on these results, we propose that MamE's protease activity is required for a previously unidentified crystal size transition from 20nm crystals too small to hold a fixed magnetic dipole moment, to large crystals that can contribute to the cell's magnetic response.

Results

MamE and MamO act as proteases *in vivo*

MamE and MamO are putative DegP/HtrA family proteases encoded by genes found within the MAI. In their absence, cells are non-magnetic yet still possess the ability to form magnetosome membranes (13, 17). Members of the HtrA/DegP family of proteins are trypsin-like serine proteases that share a high degree of sequence homology within their protease domains, including a highly conserved active site triad (14). Primary sequence alignment of MamE and MamO with *E. coli* DegP allowed identification of their putative active site residues. MamE shares the conserved histidine-aspartate-serine active site (Fig 1A), whereas MamO has a threonine in place of the serine as the predicted active site nucleophile (Fig 1B). To determine whether MamE and MamO's putative protease functions are required for magnetite crystal formation, we generated protease-inactive constructs, $mamE^{P}$ and $mamO^{P}$, by site-directed mutagenesis of the active site triad residues to alanines. As a preliminary assay for the activity of these variants *in vivo,* we relied on the Cmag measurement, a differential spectrophotometric assay that quantitates the ability of the bacteria to orient in an external magnetic field (18). In this assay, $mamO^{P}$ fully complemented the *mamO* deletion, and $mamE^{P}$ partially complemented the *mamE* deletion (Fig. 1D), suggesting that the protease functions are not essential for crystal formation.

The MAI, however, encodes paralogues of both MamE and MamO, Amb1002 and Amb1004, respectively (Figs. 1A and 1B). Since DegP/HtrA proteases are known to function as oligomeric assemblies (14, 15) we hypothesized that these paralogues could form hetero-oligomeric complexes with MamE and MamO and thus provide active protease domains in *trans*. To test this hypothesis, we deleted *mamE* and *mamO* in the R9 deletion background. R9 is a region of the MAI containing both *amb1002* and *amb1004* that can be deleted in the wild type background without a detectable phenotype (13). The resulting double deletion strains, ΔR9Δ*mamE* and ΔR9Δ*mamO*, could be complemented to the same degree as the single deletion strains by wild type *mamE* and *mamO*, respectively. However, protease-inactive MamE and MamO mutants could not restore a wild type Cmag in these double deletion backgrounds (Fig. 1D). This suggests that the two proteins function as proteases *in vivo* and that they may act within hetero-assemblies with Amb1002 and Amb1004, respectively. To build on these initial results we chose to focus on MamE, with the aim of defining the

specific function of its protease activity in magnetosome protein sorting and magnetite formation. Additionally, to avoid background effects from the unusual cross-complementation observed above, all subsequent experiments were performed in the ΔR9Δ*mamE* background.

MamE protease mutant makes small crystals of magnetite

To further characterize the phenotype of the *mamE*^{P} mutant, cells were imaged by transmission electron microscopy (TEM). As described above, this mutant could not restore a magnetic response in the ΔR9Δ*mamE* strain. However, when visualized by TEM, MamE^{P} still allowed for synthesis of chains of small electron dense structures (Fig. 2). Under the same growth conditions, the ΔR9Δ*mamE* strain complemented with wild type *mamE* showed a bimodal crystal size distribution with peaks centered in the 51-55 nm and 36-40 nm size ranges (Fig 2). In contrast, MamE^{P}'s crystal size distribution was centered at 16-20 nm, and only 3% of crystals observed were larger than 35nm. Magnetite crystals smaller than 35 nm are too small to hold a permanent magnetic dipole moment (19), thus explaining the inability of the *mamE*^{P} mutant to align in a magnetic field. High resolution TEM confirmed that these 16-20 nm particles, and even those that were smaller and irregular in shape, were indeed crystalline (Fig. 3B). In addition, spectra from energy dispersive x-ray spectroscopy (EDS) of these small crystals are consistent with the presence of magnetite (Fig. 3C). Further, small crystals were observed within mature sized magnetosome membranes, suggesting that their growth is not restrained by smaller magnetosome membranes (Fig. 3A). Recently, a second MamE paralog, MamE-like, was annotated outside of the MAI as part of the newly identified magnetosome islet (20). To rule out the possibility that MamE-like can cross-complement MamE protease activity and is responsible for the 20 nm crystals observed in the ΔR9Δ*mamE*/*mamE*^{P} strain, the triple *mamE* deletion strain ΔR9Δ*mamE*Δ*mamE-like* was generated. The triple deletion strain could be complemented with wild type *mamE* to the same extent as the ΔR9Δ*mamE* and Δ*mamE* strains, and MamE^{P} still supported the growth of small 20nm crystals in this background (Fig. S1), suggesting that unlike Amb1002, MamE-like is not capable of cross-complementing protease activity. Together, these data suggest that MamE's putative protease function is not essential for initiation of biomineralization.

MamE's protease activity is required for a novel crystal size transition step

The above results suggest that the protease activity of MamE is required for continued growth of magnetite crystals beyond the 16-20 nm size range. The results could also be consistent with a delay in the initiation of biomineralization rather than a change in the kinetics of crystal growth. To distinguish between these two models, we examined the development of the magnetic phenotype and biomineralization of magnetite over time. Briefly, we passaged strains carrying different versions of *mamE* in the absence of iron until no electron-dense structures were detectable by TEM. Cultures were then moved to iron-containing medium, and their optical densities and Cmag values were monitored over time. As expected, cells expressing only MamE^{P} do not become magnetic (Fig. 4A).

To visualize biomineralization by TEM, time points were chosen to cover early events: (1) before any strain becomes magnetic; (2) the point at which the wild type strain becomes magnetic; and (3) late time points after both strains have been growing in iron for some time. After one hour in iron-containing media, the earliest point in our time course, both strains had produced electron-dense structures of similar size and shape, suggesting that at the time resolution of our experiments, MamE^{P} was not defective in initiation of biomineralization (Figs. 4B and 5). After two hours, TEM showed large crystals in the wild type cells, whereas MamE^{P} showed only small electron-dense structures. In the presence of MamE^{P}, cells were never able to build large crystals, confirming that its crystals are arrested at the 16-20 nm growth stage and suggesting that the protease function of MamE is not required for initiation of biomineralization but for a potential novel crystal size transition step. It should, however, be noted that a small number of crystals (~3%) seem to escape this 16-20 nm arrest and attain fixed single domain sizes.

MamE's putative heme-binding motifs are required for wild type biomineralization

Unlike most other Deg family proteases, MamE is predicted to have additional functional domains. Specifically, MamE contains two putative CXXCH heme-binding motifs (Fig. 1C), which in *c*-type cytochromes are known to bind heme covalently via thioether bonds formed through the two conserved cysteines (21). To determine whether MamE's CXXCH motifs are required for magnetosome formation, we used site-directed mutagenesis to change the conserved cysteine residues of these motifs to alanines. This construct, *mamE*^{C2}, can only partially complement magnetite formation in the ΔR9Δ*mamE* strain (Fig. 1D), restoring a Cmag of 1.14±0.03 as opposed to 1.84±0.05 when complemented with wild type *mamE*. This suggests a role for MamE's putative heme-binding motifs in crystal formation.

TEM analysis revealed that this mutant formed large, wild type-sized crystals. However, complementation with *mamE*^{C2} yielded only ~30% of crystals larger than 35 nm, compared to 82% when the ΔR9Δ*mamE* strain was complemented with wild type *mamE*. The crystal size distribution of *mamE*^{C2} was shifted to smaller crystal sizes with a bimodal crystal size distribution centered at 36-40 nm and 16-20 nm (Fig. 2). The 16-20 nm peak observed in this strain clearly overlapped with the crystal size distribution of *mamE*^{P}. Additionally, HRTEM and EDX spectroscopy confirmed that the 16-20 nm crystals in the *mamE*^{C2} complemented strain are of similar composition to those found in the *mamE*^{P} complemented strain (data not shown). Interestingly, in time course experiments, *mamE*^{C2} was always delayed in the onset of its magnetic response as compared to wild type *mamE* (Fig. 4A), even though growth rates of these strains were not significantly different (data not shown). TEM analysis showed that like *mamE*^{P}, *mamE*^{C2} does not show obvious defects in the early steps of biomineralization leading to 20 nm crystals (Figs. 4B and 5). Instead, MamE^{C2}'s decreased number of large magnetite crystals is due to a defect in the post 20 nm steps of biomineralization.

This suggests that these 20 nm crystals may be an early intermediate in magnetite biomineralization and further supports the hypothesis that MamE is required for the transition from 20 nm crystals to larger crystals that can contribute to a cell's magnetic response.

MamE is a bifunctional protein with roles in protein sorting and biomineralization

The absence of crystals in the Δ*mamE* strain had previously been attributed to a defect in magnetosome protein sorting as two soluble magnetosome proteins, MamA and MamJ, were mislocalized in this mutant strain (13). To determine whether this defect extends to integral magnetosome membrane proteins, we generated C-terminal GFP fusions to MamC and MamF using a ten-glycine linker, as described by Lang *et al.* (22). We also assayed localization of GFP-MamI (13). All three proteins form linear structures in wild type AMB-1 that are reminiscent of the localization of the magnetosome chain. This pattern is disrupted in the ΔR9Δ*mamE* (Fig. 6A) and Δ*mamE* strains (data not shown). Several localization patterns were observed for the GFP constructs in these deletion backgrounds, ranging from one or multiple foci to evenly distributed membrane localization. This suggests that MamE is required for the proper localization of not only soluble but also membrane-bound magnetosome proteins. It thus seemed likely that MamE's protease function is responsible for magnetosome protein sorting. To test this hypothesis, localization of MamC-GFP and GFP-MamI were assessed in the ΔR9Δ*mamE* strain complemented by wild type *mamE*, $mamE^{P}$, or $mamE^{C2}$. Wild type MamE complemented both the magnetic response (Cmag) and protein localization in ΔR9Δ*mamE* (Fig. 6B). To our surprise, $MamE^{P}$, which cannot restore a magnetic response in the ΔR9Δ*mamE* strain, could complement the protein localization defect. Similar levels of restoration of protein localization were also observed for the strain complemented with $mamE^{C2}$ (Fig. 6B). This suggests that MamE is a bifunctional protein with independent roles in protein sorting to the magnetosome and in biomineralization.

Discussion

To date, most molecular studies of magnetosome formation have focused on identifying magnetosome-associated proteins and determining the phenotypes of deletion or disruption mutants (7, 8, 23-25). These studies have been powerful in providing a list of suspects involved in this intricate process and have laid the foundations for more detailed mechanistic studies. In this work, we have used a mutational dissection of the DegP/HtrA family protease MamE to show that this protein acts at two functionally distinct steps of magnetosome formation. First, MamE is required for proper magnetosome protein sorting. This role does not require MamE protease activity, and proper sorting of magnetosome proteins is not sufficient to produce large magnetic minerals. Since localization of magnetosome proteins does not require MamE protease activity, it could be accomplished through physical interaction of MamE with one or more magnetosome proteins at the magnetosome. Alternatively, it may be mediated

by a chaperone-like activity of MamE, which has been attributed to some DegP/HtrA proteins and is separable from their protease activity (26, 27). Once magnetosome proteins are correctly localized, MamE's protease activity is required for its second role in magnetosome formation, the maturation of small, 20 nm crystals into larger single-domain crystals with fixed dipole moments.

We also show that MamO, a second HtrA/DegP family protease encoded by the MAI, likely has protease activity *in vivo.* Constructs of MamO in which all putative active site triad residues of the protease domain are mutated to alanines cannot restore a magnetic phenotype to the ΔR9Δ*mamO* strain. MamO, however, has a threonine in the position of the conserved active site serine residue. This threonine can be changed to an alanine without reduction of MamO's ability to complement ΔR9Δ*mamO*(Fig. S1). A single point mutation of the putative active site histidine, however, decreased MamO activity, a phenotype that would be expected if this residue were part of the serine protease active site triad (Fig. S1). Further biochemical characterization is required to determine conclusively whether MamE and MamO possess protease activity and if so, what their substrates might be.

Canonical DegP/HtrA proteases consist of a protease domain coupled to one or multiple PDZ domains (14, 15). Strikingly, MamE and MamO have additional functional domains and we show these domains to be important for their function. MamO contains a seven transmembrane spanning domain of unknown function (DUF81). MamO's paralogue, Amb1004, is identical to MamO except that it lacks the DUF81 domain (Fig. 1C). Previous proteomic work has suggested that Amb1004 is expressed in wild-type cells (8). We show that Amb1004 can cross-complement the protease function of MamO when only a protease-inactive version of MamO is expressed in AMB-1. Thus, if Amb1004 is expressed in the Δ*mamO* strain, as it is in wild-type cells and in the protease inactive *mamO* complemented ΔR9Δ*mamO* strain, the non-magnetic phenotype of Δ*mamO* can be attributed to the lack of a DUF81 domain in Amb1004. This is consistent with the inability of *mamO* lacking DUF81 to complement a *mamO* disruption strain in *Magnetospirillum gryphiswaldense* MSR-1, a species that only contains one copy of *mamO* (17, 28, 29). The function of the DUF81 domain remains mysterious. While it has been suggested to function as an anion transporter in some systems, direct experimental evidence for such an activity is lacking. Alternatively, it is possible that this portion of MamO acts as a localization determinant to bring the protein to the magnetosome.

Similar to MamO, MamE is an unusal HtrA/DegP family protease, in that it also has additional functional domains, two putative CXXCH heme-binding motifs. These motifs are known to bind heme covalently via thioether bonds between the cysteines of the CXXCH motif and the heme vinyl group, and are most commonly associated with *c*-type cytochromes (21). *c*-type cytochromes have been shown to function in the oxidation and reduction of metals (30) and to act as gas sensors (31). MamE could thus act in the reduction and/or oxidation of iron required for magnetite formation. However, MamE cannot be the sole player in this role, since the heme-binding mutant is still capable of biomineralization of mature magnetite crystals. Alternatively, it is possible that MamE's CXXCH

domains are regulatory in nature. If so, this regulation does not seem to be at the level of oxygen sensing, as the heme-binding mutant's biomineralization in response to varying oxygen levels resembles the wild type response (data not shown). Interestingly, two other magnetosome proteins implicated in biomineralization, MamP and MamT, also have CXXCH motifs, raising the possibility that a network of redox activity may be at the center of magnetite biomineralization. Another possible function for the CXXCH motifs is that they could modulate MamE's protease activity. Time course experiments showed that although *mamE*^{C2} is capable of synthesizing large fixed single-domain magnetite crystals, it is delayed or slowed in this process and forms a significant number of small 20 nm crystals similar to those found in *mamE*^{P}. This similarity in phenotype to *mamE*^{P} suggests that MamE's CXXCH motifs may serve to activate or enhance proteolysis required for crystal size transition.

While it is clear that protease activity of MamE is linked to a specific step of biomineralization, the mechanisms by which this is achieved remain mysterious. One could envision that once a crystal has reached the 20 nm transition point, MamE degrades one or several inhibitors of biomineralization (Fig. 7A), or proteolytically activates proteins essential for further crystal growth (Fig. 7B). If proteolysis by MamE activates biomineralization factors, then these should be proteins that act in the post-nucleation steps of biomineralization and their deletion phenotypes should be similar to that of the MamE protease mutant. Thus, possible substrates of MamE, based on our current knowledge of biomineralization, could include MamS, MamR, MamT and the proteins encoded by the R2 and R3 genomic regions, which include the *mms6* and *mamCDFG* gene clusters (10, 12, 13). Inhibitors of crystal size transition would have eluded identification by methods currently used to screen biomineralization mutants, since their deletion or disruption would presumably lead to larger magnetite crystals, a phenotype that likely would not have caused a noticeable difference in the cells' magnetic response. Interestingly, MamE and MamO are not the only examples of serine proteases essential for biomineralization. Enamel proteases have long been known for their role in tooth formation, where they act to remove an organic matrix from nucleated enamel crystallites allowing for growth of the crystallites into mature-sized enamel (32). Additionally, some serine proteases are capable of precipitating metal oxides *in vitro*, raising the intriguing possibility that MamE or MamO could play a direct role in formation of iron oxide crystals (33). Thus, identification of MamE and MamO's substrates may shed light on the potential similarities between the biomineralization pathways of magnetotactic bacteria and those found in other organisms.

The work presented here helps define the functional relevance of MamE and MamO in more detail. More significantly, our results may also have uncovered a previously unrecognized checkpoint step in magnetite biomineralization. When the protease-deficient version of MamE is the sole copy of this protein in the cell, initiation of biomineralization occurs in a timely fashion and crystal growth kinetics are similar to those of wild-type cells until a size of 16-20 nm is reached. At this point the protease activity of MamE is required to develop mature crystals of magnetite. It should, however, be noted that ~3% of crystals can escape this

block in crystal growth, a number too small to generate cells with a permanent magnetic dipole moment.

What would be the potential selective advantage of such a decision making step during biomineralization in wild type cells? The transition from small superparamagnetic crystals to larger single domain crystals is an important decision point for the bacterium, one that will trap the cell in a forced biased swim guided by the geomagnetic field, leaving it to use magnetoaerotaxis as its sole mode of exploring the environment. Thus, if MamE's protease activity could be modulated, cells could arrest biomineralization at the 20 nm stage and be primed for the formation of larger crystals without committing themselves to magnetoaerotaxis. When desirable conditions are reached, biomineralization could be resumed by simply activating MamE protease activity. Such a system would allow cells to align with the earth's magnetic field lines when favorable without being committed to a forced directional swim under all environmental conditions. In addition, the two-fold increase in the diameter of the crystal represents an approximately eight-fold increase in its volume, meaning that significant resources must be dedicated to build a magnetosome chain after this transition point. MamE's protease activity could integrate the availability of iron with the need to maximize the production of large single domain crystals. While it remains to be determined whether MamE's protease activity can be modulated, potentially via its putative heme-binding motifs, the findings presented help to inform future work on the molecular mechanisms of magnetosome biogenesis and magnetite biomineralization.

Materials and Methods

Growth conditions

Cells were grown in MG media supplemented with both Wolfe's Vitamin Solution and 3mM iron chloride 9mM malate at 1/100 (13). Additional iron sources were omitted when preparing Wolfe's Mineral Solution. For fluorescence microscopy cells were grown in 10ml of MG with 10ml of head space in a microaerobic chamber kept at 30C and less than 10% oxygen. To assay complementation and to measure crystal size distributions cells were grown in a 30C incubator in sealed Balch tubes containing 10ml of MG and 20ml headspace. Balch tubes were flushed briefly after autoclaving and for 10min after addition of iron and vitamins before cells were added. No additional air was added to the tubes. For timecourse experiments cells were grown in Balch tubes as just described but the volume increased to 15ml. For these experiments all glassware was soaked in oxalic acid for 24h before use, cells were passaged twice in MG containing no iron until the cultures were non-magnetic and no crystals or inclusions were observable by TEM. Antibiotics were used at the following concentrations: kanamycin 15uM on plates, 10uM in liquid, 7uM in liquid when plasmid was integrated on the chromosome. carbenicillin 20uM on plate and in liquid.

Plasmids, Primers and Strains
Primers, plasmids and strains used in this study are listed in supporting information tables 1 and 2 and 3.

Timecourse experiments
For timecourse experiments cells were passaged twice in 10ml of MG medium containing no iron in 20ml tubes incubated in a microaerophillic chamber. Cells in exponential phase were then passaged into 15ml MG plus iron malate in Balch tubes and their increase in Cmag was monitored. To follow crystal growth, cells were collected by filtration, washed in PBS and fixed in .25% gluteraldehyde for TEM analysis. Crystal size was measured by hand using GIMP software and the long axis is reported as crystal size.

Generation of ΔR9Δ*mamE*, Δ*mamO*Δ*R9* and ΔR9Δ*mamE*Δ*mamE-like*
All deletions were generated using the two-step recombination method previously described (13, 24). *mamE* and *mamO* were deleted in the ΔR9 background using the plasmids pAK241 and pAK243 described in Murat *et al* (13) To delete *mamE-like* in the ΔR9Δ*mamE* background, regions flanking the gene were amplified and combined into the deletion plasmid pAK453 by fusion PCR.

Generation of MamC-GFP and MamF-GFP
All PCR except for QuikChange® site directed mutagenesis were carried out using the Promega GoTaq® Green Master Mix. MamC was C-terminally GFP tagged by fusion PCR. MamC was amplified using a forward primer adding an EcoRI site and a reverse primer deleting the stop codon and adding 10 C-terminal Glycines as a linker. A BamHI site was placed at the end of the *mamC* sequence. GFP was amplified using a forward primer adding 10 N-terminal Glycines and a reverse primer adding a SpeI site. The MamC-BamHI-10Glycine-GFP construct was then generated by fusion PCR using the MamC forward and GFP reverse primers. This fragment was EcoRI-SpeI cloned into pAK22 to generate pAK450. To confer carbenicillin resistance the ampicillin resistance gene (*bla*) placed downstream of the *tac* promoter was isolated from pAK237 by SpeI digest and then SpeI cloned into pAK450 to generate pAK451. MamF was amplified adding an N-terminal EcoRI and a C-terminal BamHI site, deleting the STOP codon. This fragment was cloned into pAK450 to replace MamC generating pAK452.

Fluorescence microscopy
Cells were imaged in early stationary phase on 1% agarose pads using a Nikon Eclipse 80i microscope. Images were acquired with the x100 oil objective using a QImaging® RETIGA 2000R Fast 1394 camera.

Generation of *mamO* and *mamE* complementation plasmids
The previously described plasmids pAK263 and pAK250 (13) were used for wild type complementation of the *mamO* and *mamE* deletion strains respectively. To identify *mamO* and *mamE*'s putative active site residues, their amino acid

sequence was aligned to *E.coli* DegP, DegQ and DegS using ClustalW2 (34). Putative active site residues were changed to alanines using Stratagene QuikChange® mutagenesis as directed by the manufacturer. MamE's putative heme-binding domains were inactivated using the same strategy to change the two cysteines of the CXXCH domains to alanines. The *mamO* deletion strains were complemented with *mamO* on a plasmid expressed off of the *tac* promoter (pAK263) whereas *mamE* deletion strains were complemented with *mamE* expressed from its endogenous promoter by integrating *mamE* into the chromosome (pAK250) (13).

Complementation assays

Cmags were measured in cultures grown in 10ml of MG in sealed 20ml Balch tubes after two days of growth at 30°C. For *mamO* complementation, Cmags were measured in the presence of kanamycin. For *mamE* complementation, Cmags were measured in the absence of any antibiotics. Complementation of protein localization was assayed by growing complemented cells in 10ml of MG+carbenicillin in 20ml tubes in a microaerobic chamber.

TEM

400mesh copper grids (Ted Pella Inc, Redding, CA) were coated with 0.5% Formvar in ethylene dicholoride. Cells were spun down (for crystal size distribution) or collected by filtration and washed in PBS for timecourse experiments. Cells were resuspended in 20ul of MG/-Fe and adsorbed to the TEM grids. A TECNAI 12 operating at 100kV was used to analyze sample. Images were taken with a Gatan UltraScan 1000 (2k x 2k) digital camera (Pleasanton, CA).

Cryo-ultramicrotomy and EDS spectroscopy

Cryo-ultramicrotomy was performed as previously described (13, 24, 35).

References

1. Shively JM (2006) *Complex intracellular structures in prokaryotes* (Springer, Berlin) pp viii, 379 p.
2. Fuerst JA (2005) Intracellular compartmentation in planctomycetes. *Annu Rev Microbiol* 59:299-328.
3. Murat D, Byrne M, & Komeili A (2010) Cell biology of prokaryotic organelles. *Cold Spring Harb Perspect Biol* 2(10):a000422.
4. Frankel RB, Bazylinski DA, Johnson MS, & Taylor BL (1997) Magneto-aerotaxis in marine coccoid bacteria. *Biophys J* 73(2):994-1000.
5. Smith MJ*, et al.* (2006) Quantifying the magnetic advantage in magnetotaxis. *Biophys J* 91(3):1098-1107.
6. Komeili A (2007) Molecular mechanisms of magnetosome formation. *Annu Rev Biochem* 76:351-366.
7. Grunberg K*, et al.* (2004) Biochemical and proteomic analysis of the magnetosome membrane in Magnetospirillum gryphiswaldense. *Appl Environ Microbiol* 70(2):1040-1050.

8. Tanaka M*, et al.* (2006) Origin of magnetosome membrane: Proteomic analysis of magnetosome membrane and comparison with cytoplasmic membrane. *Proteomics* 6(19):5234-5247.
9. Schuler D & Frankel RB (1999) Bacterial magnetosomes: microbiology, biomineralization and biotechnological applications. *Appl Microbiol Biotechnol* 52(4):464-473.
10. Arakaki A, Webb J, & Matsunaga T (2003) A novel protein tightly bound to bacterial magnetic particles in Magnetospirillum magneticum strain AMB-1. *J Biol Chem* 278(10):8745-8750.
11. Arakaki A, Masuda F, Amemiya Y, Tanaka T, & Matsunaga T (2010) Control of the morphology and size of magnetite particles with peptides mimicking the Mms6 protein from magnetotactic bacteria. *J Colloid Interface Sci* 343(1):65-70.
12. Scheffel A, Gardes A, Grunberg K, Wanner G, & Schuler D (2008) The major magnetosome proteins MamGFDC are not essential for magnetite biomineralization in Magnetospirillum gryphiswaldense but regulate the size of magnetosome crystals. *J Bacteriol* 190(1):377-386.
13. Murat D, Quinlan A, Vali H, & Komeili A (2010) Comprehensive genetic dissection of the magnetosome gene island reveals the step-wise assembly of a prokaryotic organelle. *Proc Natl Acad Sci U S A* 107(12):5593-5598.
14. Kim DY & Kim KK (2005) Structure and function of HtrA family proteins, the key players in protein quality control. *J Biochem Mol Biol* 38(3):266-274.
15. Clausen T, Southan C, & Ehrmann M (2002) The HtrA family of proteases: implications for protein composition and cell fate. *Mol Cell* 10(3):443-455.
16. Schuhmann H, Huesgen PF, Gietl C, & Adamska I (2008) The DEG15 serine protease cleaves peroxisomal targeting signal 2-containing proteins in Arabidopsis. *Plant Physiol* 148(4):1847-1856.
17. Yang W*, et al.* (2010) mamO and mamE genes are essential for magnetosome crystal biomineralization in Magnetospirillum gryphiswaldense MSR-1. *Res Microbiol* 161(8):701-705.
18. Schuler D, Rainer U, & Bauerlein E (1995) A Simple Light-Scattering Method to Assay Magnetism in Magnetospirillum Gryphiswaldense. *Fems Microbiol Lett* 132(1-2):139-145.
19. Butler RF & Banerjee SK (1975) Theoretical Single-Domain Grain-Size Range in Magnetite and Titanomagnetite. *J Geophys Res* 80(29):4049-4058.
20. Rioux JB*, et al.* (2010) A Second Actin-Like MamK Protein in Magnetospirillum magneticum AMB-1 Encoded Outside the Genomic Magnetosome Island. *Plos One* 5(2):-.
21. Bowman SEJ & Bren KL (2008) The chemistry and biochemistry of heme c: functional bases for covalent attachment. *Nat Prod Rep* 25(6):1118-1130.

22. Lang C & Schuler D (2008) Expression of green fluorescent protein fused to magnetosome proteins in microaerophilic magnetotactic bacteria. *Appl Environ Microbiol* 74(15):4944-4953.
23. Fukuda Y, Okamura Y, Takeyama H, & Matsunaga T (2006) Dynamic analysis of a genomic island in Magnetospirillum sp. strain AMB-1 reveals how magnetosome synthesis developed. *FEBS Lett* 580(3):801-812.
24. Komeili A, Vali H, Beveridge TJ, & Newman DK (2004) Magnetosome vesicles are present before magnetite formation, and MamA is required for their activation. *Proc Natl Acad Sci U S A* 101(11):3839-3844.
25. Okuda Y, Denda K, & Fukumori Y (1996) Cloning and sequencing of a gene encoding a new member of the tetratricopeptide protein family from magnetosomes of Magnetospirillum magnetotacticum. *Gene* 171(1):99-102.
26. Spiess C, Beil A, & Ehrmann M (1999) A temperature-dependent switch from chaperone to protease in a widely conserved heat shock protein. *Cell* 97(3):339-347.
27. Rizzitello AE, Harper JR, & Silhavy TJ (2001) Genetic evidence for parallel pathways of chaperone activity in the periplasm of Escherichia coli. *Journal of Bacteriology* 183(23):6794-6800.
28. Mampel J*, et al.* (2004) A novel outer-membrane anion channel (porin) as part of a putatively two-component transport system for 4-toluenesulphonate in Comamonas testosteroni T-2. *Biochem J* 383:91-99.
29. Weinitschke S, Denger K, Cook AM, & Smits THM (2007) The DUF81 protein TauE in Cupriavidus necator H16, a sulfite exporter in the metabolism of C-2 sulfonates. *Microbiol-Sgm* 153:3055-3060.
30. Paquete CM & Louro RO (2010) Molecular details of multielectron transfer: the case of multiheme cytochromes from metal respiring organisms. *Dalton Trans* 39(18):4259-4266.
31. Takayama Y*, et al.* (2006) Specific binding of CO to tetraheme cytochrome c(3). *Biochemistry-Us* 45(10):3163-3169.
32. Bartlett JD & Simmer JP (1999) Proteinases in developing dental enamel. *Crit Rev Oral Biol Med* 10(4):425-441.
33. Smith GP, Baustian KJ, Ackerson CJ, & Feldheim DL (2009) Metal oxide formation by serine and cysteine proteases. *J Mater Chem* 19(44):8299-8306.
34. Chenna R*, et al.* (2003) Multiple sequence alignment with the Clustal series of programs. *Nucleic Acids Res* 31(13):3497-3500.
35. Byrne ME*, et al.* (2010) Desulfovibrio magneticus RS-1 contains an iron- and phosphorus-rich organelle distinct from its bullet-shaped magnetosomes. *Proc Natl Acad Sci U S A* 107(27):12263-12268.
36. Jomaa A, Iwanczyk J, Tran J, & Ortega J (2009) Characterization of the autocleavage process of the Escherichia coli HtrA protein: implications for its physiological role. *J Bacteriol* 191(6):1924-1932.

A

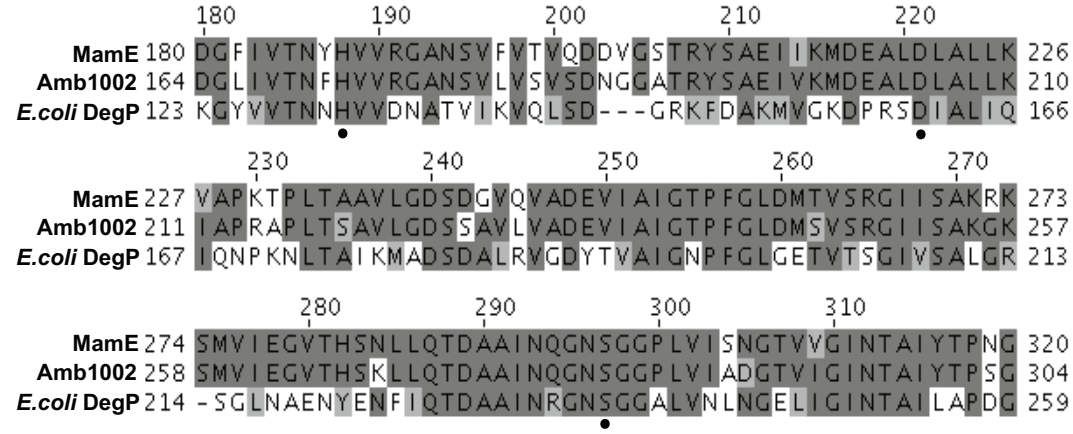
180 190 200 210 220
MamE 180 DGFIVTNYHVVRGANSVFVTVQDDVGSTRYSAEIIKMDEALDLALLK 226
Amb1002 164 DGLIVTNFHVVRGANSVLVSVSDNGGATRYSAEIVKMDEALDLALLK 210
E.coli DegP 123 KGYVVTNNHVVDNATVIKVQLSD---GRKFDAKMVGKDPRSDIALIQ 166
230 240 250 260 270
MamE 227 VAPKTPLTAAVLGDSDGVQVADEVIAIGTPFGLDMTVSRGIISAKRK 273
Amb1002 211 IAPRAPLTSAVLGDSSAVLVADEVIAIGTPFGLDMSVSRGIISAKGK 257
E.coli DegP 167 IQNPKNLTAIKMADSDALRVGDYTVAIGNPFGLGETVTSGIVSALGR 213
280 290 300 310
MamE 274 SMVIEGVTHSNLLQTDAAINQGNSGGPLVISNGTVVGINTAIYTPNG 320
Amb1002 258 SMVIEGVTHSKLLQTDAAINQGNSGGPLVIADGTVIGINTAIYTPSG 304
E.coli DegP 214 -SGLNAENYENFIQTDAAINRGNSGGALVNLNGELIGINTAILAPDG 259

B

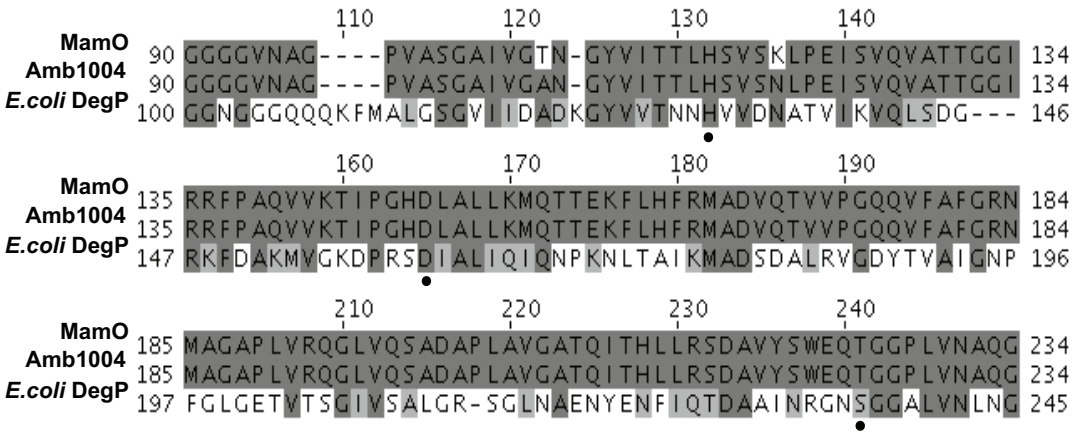
110 120 130 140
MamO 90 GGGGVNAG----PVASGAIVGTN-GYVITTLHSVSKLPEISVQVATTGGI 134
Amb1004 90 GGGGVNAG----PVASGAIVGAN-GYVITTLHSVSNLPEISVQVATTGGI 134
E.coli DegP 100 GGNGGGQQQKFMALGSGVIIDADKGYVVTNNHVVDNATVIKVQLSDG--- 146
160 170 180 190
MamO 135 RRFPAQVVKTIPGHDLALLKMQTTEKFLHFRMADVQTVVPGQQVFAFGRN 184
Amb1004 135 RRFPAQVVKTIPGHDLALLKMQTTEKFLHFRMADVQTVVPGQQVFAFGRN 184
E.coli DegP 147 RKFDAKMVGKDPRSDIALIQIQNPKNLTAIKMADSDALRVGDYTVAIGNP 196
210 220 230 240
MamO 185 MAGAPLVRQGLVQSADAPLAVGATQITHLLRSDAVYSWEQTGGPLVNAQG 234
Amb1004 185 MAGAPLVRQGLVQSADAPLAVGATQITHLLRSDAVYSWEQTGGPLVNAQG 234
E.coli DegP 197 FGLGETVTSGIVSALGR-SGLNAENYENFIQTDAAINRGNSGGALVNLNG 245

C

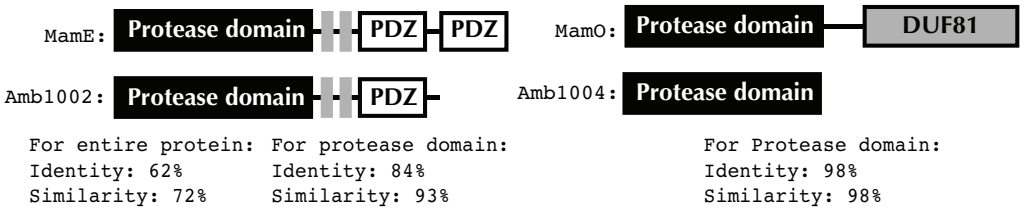

For entire protein:
Identity: 62%
Similarity: 72%

For protease domain:
Identity: 84%
Similarity: 93%

For Protease domain:
Identity: 98%
Similarity: 98%

D

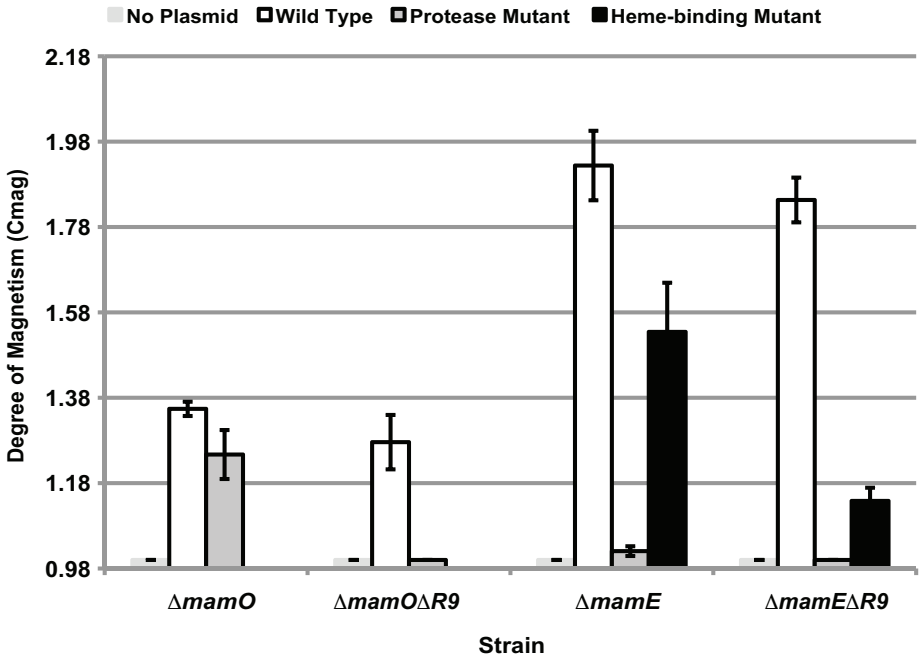

Figure 1: Dependence of AMB-1 magnetic response (Cmag) on MamE and MamO protease activity.
A. Alignments of MamE and Amb1002 protease domains with *E.coli* DegP.
B. Alignments of MamO and Amb1004 protease domains with E. *coli* DegP. Active site triad residues of MamE and MamO, indicated by black dots, were identified based on homology with DegP. Identical residues are highlighted in dark grey and conserved substitutions in light grey.
C. Domain architecture of MamE, Amb1002, MamO and Amb1004. For MamE and Amb1002, identity for both the entire protein and for just the protease domains are shown. For MamO identity over protease domain of MamO and Amb1004 is shown.
D. Complementation of magnetic response of the single and double *mamO* and *mamE* deletion strains with wild type and protease inactive constructs. For MamE complementation by the heme-binding deficient construct is also shown. Error bars represent one standard deviation.

A

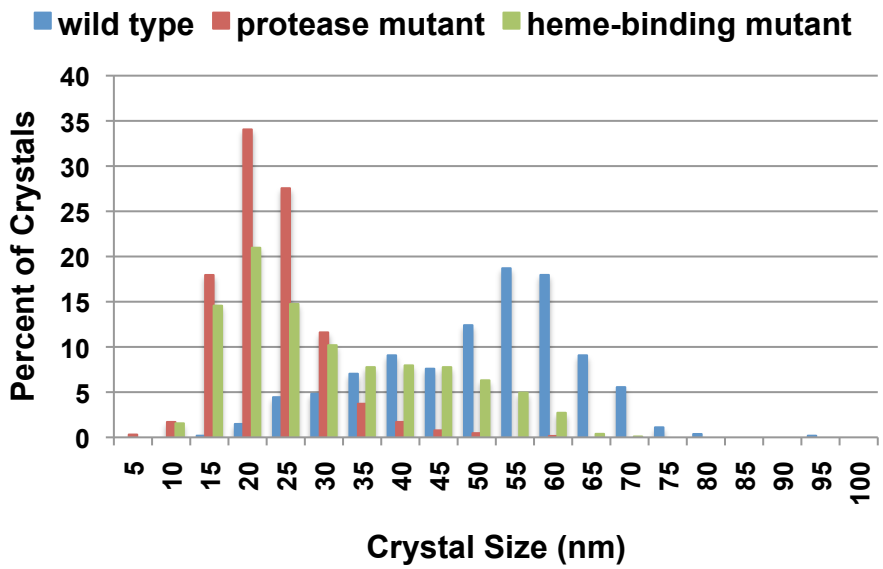

B

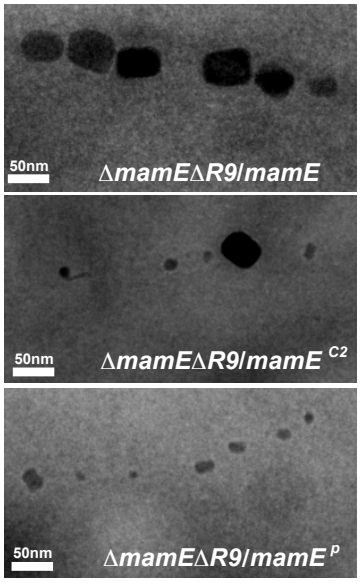

Figure 2: MamE protease domain is essential for crystal maturation.
A. Crystal size distribution of ΔR9Δ*mamE* complemented with wild type, protease inactive, and heme-binding deficient *mamE*. Crystal size is plotted as the percent of the total number of crystals that fall into each 5nm bin. n>500 crystals from several cultures of each strain.
B. Representative TEM images of crystals for each of the three complemented strains.

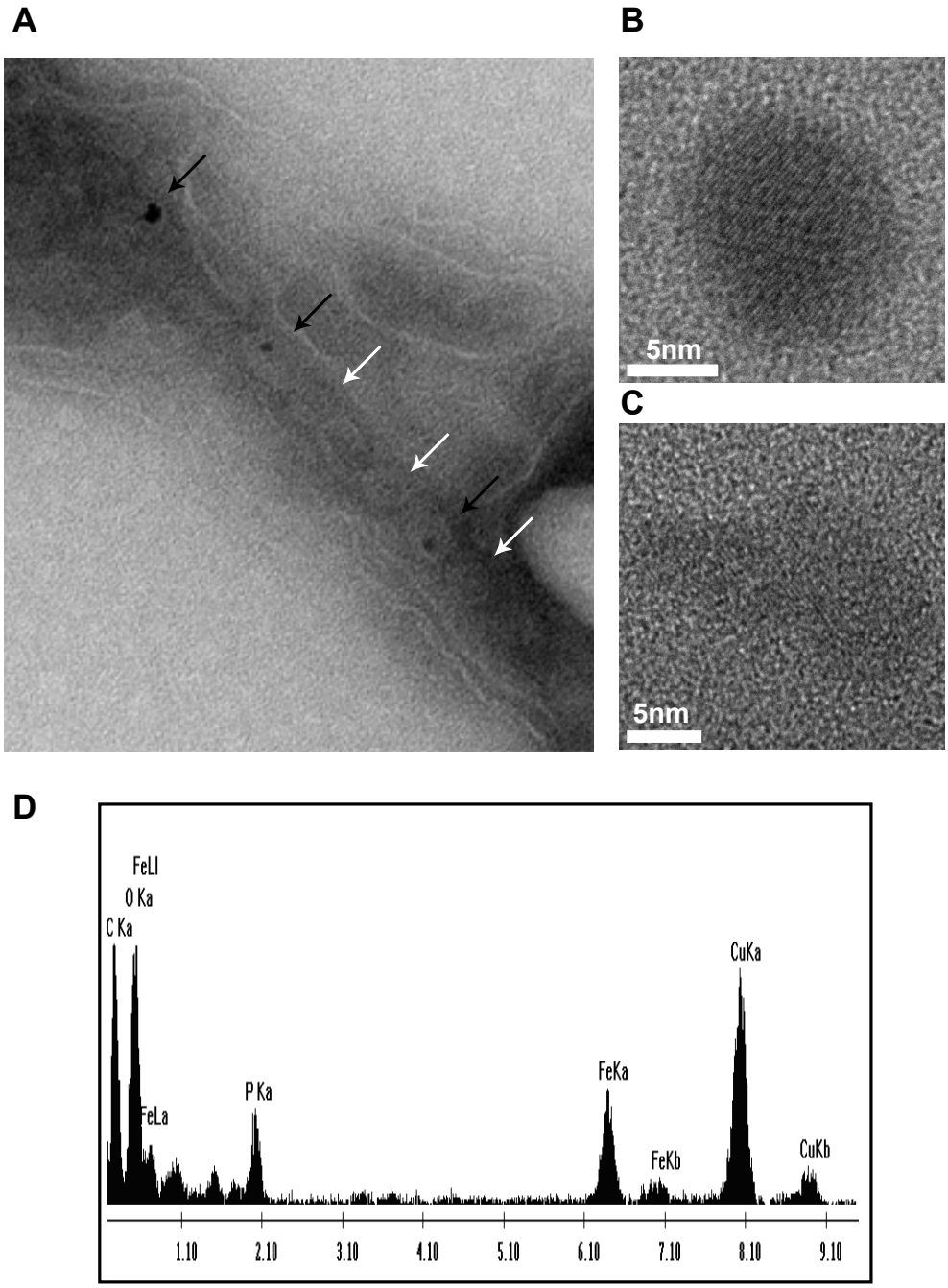

Figure 3: MamE protease mutant 20nm structures are crystalline.
A. Representative TEM image of a cryo-sectioned ΔR9Δ*mamE* cell complemented with the MamE protease mutant showing that the small 20nm inclusions grow within mature-sized magnetosome membranes.
B. HRTEM shows that 20nm electron dense structures formed by the protease mutant are crystalline.
C. Even amorphous electron-dense structures are crystalline.
D. EDS spectra show iron and oxygen peaks consistent with the presence of magnetite. Copper signal is due to copper grids, and phosphorous and carbon peaks from media/cells.

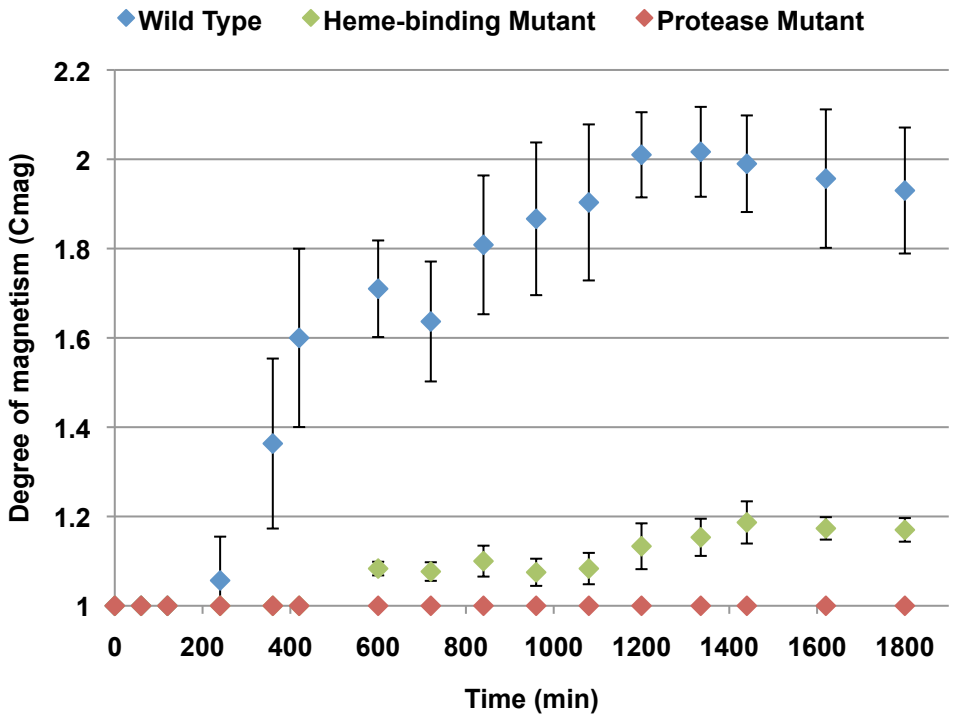

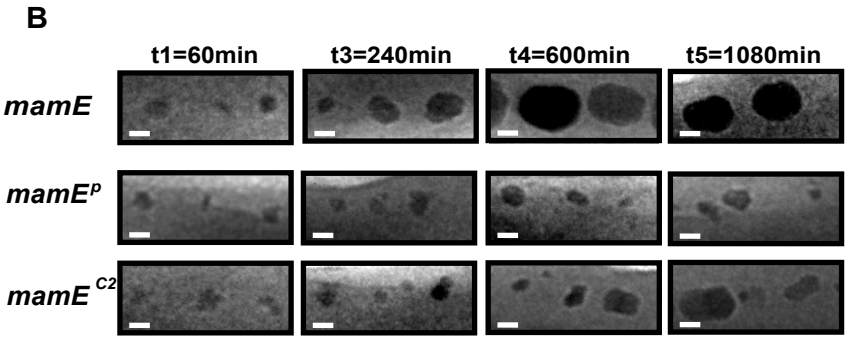

Figure 4: Time course experiments show protease and heme-binding mutants are not defective in early steps of biomineralization. A. Time course of increase in magnetic response of complemented strains. Cells were passaged in the absence of iron until no electron dense structures were visible by TEM, at which point they were passaged into iron containing media. The protease mutant never becomes magnetic whereas the heme-binding mutant does but is always delayed in the onset of its magnetic response as compared to wild type complemented ΔR9Δ*mamE*. Error bars represent one standard deviation of three separate cultures. Arrows indicated points at which cells were fixed for TEM imaging.
B. Representative TEM images of electron dense inclusions made by wild type complemented, protease mutant complemented and heme-binding mutant complemented ΔR9Δ*mamE*. At the earliest time point, 1h, all three strain are making similar-sized electron dense inclusions.

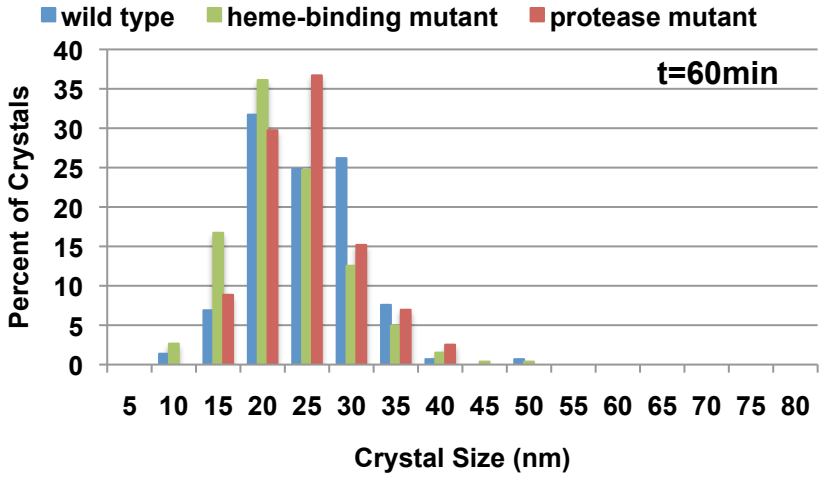
wild type
heme-binding mutant
protease mutant
t=60min
Percent of Crystals
0
5
10
15
20
25
30
35
40
5 10 15 20 25 30 35 40 45 50 55 60 65 70 75 80
Crystal Size (nm)

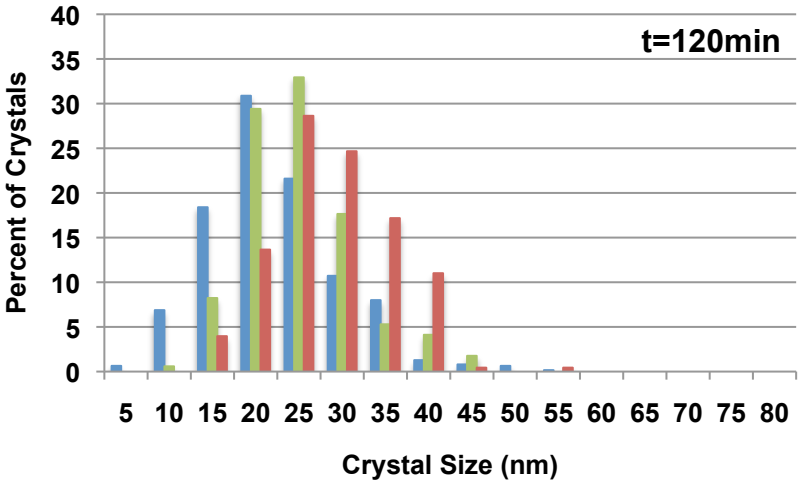
t=120min
Percent of Crystals
0
5
10
15
20
25
30
35
40
5 10 15 20 25 30 35 40 45 50 55 60 65 70 75 80
Crystal Size (nm)

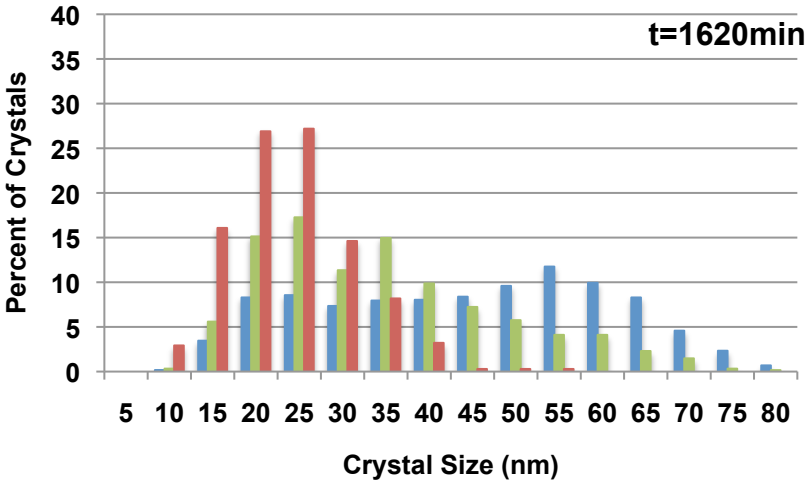
t=1620min
Percent of Crystals
0
5
10
15
20
25
30
35
40
5 10 15 20 25 30 35 40 45 50 55 60 65 70 75 80
Crystal Size (nm)

Figure 5: Crystal size distributions of complemented strains during time course. At early time points, one hour or two hours after addition of iron all three strains are behaving similarly. Only at later time points do the crystal growth defects of the protease mutant and heme-binding mutant complemented strains become apparent.

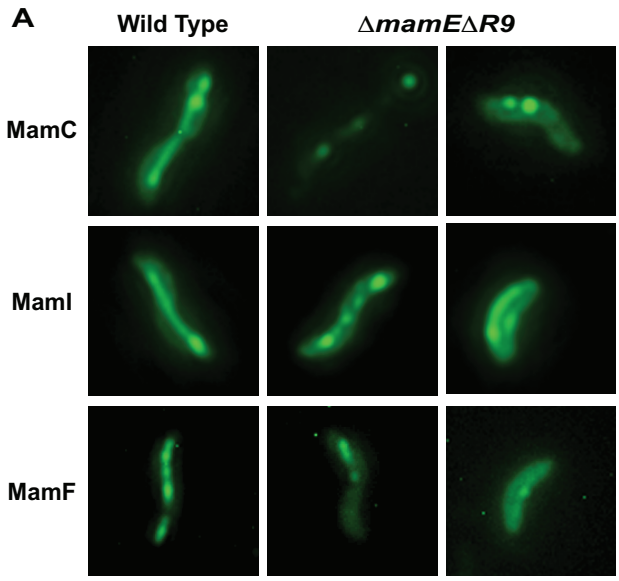

B MamC-GFP

Strain	Cmag	% linear localizatior	n
Δ*mamE*Δ*R9*	1.0+/-0	1+/-1	259
Δ*mamE*Δ*R9*/ *mamE*	1.52+/-0.07	85+/-12	400
Δ*mamE*Δ*R9*/ $mamE^{p}$	1.0+/-0	75+/-7	464
Δ*mamE*Δ*R9*/ $mamE^{C2}$	1.10+/-0.03	63+/-6	631

C GFP-MamI

Strain	Cmag	% linear localizatior	n
Δ*mamE*Δ*R9*	1.0+/-0	0+/-0	523
Δ*mamE*Δ*R9*/ *mamE*	1.5+/-0.15	82+/-8	1278
Δ*mamE*Δ*R9*/ $mamE^{p}$	1.0+/-0	73+/-10	1061
Δ*mamE*Δ*R9*/ $mamE^{C2}$	1.07+/-0.03	63+/-7	1018

Figure 6: MamE is a bifunctional protein with a protease-independent role in magnetosome protein sorting. A. Representative images of localization pattern of GFP-MamI, MamC-GFP and MamF-GFP in the wild type AMB-1 and in the ΔR9Δ*mamE* background. These constructs form linear structures reminiscent of the localization of the magnetosome chain in wild type cells that are disrupted in the absence of MamE. B. MamC-GFP localization in complemented strains. C.GFP-MamI localization in complemented strains. Magnetic response and percent of cells with linear, wild type-like linear localization patterns are reported. n is the number of cells scored for GFP localization. Error is reported as one standard deviation representative of variation between different cultures.

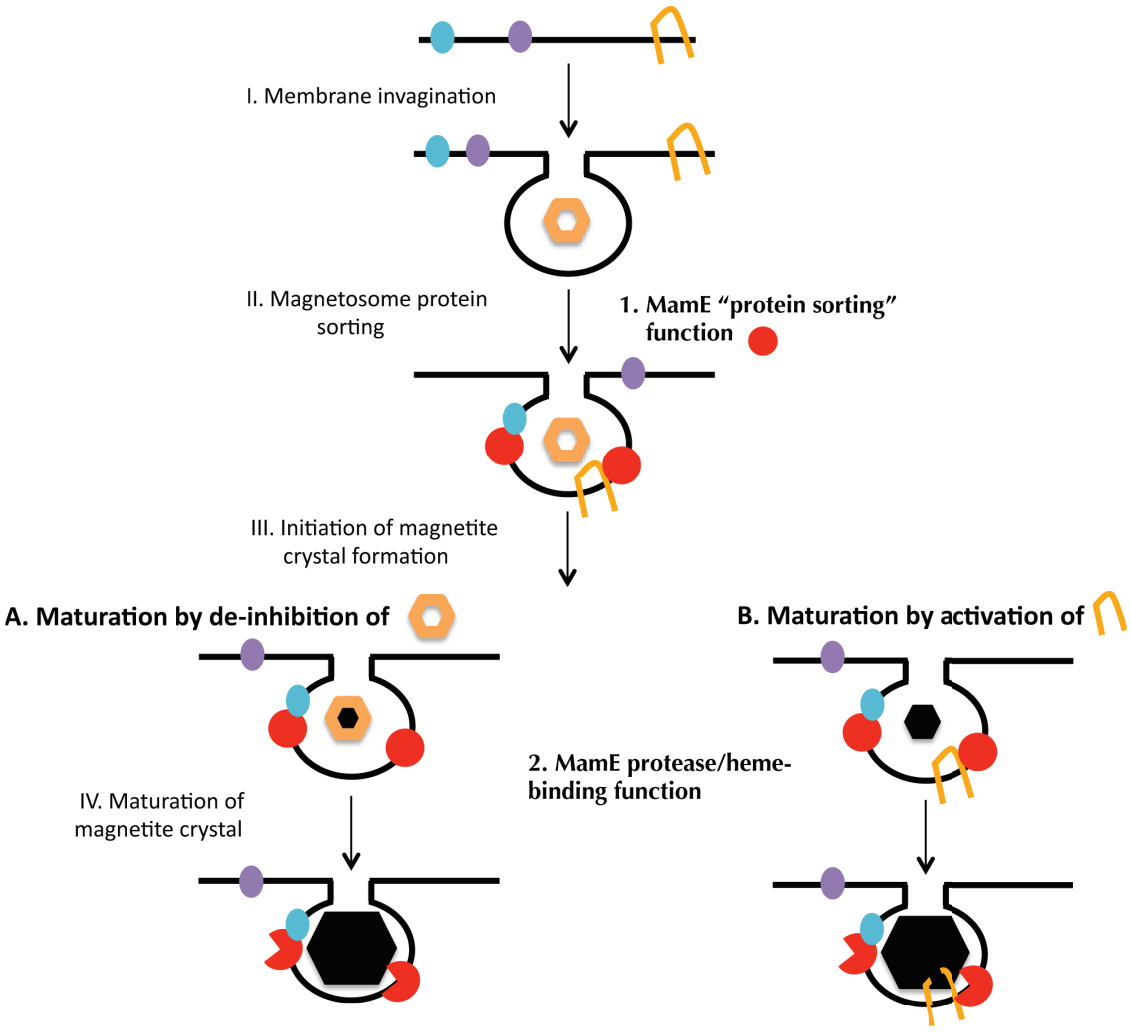

Figure 7: Model for MamE's role in magnetosome formation. After magnetosome membranes are formed MamE is required in a protease independent fashion for the proper localization of at least a subset of magnetosome proteins. This activity is sufficient for the formation of 20 nm crystals of magnetite. MamE's protease function is then required to mature these crystals into large fixed single domain crystals of magnetite. This could be achieved either by (A) proteolytically removing one or several inhibitors of magnetosome formation, or by (B) proteolytically activating one or several biomineralization promoting proteins. Blue oval: magnetosome membrane protein; purple oval: inner membrane protein; orange symbol: inhibitor or activator of biomineralization; red circle: MamE protease independent function; red pacman: MamE protease-dependent activity. I.-IV.: proposed steps in magnetosome formation.

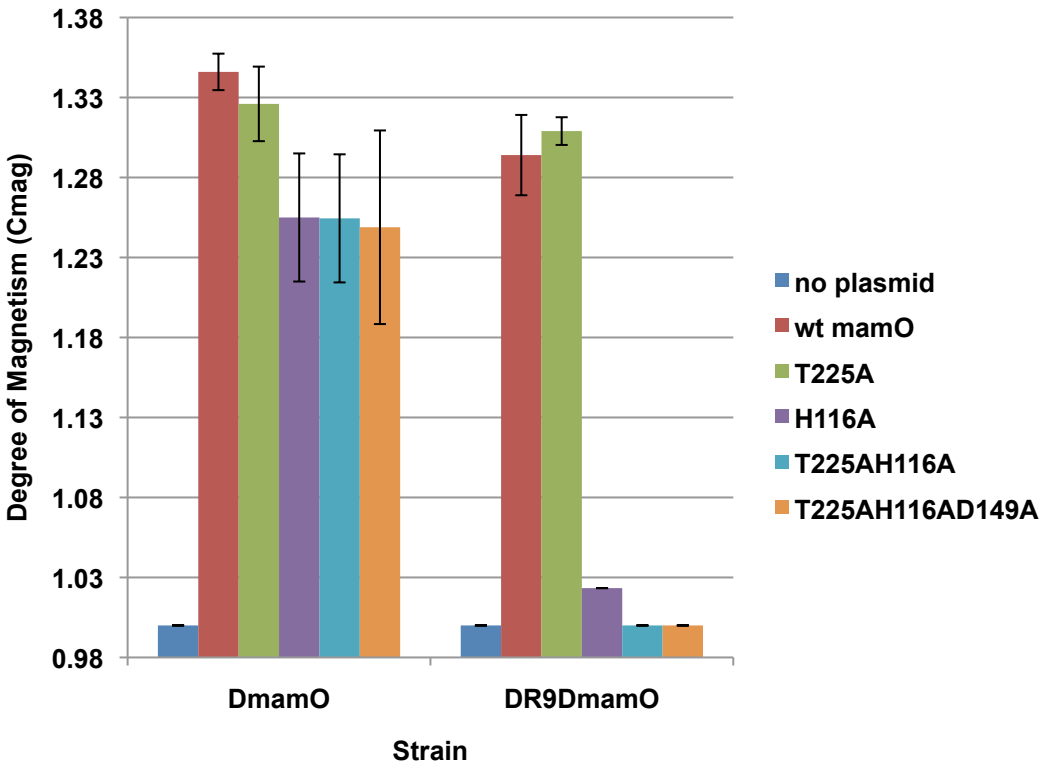

Supporting Information Figure 1: Complementation of Δ*mamO* and Δ*mamO*Δ*R9* by various protease mutants of MamO. Δ*mamO* and ΔR9Δ*mamO* were complemented with wild type MamO and MamO in which the active site threonine alone, the active site histidine alone, the active site threonine and histidine and all three active site residues were inactivated. Error bars indicated variability between individual cultures.

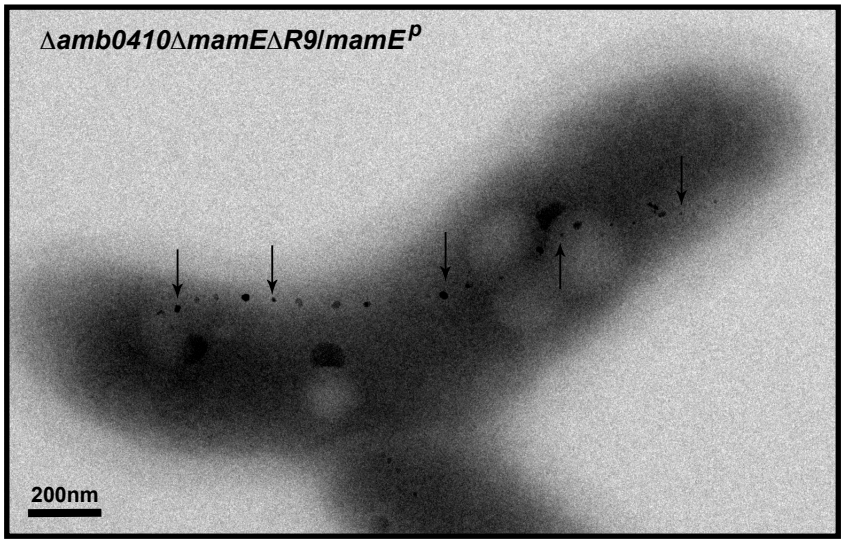

Supporting Information Figure 2: Amb0410 cannot complement MamE protease activity. The small 25nm crystals formed in the ΔR9Δ*mamE*/*mamE*^{P} strain are not do to Amb0410's protease activity as a ΔR9Δ*mamE*Δ*amb0410* triple deletion strain complemented with *mamE*^{P} still forms small electron dense structures similar in size and morphology to those formed in the ΔR9Δ*mamE*/*mamE*^{P} strain. Arrows highlight the chain of magnetite crystals.

Primer Name	Primer Sequence	Target
S297A-F2	aaccagggcaatgccggcggtccgctggtg	*mamE*
S297A-R2	caccagcggaccgccggcattgccctggtt	*mamE*
H188A-F	atcgtcaccaactatgctgtggtgcgcgg	*mamE*
H188A-R	ccgcgcaccacagcatagttggtgacgat	*mamE*
D221A-F	atggacgaggctctggctctcgccttgct	*mamE*
D221A-R	agcaaggcgagagccagagcctcgtccat	*mamE*
CXXCH1-F	atggccgccagaacatggatgccaccaccgcccacgatctgatt	*mamE*
CXXCH1-R	aatcagatcgtgggcggtggtggcatccatgttctggcggccat	*mamE*
CXXCH2-F	tcagaacatgaacgccgccaatgccaatcagatgct	*mamE*
CXXCH2-R	agcatctgatgggcattggcggcgttcatgttctga	*mamE*
T225A-F	tctacagctgggaacaggccggcggcccgctg	*mamO*
T225A-R	cagcgggccgccggcctgttcccagctgtaga	*mamO*
H116A-Fb	tgatcaccaccttggcttcggtgtccaagct	*mamO*
H116A-Rb	agcttggacaccgaagccaaggtggtgatca	*mamO*
D149A-Fc	attccggggcatgctctggcgctgctgaag	*mamO*
D149A-Rc	cttcagcagcgccagagcatgccccggaat	*mamO*
0410along	ggcactagtggtcggttcggcgtcttcctcgggccactcgaccaagaaccatt	*mamE-like*
0410b	tatttaaatttagtggatgggatctgcgctacgattgaacat	*mamE-like*
0410c	cccatccactaaatttaaatagaagtgtgggttgttctgtaa	*mamE-like*
0410dlong	ggcactagtaacggtcgtgagattttgaacgagtacagaacgttgcgatgagc	*mamE-like*
cMamC-F	ggcgaattcatgcgctcctggctgcggccggggaag	mamC
3'C10Gly-R	ggcgccgccgccgccgccgccgccgccgccgccggatccggccagtt cgtcccgcaagat	mamC
cMamF-F	ggcgaattcatggctgaggcaatcttgctcgaaacc	mamF
cMamF-R	gccggatccgatcaacgcgacgaaatagccgac	mamF
10GlyGFP-F	gccggcggcggcggcggcggcggcggcggcggcatgagtaaaggaga agaacttttt	GFP
3'GFPSpe	ggactagtctatttgtatagttcatccatg	GFP

Table S1: Primers used in this study

Plasmid name	Content
pAK439	MamES297A
pAK441	MamES297AH188AD221A
pAK445	MamEAXXAH1AXXAH2
pAK448	MamOT225AH116AD149A
pAK446	MamOT225A
pAK449	MamOH116A
pAK454	MamF10GlyGFP
pAK452	MamC10GlyGFP
pAK453	MamC10GlyGFPtacbla
pAK437	GFP-HL4MamI
pAK455	*amb0410* flanking regions for deletion

Table S2: Plasmids used in this study

Strain name	Genetic background
AK30	Wild type AMB-1
AK42	Δ*mamE*
AK34	Δ*mamO*
AL93	ΔR9Δ*mamE*
AK96	ΔR9Δ*mamE*Δ*mamE-like*
AK94	ΔR9Δ*mamO*
AK57	ΔR9

Table S3: Strains of AMB-1 used in this study

Appendix 1: MamE Self-Processing

In the hope of identifying MamE substrates, confirming MamE protease activity *in vitro* and assaying MamE for heme-binding, I generated a dual C- and N-terminally 6His tagged version of MamE for over-expression in *E.coli*. Intriguingly, I was unable to over-express wild type MamE, as assessed by Coomassie stain (Fig. A1-1). Western blotting using an anti-6His antibody showed expression of smaller, possibly processed, versions of MamE (Fig. A1-2). Accordingly, I was able to express full-length protease-inactive MamE ($MamE^{P}$) at levels detectable by Coomassie (Fig. A1-1). Western blotting revealed fewer processed products of $MamE^{P}$ (Fig. A1-2), and I was able to enrich what I believed to be the full-length version of $MamE^{P}$ over an Ni-NTA resin (Fig. A1-3). Most of the over-expressed $MamE^{P}$, however, was found in the flow-through, which may be expected for a membrane protein. For purification of MamE for biochemical analysis, it may be advisable to work with a soluble version of MamE or to attempt to detergent extract full-length MamE from the membrane before subsequent purification steps. The heme-binding mutant of MamE ($MamE^{C2}$) seemed to be processed in *E.coli* similarly to wild type MamE (Fig. A1-1 and data not shown).

These preliminary data suggest that MamE may process itself. Such activity has previously been shown for *E.coli* HtrA (36), which is believed to process itself in response to the presence of substrate peptides in order to down-regulate its activity. I have shown that MamE protease activity is not required for formation of 20nm crystals. This suggests that MamE may need to process itself for biomineralization to proceed beyond 20nm crystals. Future experiments will assess whether self-processing is also seen in AMB-1, and at what stage during magnetosome formation.

Materials and Methods

Generation of 6His-MamE-6His constructs

MamE was amplified using the forward primer nc6HisE-F adding an EcoRI site and the reverse primer nc6HisE-R adding a NotI site and deleting the stop codon. This fragment was EcoRI-NotI cloned into the pET28 vector pAK137 to generate pAK456. The protease and heme-binding mutant versions of this plasmid, pAK457 and pAK459 respectively, were generated by Quickchange mutagenesis using the primers described in the materials and methods section of Chapter 3 of this dissertation.

Expression and purification of 6His-MamE-6His constructs

pAK456, pAK457 and paK459 were transformed into BL21 *E.coli* cells. Cells were grown at 37°C, and overexpression of the His-tagged MamE constructs was induced when cells reached an OD_{600} of ~0.3 by addition of IPTG to a final concentration of 1mM. Cells were harvested by centrifugation after four hours of growth. For comparison of expression of the three constructs, cells were resuspended in a small volume of Lysis buffer (50mM NAH_2PO_4, 300mM NaCl, lysozyme, DNaseI) and incubated on ice for 30min. Protein concentration was

determined, and equal amounts of proteins were analyzed by SDS-PAGE and Western blotting. A Covance monoclonal antibody against the 6His tag was used to assess expression.

To purify MamE^{P}, one liter of *E.coli* carrying the protease mutant construct and one liter of *E.coli* carrying no plasmid were grown and induced. Cells were harvested by centrifugation and lysed by French press in 5ml of lysis buffer (50mM NaH_2PO_4, 300mM NaCl) supplemented with 10mM imidazole. Lysate was then incubated with 2ml of packed Ni-NTA resin for 2h at 4°C. The lysate-resin slurry was packed into an empty BioRad column and the flow through collected. The resin was then washed twice with 20ml of wash buffer (lysis buffer + 20mM imidazole). Protein was eluted manually using a step-wise gradient: two 5ml fractions were eluted with elution buffer 1 (lysis buffer + 50mM imidazole); three 1ml fractions eluted with elution buffer 2 (lysis buffer + 100mM imidazole); six 500ul fractions with elution buffer 3 (lysis buffer + 150mM imidazole); ten fractions with elution buffer 4 (lysis buffer + 250mM imidazole). Protein concentrations of the elution fractions were determined by Bradford Assay and fractions were loaded onto an SDS-PAGE gel for resolution.

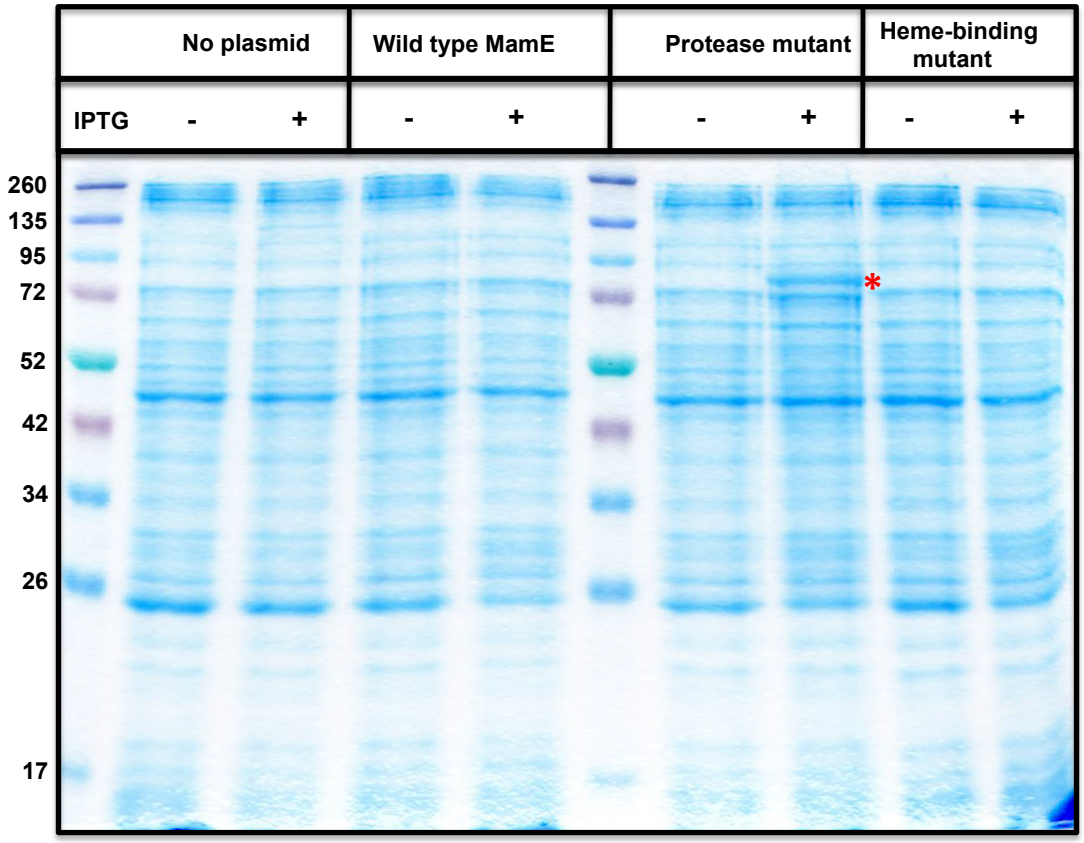

FigureA1-1: Overexpression of wild type MamE, protease mutant MamE ($MamE^{P}$) or heme-binding mutant MamE ($MamE^{C2}$) in *E.coli*. No vector control is shown in lane 2 and 3. Red asterix indicates overexpressed protein of expected size for MamE.

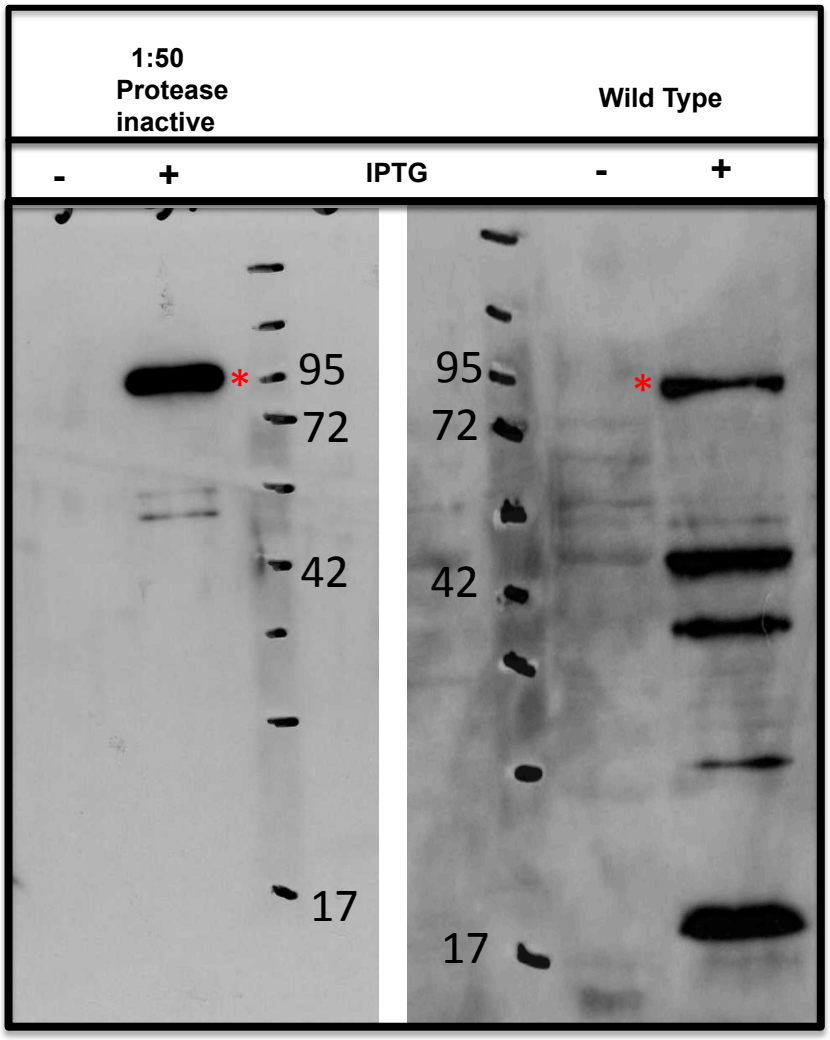

Figure A1-2: Western blot against 6His-MamE-6His using Covance monoclonal anti-6His antibody. Lane 1: uninduced 1:50 dilution of *E.coli* culture expressing protease inactive MamE. Lane 2: induced 1:50 dilution of *E.coli* culture expressing protease inactive MamE. Lane 3: Molecular weight markers. Lane 4: Molecular weight markers. Lane 5: uninduced 1:50 dilution of *E.coli* culture expressing wild type MamE. Lane 6: Induced 1:50 dilution of *E.coli* culture expressing wild type MamE.

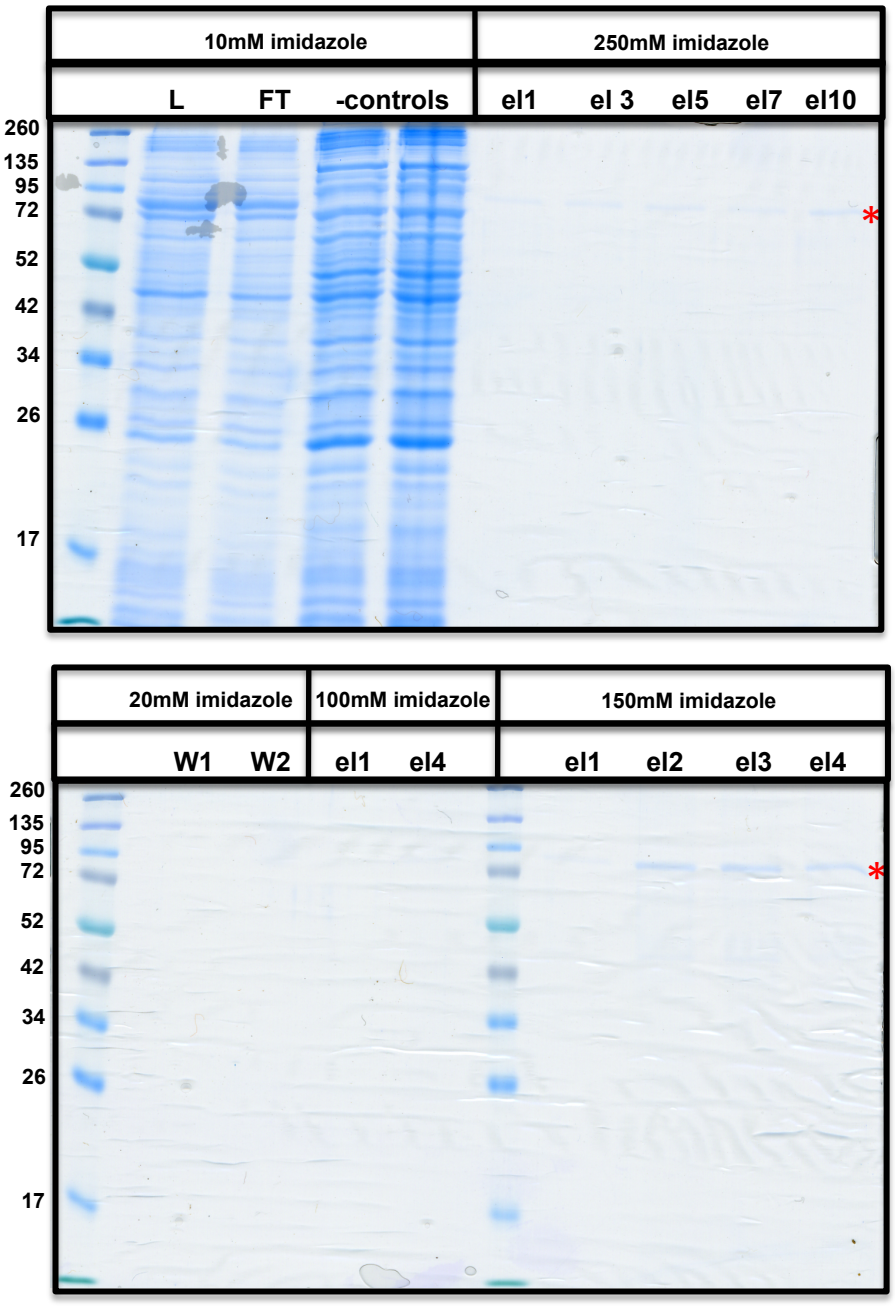

Figure A1-3: Coomassie stained SDS-PAGE gel of fractions from Ni-NTA purification of protease mutant construct of 6His-MamE^{P}-6His overexpressed in *E.coli* BL21. L: load; FT: flowthrough; - controls: no plasmid controls; W: washes; el: elution fractions.

Appendix 2: Cell Fractionation of Δ*mamO* and Δ*mamE* Strains

Since MamE and MamO are annotated as HtrA/DegP family proteases, we wanted to determine what the proteases may be processing to allow for magnetosome formation. One approach taken to answer this question was to attempt to identify proteins that are expressed only in the absence of MamE and MamO, as these proteins would be potential candidate substrates of the two proteases. No detectable differences were observed when whole lysates or soluble and insoluble fractions of Δ*mamE* and Δ*mamO* were compared to wild type AMB-1 (Fig. A2-1). Since magnetosome proteins are the likely targets of MamE and MamO activity, and these proteins are not abundant in the cell, I undertook further cell fractionation to improve my chances of observing small changes in protein expression when Δ*mamE* and Δ*mamO* were compared to wild type AMB-1. I identified one possible ~40kD band and one ~30kD band that were enriched in the membrane fraction of Δ*mamE*, not present in the ΔMAI strain and only present in smaller amounts in the wild type and Δ*mamO* strains (Fig. A2-2). This suggests that this protein may be a target of MamE proteolysis that is encoded by the MAI. This work was not repeated, and it remains to be shown that this protein is a true target of MamE proteolysis. In light of the cross-complementation observed, these types of experiments should be performed in the ΔR9Δ*mamE* and ΔR9Δ*mamO* backgrounds.

Materials and Methods

For whole-cell lysate analysis cells were grown to an OD_{400} of 0.20, and 1ml or 3ml of cell material was loaded per well. To separate the soluble and insoluble fractions cells were lysed in 1ml lysis buffer (20mM HEPES pH7.5; 25mM NaCl; 0.5mM EDTA; 20ug/ml lysozyme; 25ug/ml DNaseI; 14.1mM BME; 1mM PMSF) for 10 minutes after three rounds of freeze-thaw in liquid nitrogen. Lysate was then sonicated at 30% output power in two-second bursts for a total of 10 seconds of sonication. The insoluble fraction was then isolated by centrifugation for 1h at 32 000rpm in a SW60 rotor at 4°C. The supernatant was removed, and the pellet resuspended in 0.5% sarkosyl, 10mM TrisCl pH8.0.

For cell fractionation, 100ml of cells were grown to an OD_{400} of .20. The pellet was resuspended in 0.5ml of periplasting buffer (20% sucrose; 1mM EDTA; 20ug/ml lysozyme) and incubated on ice for 20 minutes. 0.5ml of ice-cold ddH2O were added and cells were mixed gently by slow pipetting to induce osmotic shock. Cells were then incubated on ice for 20 minutes followed by a 5 minute spin at 12,000xg to remove spheroplasted and intact cells. The supernatant was retained as the periplasmic fraction. Spheroplasts were the lysed in 500ul lysis buffer (ddH2O with 25ug/ml DNaseI) and incubated on ice for 5 minutes. Cells were then sonicated four times in two-second bursts at 30-40% full power. Non-spheroplasted cells were then removed by centrifugation at 12000xg for 5 minutes. The supernatant was removed and centrifuged again. The remaining supernatant was kept as the spheroplasmic fraction. To isolate the membrane fraction from the spheroplasmic fraction, the supernatant was

spun for 1h at 138,000xg. The membrane pellet was solubilized in 0.5% Sarkosyl, 10mM TrisCl pH8.0.

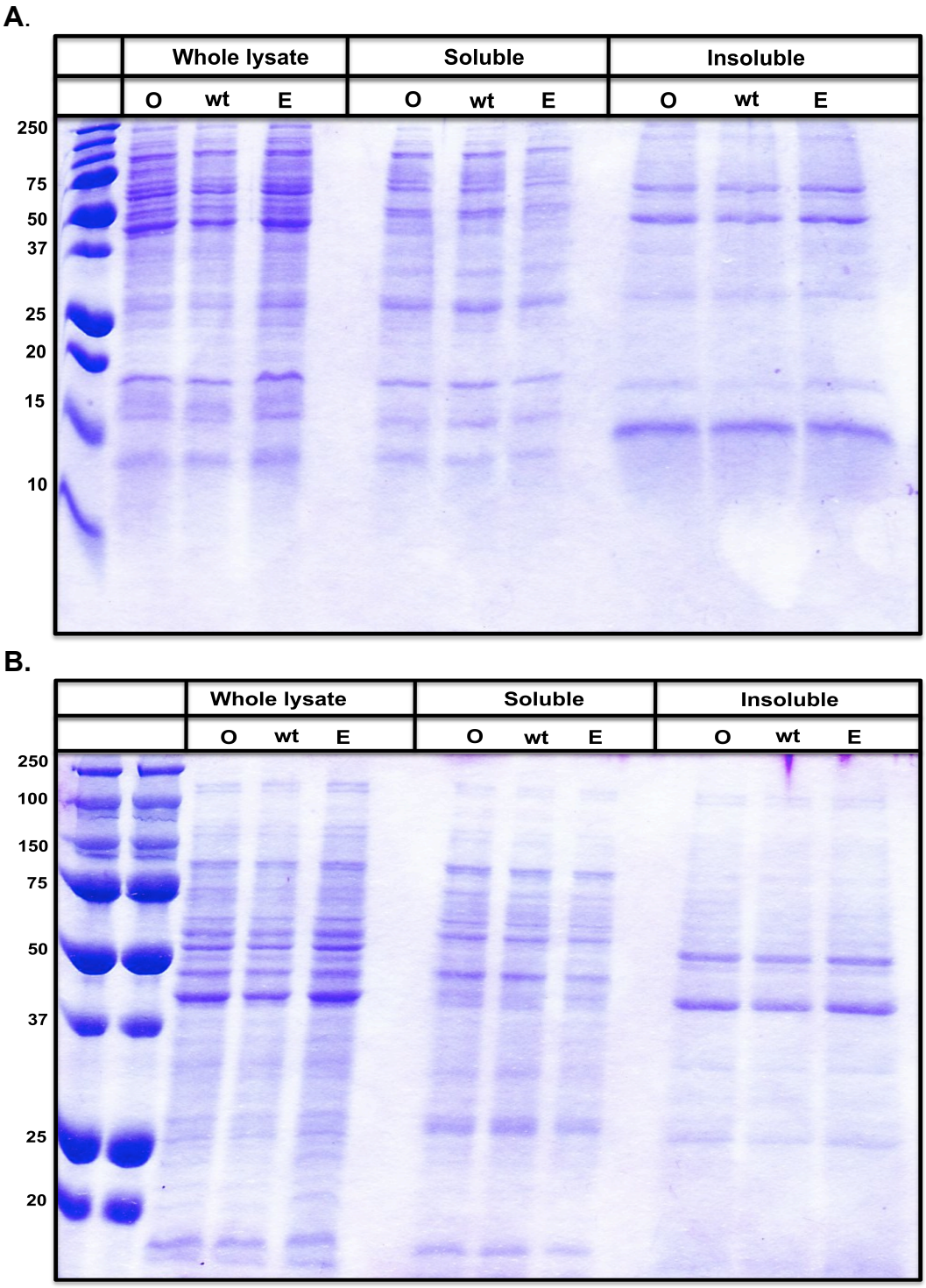

Figure A2-1: SDS-PAGE analysis of whole cell lysates, soluble and insoluble fractions of wild type AMB-1, wt; Δ*mamO*, O; Δ*mamE*, E. A. 15% SDS-PAGE gel. B. 10% SDS-PAGE gel.

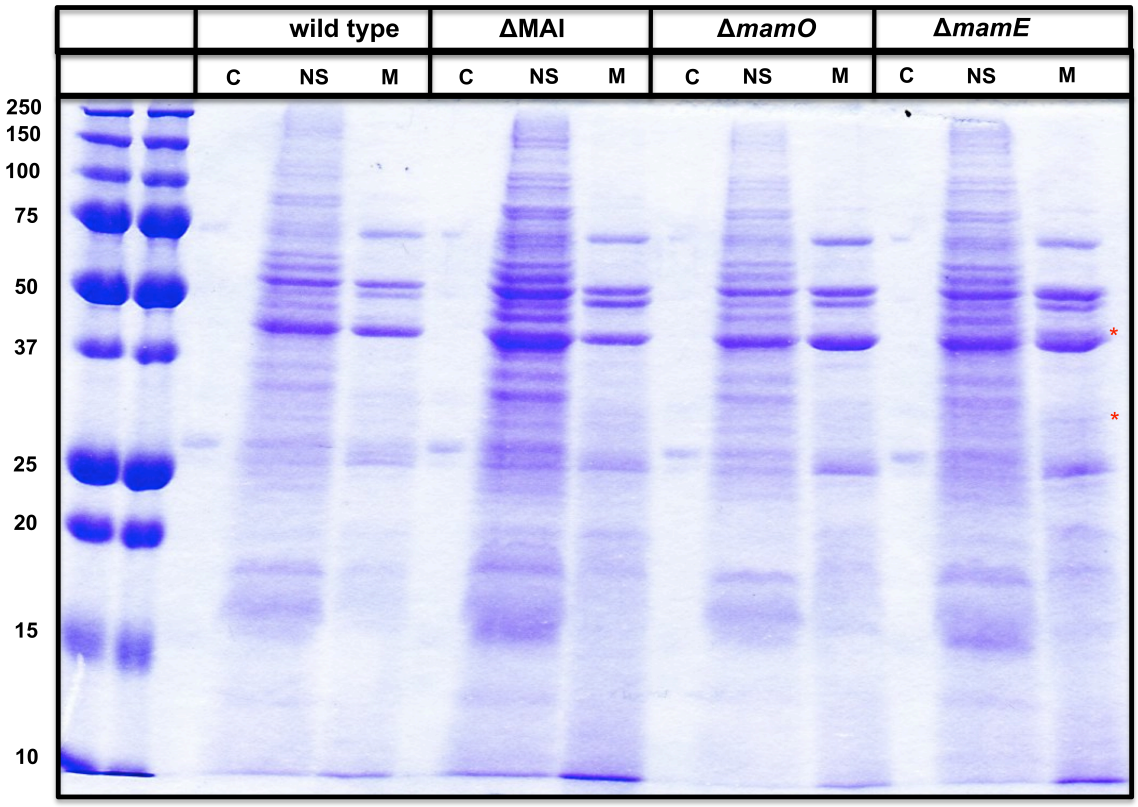

Figure A2-2: SDS-PAGE gel of wild type AMB-1, ΔMAI, Δ*mamO*, and Δ*mamE* strains after further fractionation. Cytoplasmic, C; nonspheroplasted fraction, NS; and membrane fraction, M; red asterisks indicate bands potentially enriched in Δ*mamE* strain. Surprisingly, the cytoplasmic fraction does not contain as many proteins as expected, suggesting this protocol needs optimization.

Appendix 3: GFP-MamI localization

Protein localization was usually assessed in early stationary phase for all experiments described in this chapter. It became obvious, however, that in early and mid-exponential phase, more Δ*mamE* cells had linear localization patterns of MamI, suggesting that the defect in MamI localization was not complete. Similar changes in MamI localization were observed for wild type cells although mislocalization occurred only after extended periods of growth in stationary phase, and always at least 55% of cells had linear MamI localization. This could be interpreted as follows: Since MamI is essential for magnetosome membrane formation, it may be passively brought to the magnetosome but potentially requires other magnetosome proteins to remain there. In the absence of *mamE* at least some MMPs are mislocalized, some of which may be responsible for maintaining MamI at the magnetosome. One could thus imagine that in the absence of *mamE* one would see linear GFP-MamI localization as long as new magnetosomes are formed and MamI localized to the magnetosome passively through its role in magnetosome membrane formation. As cells enter stationary phase and no new magnetosomes are formed, MamI localization is lost as it is not actively maintained at the magnetosome.

Materials and Methods

MamI-GFP construct was generated by Dorothée Murat. Cells were grown in green capped tubes in a microaerphillic chamber in 10ml MG supplemented to 10ug/ml of kanamycin. At the indicated time points, cells were collected, spotted onto 1% agarose pads and imaged using a Nikon Eclipse 80i microscope. Images were acquired with the x100 oil objective using a QImaging® RETIGA 2000R Fast 1394 camera. After cells reached stationary phase they were passaged at 1:10 dilution into fresh MG and growth and MamI-GFP localization were monitored.

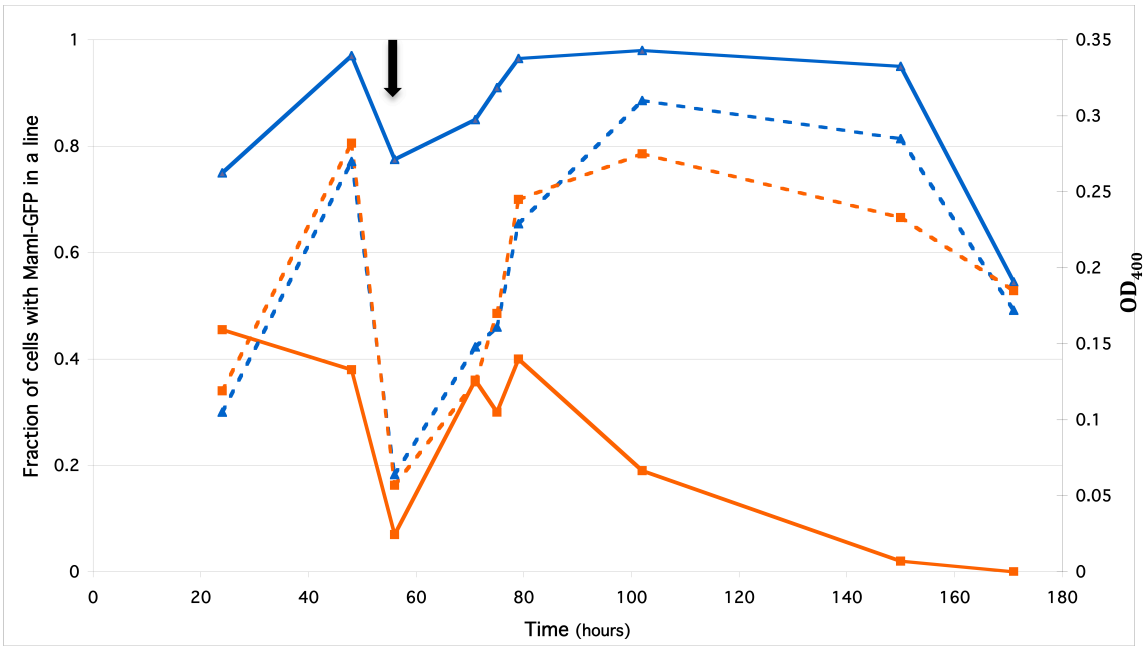

Figure A3-1: MamI-GFP localization throughout cell growth. Solid blue line represents MamI-GFP localization in wild type AMB-1; solid orange line MamI-GFP localization in Δ*mamE*; dotted blue line wild type OD_{400}; dotted orange line Δ*mamE* OD_{400}. Black arrow indicates time at which cultures were diluted 1:10 into fresh media.

Chapter 4: Magnetosome Membrane Protein Sorting

Introduction

Magnetosomes are membrane-bound crystals of magnetite or greigite found in magnetotactic bacteria. By aligning magnetosomes in chains, cells attain a fixed net magnetic dipole moment large enough to align with the earth's magnetic field lines. This alignment is thought to facilitate the cells' search for favorable environments within the water column (1-3). Magnetotactic bacteria share a conserved genomic island, the magnetosome island (MAI), which is essential for magnetosome formation; upon spontaneous loss of this island, cells are no longer magnetic and do not form magnetosomes or magnetosome membranes (4, 5). This suggests that at least a subset of the proteins required for magnetosome formation is encoded by this island. Proteomic studies strengthened this hypothesis when it was found that magnetosomes are enriched for a specific set of soluble and transmembrane proteins, many of which are encoded by the MAI (6, 7). Subsequently, some of these proteins have been shown to be essential for magnetosome membrane formation (*mamI*, *mamL*, *mamQ*, *mamB*) (8), others for various aspects of biomineralization (*mamA*, *mamC*, *mamD*, *mamF*, *mamG*, *mamT*, *mamS*, *mamR*, *mms6*) (8-10) and yet others for magnetosome chain organization (*mamK*, *mamJ*) (11-14). How these magnetosome proteins (MPs) are sorted/localized to the magnetosome is unknown. Besides shedding light on the process of magnetosome formation, understanding how proteins are targeted to the magnetosome would also inform many proposed applications that aim to functionalize magnetosomes (15). Current methods to functionalize magnetosomes rely on gene fusions to known magnetosome proteins (16). Understanding how MPs are targeted for magnetosome localization would potentially allow for functionalization of magnetosomes independent of such gene fusions.

A deeper understanding of magnetosome protein localization would also add to our currently limited understanding of how protein sorting in general is accomplished in bacteria. First assumed to be uniform "bags of enzymes", it has become ever more clear that bacteria possess much greater degrees of complexity that require the ability to sort effector proteins to subdomains of the cell, much as eukaryotes do. Many examples of subcompartments within bacteria and archaea have been identified, such as thylakoid membranes and carboxysomes (17, 18). These compartments, like magnetosomes, contain a specific set of proteins that need to be correctly localized. Other examples of localized proteins in bacteria include DivJ, PleC and DivK, localized at the poles of *Caulobacter crescentus* and essential for establishment of the two different cell fates of the organism (19), proteins localized to the forespore of *Bacillus* that are required for the process of spore formation (20), and chemoreceptor arrays found at the poles of many bacteria (21). Other striking examples are the various localization patterns of bacterial cytoskeletal proteins and septal localization of the divisisome proteins required for cell division (22). Different methods of protein targeting have been proposed for these proteins, including targeted

insertion, selected degradation and non-targeted insertion followed by diffusion and capture (23).

The goals of this project were to (a) characterize the path magnetosome membrane proteins (MMPs) take to the magnetosome, (b) identify signals and structures required for magnetosome localization, and (c) characterize the cellular machinery that accomplishes MMP sorting. The problem of magnetosome protein sorting is made more complex in AMB-1, given that that the magnetosome membrane is continuous with the inner membrane. It is currently unknown whether cells establish a diffusion barrier between these two membrane compartments or whether proteins are free to move into and out of the magnetosome. Based on the current knowledge of bacterial protein targeting, one could envision the following five models (illustrated in Fig. 1) for sorting of magnetosome membrane proteins:

Model 1: MMPs could be localized via sorting signal-mediated insertion directly into the magnetosome membrane. Such signal sequence-mediated sorting mechanisms have been proposed for the cyanobacterium *Synechocystis*, which encounters a similar protein sorting conundrum as magnetotactic bacteria; cyanobacteria, like magnetotactic bacteria contain a third membrane system in addition to the inner and outer membranes, the thylakoid membranes. All three membranes possess distinct sets of proteins and Rajalahti *et al.* (24) found that resident proteins of different compartments have differential signal sequence and N-terminal segment properties. They propose that this allows for targeting of proteins, assuming that Sec and Tat translocons have different substrate affinities in different compartments. They suggest that this could be achieved through differential chemical modification of translocon components, differential lipid content of the membrane systems, or additional translocon components present in different compartments. If such a mechanism acted to sort magnetosome proteins, one would expect that MPs are inserted into a pre-formed magnetosome. This model predicts that magnetosome membrane proteins should never be found at the inner membrane, a testable hypothesis. Such a model would also require the presence of protein translocation machinery, such as SecYEG or YidC homologues, at the magnetosome. These components were not found in the proteomics studies of either MSR-1 nor AMB-1, suggesting that direct insertion into the magnetosome may be unlikely.

Model 2: Another possible mechanism is one of diffusion and capture, similar to the model proposed for the forespore protein SpoIVB in *Bacillus subtilis* (25). In this model, proteins are inserted at random into the inner membrane and then diffuse to their site of activity, where they are captured and retained. Any protein could thus diffuse into or out of the magnetosome, but MMPs are retained at the magnetosome through interactions with each other. Such a model would predict that inner membrane proteins should be able to sample the magnetosome environment and could possibly be trapped by crosslinking experiments. Depending on the rate of diffusion into the magnetosome, this model would also suggest that magnetosome membrane proteins should be found at the inner membrane as well as at the magnetosome. A diffuse and capture model, however, does not explain how magnetosomes are defined as the preferred site

of MMP localization. A possible way to define the magnetosome would be the presence of “founder” or “anchor” proteins. MamI, MamL, MamQ and/or MamB could perform this function, since they have been shown to be essential for magnetosome membrane formation (8). One could thus imagine that these four proteins passively localize to the magnetosome due to their involvement in magnetosome membrane formation and then remain there to capture other MMPs as they diffuse into the magnetosome. MamB was found at the magnetosome in both MSR-1 (6) and AMB-1 (7) and magnetosome membrane localization has been suggested for MamI, as a GFP fusion to this protein shows a linear localization pattern reminiscent of the position of the magnetosome chain (8). The presence of these two proteins at the magnetosome might make a model of diffusion and capture by magnetosome “anchor” proteins a feasible hypothesis.

Model 3: One could envision a magnetosome protein-specific protease that is excluded from the magnetosome, but present at the inner membrane. In this case MMPs would be inserted into the inner membrane throughout the cell but locally stabilized at the magnetosome membrane. Such a mechanism is thought to be in part responsible for polar localization of the *Shigella flexneri* protein IcsA (26). Such a model would require a magnetosome protein specific motif that would identify magnetosome proteins but not general inner membrane proteins as targets for the protease.

Model 4: Lipid-mediated sorting is yet another means of localizing proteins to specific membrane subdomains. MMPs could be sorted to the magnetosome through interaction with a magnetosome-specific lipid as is seen for the *E.coli* osmosensory transporter ProP, whose polar localization is achieved by preferential interaction with cardiolipin (27). Analysis of the composition of the magnetosome membrane has been performed for *Magnetospirillum gryphiswaldense* MSR-1 (6), *Magnetospirillum magnetotacticum* MS-1 (28), and *Magnetospririllum magneticum* AMB-1 (7), but no study suggested a distinct lipid content for the magnetosome membrane. None of the studies, however, performed an exhaustive analysis of lipid composition, and subtle differences in lipid content could have eluded detection. Alternatively, differences in membrane thickness could lead to partitioning of MMPs into the magnetosome membrane based on the length of their transmembrane domains, as has been proposed for SNARE sorting (29). Membrane curvature itself has also been suggested as a means of protein sorting. Lenarcic *et al.* (30) showed that the *Bacillus* protein DivIVA preferentially localizes to the highly negatively curved division septa and poles of the cells. Similarly, positive membrane curvature has been shown to act as a cue for the localization of peripheral membrane proteins such as the spore coat protein SpoVM (31).

Model 5: Lastly, magnetosomes could form through a process of self-assembly analogous to formation of clathrin-coated vesicles (32). In such a scenario, magnetosome formation/membrane deformation would follow assembly of a complex of magnetosome proteins at the inner membrane. In such a model there would be no turnover of proteins at the magnetosome; once a magnetosome is formed it is no longer accessible to nascent MMPs. Given the

advances described in Chapter 2 of this thesis, this model seems less likely as a general magnetosome protein sorting mechanism since many magnetosome membrane proteins can be deleted without resulting in a defect of magnetosome formation, and a single gene deletion mutant has been identified in which a subset of MPs is mislocalized, yet magnetosome membranes are still formed (8). Self-assembly could, however, be the means for MamB, MamQ, MamL and MamI localization to the magnetosome; these founder proteins could be passively brought to the magnetosome as part of their involvement in the process of magnetosome membrane formation.

Although I have presented these models as separate possibilities, MMP sorting may very likely be accomplished by a combination of all or a subset of these mechanisms. To begin to address the question of MMP sorting, I chose a classical approach to identifying sorting signals by assaying localization of truncations of various magnetosome membrane proteins. This project was abandoned for the work on MamE and MamO described in earlier chapters of this thesis, as I was unable to optimize our magnetosome purification protocol to separate what I believed to be an inner membrane marker from magnetosome proteins.

Results

Standard magnetosome purification protocol does not separate an inner membrane marker from the magnetosome protein MamB

Preliminary data suggested that the first N-terminal 75 amino acids of the magnetosome protein MamB are sufficient for localizing an inner membrane marker, the transmembrane domain of FtsQ (FtsQ1-100), to the magnetosome. Similarly, MamB could be truncated to a construct comprising only its first 110 amino acids and still localize to the magnetosome. Further attempts at MamB truncations led to constructs of MamB comprising amino acids 1-55, 1-60 and 1-65, which were not detectable by Western blot. My initial goal was to confirm that a MamB-FtsQ fusion comprising amino acids 35-70 of MamB and amino acids 1-100 of FtsQ (MamB35-70/FtsQ1-100) localized to the magnetosome, and hence that amino acids 35-70 are sufficient for magnetosome localization. The ultimate goal was to determine how these residues mediated magnetosome localization and to generate similar truncations of other magnetosome membrane proteins in the hope of identifying a consensus magnetosome localization sequence or magnetosome protein interaction surfaces that mediate magnetosome localization.

The standard magnetosome purification protocol employed by the lab uses freeze-thaw followed by lysozyme lysis to generate AMB-1 extract. This extract is then passed over a column of ferromagnetic beads that can be magnetized by application of an external magnetic field. Magnetosomes are retained on the column whereas non-magnetic material such as the cytoplasm and inner membrane fractions should pass into the flow-through and washes. Magnetosomes are then eluted by removing the external magnetic field.

Using a cytoplasmic GFP construct I showed that we can separate cytoplasmic proteins from the magnetosome fraction (Fig. 2A and C). However, our inner

membrane protein control, the transmembrane domain of FtsQ (the first 100 amino acids of FtsQ) fractionated with the magnetosomes (Fig. 2B). This presented a problem for studies of protein sorting, since I would not be able to distinguish between proteins that localize correctly to the magnetosomes and proteins that are mislocalized to the inner membrane. I thus set out to find purification conditions, which would allow me to separate the inner membrane marker from the magnetosome fraction.

Mild Sonication, Syringe Lysis, and Higher Salt Washes Do Not Allow For Separation of Inner and Magnetosome Membrane

One hypothesis was that since the magnetosome membrane is continuous with the inner membrane, large sheets of inner membrane may remain attached to the magnetosome membrane upon cell lysis. I thus attempted to use harsher cell lysis protocols to enhance membrane disruption, including various amounts of sonication as well as syringe lysis. Although these protocols yielded varying amounts of MamB and FtsQ1-100 in the magnetosome fraction, they were never able to separate FtsQ1-100 from MamB; conditions that rendered FtsQ1-100 in the flow through, such as 60-second sonication, also eliminated MamB from the magnetosome fraction (Fig. 2D and E). After 5 seconds of sonication, a condition where MamB and FtsQ1-100 were still found in the magnetosome fraction, large amounts of lipid vesicles co-purified with the magnetosome as observed by electron microscopy, supporting the hypothesis of inner membrane contamination (Fig. 2J,K and L). Syringe lysis significantly changed the elution profile of the magnetosome fraction as assessed by Coomassie stain, but FtsQ1-100 remained in the elution fraction (data not shown). Higher salt did not alter the elution profiles. I thus concluded that I was able to separate cytoplasmic proteins from the magnetosome fraction but was either (1) unable to separate inner from magnetosome membrane with the above methods or (2) that FtsQ1-100 may not be an ideal inner membrane marker.

Alternative Inner Membrane Markers

Since my results suggested that FtsQ1-100 may not be an ideal inner membrane marker, I set out to generate another such probe. One approach to asses inner membrane contamination is to follow Diphosphopyridine nucleotide (DPNH) oxidation activity associated with the inner membrane(33) in our magnetosome purification fractions. These assays showed DPNH activity in all fractions, but were inconclusive as many proteins encoded by the AMB-1 genome are able to oxidize DPNH (data not shown). Proteomic studies of magnetosome fractions (6, 7) have given some insight into which proteins are found at the magnetosome, but they by no means generate an exhaustive list. Since the exact nature of the protein content of the magnetosome is not known, it is not possible to definitively assess whether the magnetosome fraction should or should not possess DPNH oxidation activity.

To generate new inner membrane markers, I attempted to HA-tag *amb2660* (putative methyl accepting chemotaxis protein), *amb3424* (putative membrane fusion protein), *amb4179* (putative ABC-type transport system component) and

amb3111 (SecY) (Table 3). None of these constructs was detectable by anti-HA Western blotting when expressed in either AMB-1 or in *E.coli*.

GFP-Fusions to Magnetosome Proteins

Since magnetosomes form a straight line through the cell body, GFP-fusions to magnetosome proteins such as MamK, MamJ and MamA result in straight lines of GFP fluorescence within the cell (8, 11, 13, 34). As a parallel approach to optimizing our magnetosome purification protocol, I attempted to GFP-tag various magnetosome proteins to use their localization pattern as a proxy for magnetosome localization. Since GFP will not refold in the periplasm and most magnetosome membrane proteins' C-termini are localized in the periplasm, I generated two vectors for N-terminal GFP tagging of magnetosome proteins. I chose two different linker sequences, one alpha helical linker, HL4, described by Arai *et al.* (35), and an unstructured linker 1MCJ generated by the LINKER software (36). N-terminal GFP constructs were generated for several magnetosome proteins with varying success (Table1). All constructs when expressed in AMB-1 were either diffusely localized, formed foci or showed no detectable fluorescence. When expression was assessed by Western blot using a GFP antibody, all contructs, with the exception of MamT were found to be expressed as truncations (Table 2).

Since the GFP variant mCherry has been shown to fluoresce even when expressed in the periplasm, I also attempted to C-terminally mCherry tag magnetosome proteins. A cytoplasmic GFP-mcherry construct I generated for this purpose, which showed both GFP and mCherry fluorescence in *E.coli* displayed no fluorescence in AMB-1, leading me to abandon this approach (Table 1).

Immunofluorescence

In another approach to analyzing magnetosome protein localization in AMB-1. I attempted to visualize magnetosome proteins by immunofluorescence. This approach was successful using an antibody against MamK (Fig. 3A). Using both a protocol optimized for *Myxococcus xanthus* (Emilia Mauriello, personal communication) and one optimized for AMB-1 (Fukumori lab, personal communication), I was able to reproduce the clear linear localization patterns of MamK seen for MamK-GFP. As expected, only background staining was observed in a ΔMAI strain. Visualization of MamC using a MamC antibody was unsuccessful in that only patched membrane localization was observed in wild type cells, similar to the staining observed for the ΔMAI strain, which lacks MamC (Fig. 3B). This may be due to the poor specificity of the MamC antibody, which recognizes several proteins in Western blots of AMB-1 whole cell lysate. An attempt at using an HA-antibody to visualize MamB-HA, and thus potentially other HA-tagged magnetosome proteins, showed some promise. Linear structures were observed but similar structures were sometimes visible in a no plasmid control strain (Fig. 3C). If signal-to-noise ratios could be improved, immunofluoresence against HA-tagged proteins may be possible.

Discussion

Magnetosome protein sorting poses an intriguing question. How are MMPs addressed to the subcompartment of the inner membrane that is the magnetosome, and how are they concentrated there to the exclusion of general inner membrane proteins? My experiments failed to answer these questions due to the lack of a bona fide inner membrane marker that could be used to troubleshoot the lab's standard magnetosome purification protocol. My results suggest that this protocol does not purify magnetosomes to the exclusion of inner membrane, as I was never able to separate the magnetosome membrane protein MamB from the protein used as a general inner membrane marker, the first 100 amino acids of FtsQ. We were unable to ascertain whether this was due to a true inability to efficiently separate inner membrane from magnetosome membrane, or whether FtsQ1-100 was able to access the magnetosome membrane and was thus not a bona fide inner membrane marker. Several HA-fusions were generated to other candidates for an inner membrane marker. These candidates were picked based on the annotation of the AMB-1 genome and homology to known inner membrane proteins but none of the HA-fusions were detectable by Western blot in AMB-1 nor in *E.coli*. Proteomics studies of AMB-1 magnetosomes performed by Tanaka *et al* (7) showed significantly more inner membrane protein contamination than similar procedures in *Magnetospirillum gryphiswaldense* MSR-1 (6), where magnetosomes are possibly not invaginations of the inner membrane but vesicles within the cytoplasm. This may be due to an inherent difficulty of separating magnetosomes from inner membrane when the two membrane systems are continuous. A bona fide inner membrane marker is absolutely essential for the continued troubleshooting of magnetosome purification.

In the parallel approach of GFP-tagging magnetosome membrane proteins, I encountered the difficulty that most MMPs have periplasmic C-termini, which are not compatible with GFP fluorescence. mCherry-tagging these C-termini was abandoned since cytoplasmic GFP-mCherry constructs which showed both GFP and mCherry fluorescence in *E.coli* no longer displayed mCherry nor GFP fluorescence when expressed in AMB-1 (Table 1). These fusions were expressed in AMB-1 as detected by Western blot using a GFP antibody. It may, however, be worth revisiting c-terminal mCherry-tagging of MMPs since N-terminal GFP fusions to MamI using this construct were successful. Lack of fluorescence of the GFP-mCherry construct in AMB-1 is thus not an indicator of the ability of fusions that replace either GFP or potentially mCherry to be successful.

Most of the N-terminal GFP fusions generated were only expressed as truncated forms in AMB-1 and showed very faint diffuse fluorescence. Dorothée Murat, however, was able to use the GFP-HL4-MamT construct to successfully tag the magnetosome protein MamI. This construct was expressed and showed localized fluorescence (see Chapter 2 of this thesis). This approach is thus not flawed, but may not be transferable to all magnetosome membrane proteins. A GFP-independent form of fluorescence microscopy, such as the tetracysteine tag-based FlAsH protein detection technology should be attempted for

visualization of proteins that cannot be successfully GFP or mCherry tagged. An advantage of the FlAsH system is that tetracysteine tags are small enough to be inserted into protein sequences internally with minimal disruption of secondary or tertiary structure, thus circumventing the cleavage of GFP from proteins of interest.

An approach that proved more promising was the use of immunofluorescence to visualize magnetosome proteins. This technique was particularly successful when used to visualize MamK, for which a highly specific antibody exists. This technique was less successful using the less specific antibody against MamC, but showed promise using a commercially available HA antibody. It may thus be possible to use immunofluorescence to visualize tagged magnetosome proteins when highly specific antibodies are available. Immunofluorescence has been successfully used in several other instances to assess protein localization in magnetotactic bacteria and has been shown to be a powerful tool for the study of protein localization in magnetotactic bacteria(37).

In conclusion, the mechanism of magnetosome protein sorting remains an intriguing and unexplored question. With the generation of a bona fide inner membrane marker, magnetosome purification protocols can undoubtedly be optimized to allow for efficient separation of inner and magnetosome membranes and thus provide the tools for answering the questions I set out to address. My work, however, transitioned to the study of two HtrA/DegP-family proteases MamE and MamO before I could identify such an inner membrane marker because MamE was found to play a role in magnetosome protein sorting. I thus focused on elucidating the role of these proteases in magnetosome protein sorting and magnetosome formation, work that is described in Chapter 2 and Chapter 3 of this thesis.

Materials and Methods

Magnetosome Purification

50 to 100ml of AMB-1 were grown to exponential phase in MG media supplemented with both Wolfe's Vitamin Solution and 3mM iron chloride 9mM malate at 1/100 (8). Cells were collected by centrifugation at room temperature, 8000xg for 10 minutes. Pellets were then exposed to two cycles of freeze-thaw using liquid nitrogen and subsequently resuspended in 1-2ml of lysis buffer (20mM HEPES pH7.5; 25mM NaCl, 0.5mM EDTA; 20ug/ul lysozyme; 25ug/ul DNaseI; 14.6mM BME; 1mM PMSF) and incubated on ice for 1.5h. The lysate was then passed over a magnetized MACS® separation column equilibrated in 3ml of elution buffer (20mM HEPES pH7.5; 25mM NaCl, 14.1mM BME; 1mM PMSF). After 2 washes of 5ml each with elution buffer, magnetization of the column was removed and the "magnetosome fraction" eluted in 1ml of elution buffer using the plunger supplied with the columns. 500ul of the elution fraction was then concentrated by centrifugation at 4° C.

For sonication, lysate was placed into 1.5ml eppendorff tubes and sonicated on ice at 5 or 10 second intervals using a microtip at output setting 2 of a Branson Sonifier 250. For syringe lysis, lysate was treated as described above except

that lysate was passed eight times through a 30.5G needle after incubation on ice instead of being subjected to sonication.

Cloning of NGFP vectors and NGFP-MMP constructs

The alpha helical HL4 linker previously described by Arai *et al* (35) was chosen to reduce interference between GFP and the tagged protein. The amino acid sequence of this linker is LA$(EAAAK)_4$AAA. GFP was amplified from pAK22 using a forward primer including a 5' EcoRI site and a reverse primer that included the HL4 sequence followed by a BamHI site. This fragment was EcoRI-BamHI cloned into pAK22 to yield EcoRI-*gfp*-*hl4*-BamHI-*gfp*-SpeI. Clones of this backbone are referred to as 3-1 through 3-5. The second GFP can then be replaced by the gene of choice using a BamI-SpeI digest to yield EcoRI-*gfp*-*HL4*-*yfg*-SpeI. In addition the PCR product was EcoRI-BamHI cloned into pAK151 to yield EcoRI-*gfp*-*HL4*-BamHI-*mcherry*-Spe. Clones of this backbone are referred to as 7-1 through 7-5.

A second approach was to choose an unstructured, extended linker based on computational predictions of the LINKER program (36). Using this program a 20 amino acid linker termed 1MCJ was chosen. The amino acid sequence of this linker is APTECSPSALTQPPSASGSL. This linker was similarly amplified and cloned into the pAK22 and pAK151 backbones.

AMB-1 proteins were then amplified using primers listed in Table 4 and BamHI-SpeI cloned into the four vectors described above. GFP and mCherry fluorescence was assessed in *E.coli* as well as in *AMB-1* and expression was confirmed by Western blot.

Western blotting

Western blotting was performed using standard techniques. Antibodies used for detection of GFP- and HA-tagged proteins are as follows: JL8 monoclonal anti-GFP antibody from Clontech and Sigma monoclonal anti-HA antibody. Both antibodies were used at a 1:5000 dilution,

For AMB-1 whole cell lysate Westerns, at least 500ul of culture were loaded per well. For magnetosome purifications, 15ul of all unconcentrated fractions were loaded. Concentrated elution fractions were resuspended in sample buffer at 1/10 the pre-concentration volume, and 10ul were loaded per well.

Immunofluoresence

An immunofluorescence protocol optimized for *Magnetospirillum magneticum* AMB-1 by the Fukimori lab (Kanazawa University, Japan) was used: 1ml of cells was fixed for 30 minutes at room temperature by addition of 250ul 16% paraformaldehyde. Cells were pelleted by centrifugation at room temperature for 10 minutes. The resulting pellet was resuspended in 100ul ddH_2O and 10ul of this suspension was added to each well of a 15 well MP Biomedicals multitest slide and allowed to dry. Cells were then washed twice for 5 minutes with phophate buffered saline (PBS). 10ul of lysozyme buffer (50mM TrisCl pH 8; 500ug/ml EDTA, 100ug/ml lysozyme; 0.5M sucrose; 1% Triton X-100) were added and then immediately removed by two 5-minute washes with PBS buffer.

Then 10ul of 1% BSA in PBS were added and the slide incubated in a moist chamber for 10 minutes. After blocking, primary antibody was added at 1:2500 for MamC and 1:500 for MamK in 0.5%BSA/PBS. Slides were incubated for 30 minutes in a moist chamber. After this incubation, slides were washed twice with PBS and 10ul of secondary antibody in 0.5% BSA/PBS at a concentration of 1:1500 were added. The secondary antibody used was an Alexa488 labeled anti-rabbit antibody, and slides were kept in the dark for all steps after addition of this antibody. Slides were incubated again for 30 minutes in a moist chamber and washed twice with PBS before addition of Invitrogen SlowFade®Gold antifade reagent. Coverslips were then placed on top of the slides and sealed using nail polish.

For immunofluorescence against HA-tagged MamB, a *Myxococcus xanthus* protocol developed by the Zusman lab at UC Berkeley (personal communication, Emilia Mauriello) was used and optimized for AMB-1. Briefly, 2.4ul of 1M NaPO4 pH7.4 were added to 60ul of culture. This was added to 12ul of 16% paraformaldehyde+.24ul gluteraldehyde and transferred to the slide grid at 10ul/well. Cells were fixed for 20 minutes at room temperature. All liquid was then removed and cells washed 3 times in PBS followed by one wash with a Glucose-Tris-EDTA (GTE) buffer. Cells were then lysed in GTE+5ug/ml lysozyme for 10 minutes at room temperature. Subsequently cells were washed three times in PBS and allowed to dry. Cells were then re-hydrated in PBS for 5 minutes, and blocking buffer (PBS + 2%BSA) was added for 30 minutes. Cells were then incubated overnight with HA-antibody diluted to 1:500 in PBS/2%BSA. Cells were then washed ten times with PBS and incubated with an Alexa488-fused anti-mouse secondary antibody at various concentrations.

DPNH oxidase activity assay

Diphosphopyridine nucleotide (DPNH) oxidase activity assays were performed as described by Osborne *et al* (1972 Journal of Biological Chemistry 247:3062-72). Briefly 20ul of each magnetosome fraction were added to 120uM DPNH in 1ml of reaction buffer (50mM TrisCl pH 7.5; 0.2mM DTT) and the decrease in absorbance at 340nm was measured as a proxy for DPNH oxidation. Lactate dehydrogenase was used as a positive control for DPNH oxidation.

References:

1. Frankel RB, Bazylinski DA, Johnson MS, & Taylor BL (1997) Magneto-aerotaxis in marine coccoid bacteria. *Biophys J* 73(2):994-1000.
2. Smith MJ*, et al.* (2006) Quantifying the magnetic advantage in magnetotaxis. *Biophys J* 91(3):1098-1107.
3. Komeili A (2007) Molecular mechanisms of magnetosome formation. *Annu Rev Biochem* 76:351-366.
4. Matsunaga T*, et al.* (2005) Complete genome sequence of the facultative anaerobic magnetotactic bacterium Magnetospirillum sp. strain AMB-1. *DNA Research* 12(3):157-166.
5. Ullrich S, Kube M, Schubbe S, Reinhardt R, & Schuler D (2005) A hypervariable 130-kilobase genomic region of Magnetospirillum

gryphiswaldense comprises a magnetosome island which undergoes frequent rearrangements during stationary growth. *J Bacteriol* 187(21):7176-7184.
6. Grunberg K*, et al.* (2004) Biochemical and proteomic analysis of the magnetosome membrane in Magnetospirillum gryphiswaldense. *Appl Environ Microbiol* 70(2):1040-1050.
7. Tanaka M*, et al.* (2006) Origin of magnetosome membrane: Proteomic analysis of magnetosome membrane and comparison with cytoplasmic membrane. *Proteomics* 6(19):5234-5247.
8. Murat D, Quinlan A, Vali H, & Komeili A (2010) Comprehensive genetic dissection of the magnetosome gene island reveals the step-wise assembly of a prokaryotic organelle. *Proc Natl Acad Sci U S A* 107(12):5593-5598.
9. Scheffel A, Gardes A, Grunberg K, Wanner G, & Schuler D (2008) The major magnetosome proteins MamGFDC are not essential for magnetite biomineralization in Magnetospirillum gryphiswaldense but regulate the size of magnetosome crystals. *J Bacteriol* 190(1):377-386.
10. Arakaki A, Webb J, & Matsunaga T (2003) A novel protein tightly bound to bacterial magnetic particles in Magnetospirillum magneticum strain AMB-1. *J Biol Chem* 278(10):8745-8750.
11. Komeili A, Li Z, Newman DK, & Jensen GJ (2006) Magnetosomes are cell membrane invaginations organized by the actin-like protein MamK. *Science* 311(5758):242-245.
12. Scheffel A*, et al.* (2006) An acidic protein aligns magnetosomes along a filamentous structure in magnetotactic bacteria (vol 440, pg 110, 2006). *Nature* 441(7090):248-248.
13. Scheffel A & Schuler D (2007) The acidic repetitive domain of the Magnetospirillum gryphiswaldense MamJ protein displays hypervariability but is not required for magnetosome chain assembly. *J Bacteriol* 189(17):6437-6446.
14. Katzmann E, Scheffel A, Gruska M, Plitzko JM, & Schuler D (2010) Loss of the actin-like protein MamK has pleiotropic effects on magnetosome formation and chain assembly in Magnetospirillum gryphiswaldense. *Mol Microbiol* 77(1):208-224.
15. Schuler D & Frankel RB (1999) Bacterial magnetosomes: microbiology, biomineralization and biotechnological applications. *Appl Microbiol Biotechnol* 52(4):464-473.
16. Yoshino T, Shimojo A, Maeda Y, & Matsunaga T (2010) Inducible expression of transmembrane proteins on bacterial magnetic particles in Magnetospirillum magneticum AMB-1. *Appl Environ Microbiol* 76(4):1152-1157.
17. Fuerst JA (2005) Intracellular compartmentation in planctomycetes. *Annu Rev Microbiol* 59:299-328.
18. Vothknecht UC & Westhoff P (2001) Biogenesis and origin of thylakoid membranes. *Biochim Biophys Acta* 1541(1-2):91-101.

19. Ausmees N & Jacobs-Wagner C (2003) Spatial and temporal control of differentiation and cell cycle progression in Caulobacter crescentus. *Annual Review of Microbiology* 57:225-247.
20. Ramamurthi KS & Losick RM (2005) Protein localization: Reach out and touch the forespore. *Curr Biol* 15(5):R165-R167.
21. Li Z & Jensen GJ (2009) Electron cryotomography: a new view into microbial ultrastructure. *Curr Opin Microbiol* 12(3):333-340.
22. Goehring NW & Beckwith J (2005) Diverse paths to midcell: Assembly of the bacterial cell division machinery. *Curr Biol* 15(13):R514-R526.
23. Rudner DZ & Losick R (2010) Protein Subcellular Localization in Bacteria. *Csh Perspect Biol* 2(4):-.
24. Rajalahti T*, et al.* (2007) Proteins in different Synechocystis compartments have distinguishing N-terminal features: A combined proteomics and multivariate sequence analysis. *J Proteome Res* 6(7):2420-2434.
25. Rudner DZ, Pan Q, & Losick RM (2002) Evidence that subcellular localization of a bacterial membrane protein is achieved by diffusion and capture. *Proc Natl Acad Sci U S A* 99(13):8701-8706.
26. Shapiro L, McAdams HH, & Losick R (2002) Generating and exploiting polarity in bacteria. *Science* 298(5600):1942-1946.
27. Romantsov T*, et al.* (2007) Cardiolipin promotes polar localization of osmosensory transporter ProP in Escherichia coli. *Mol Microbiol* 64(6):1455-1465.
28. Gorby YA, Beveridge TJ, & Blakemore RP (1988) Characterization of the bacterial magnetosome membrane. *J Bacteriol* 170(2):834-841.
29. Sprong H, van der Sluijs P, & van Meer G (2001) How proteins move lipids and lipids move proteins. *Nat Rev Mol Cell Biol* 2(7):504-513.
30. Lenarcic R*, et al.* (2009) Localisation of DivIVA by targeting to negatively curved membranes. *Embo J* 28(15):2272-2282.
31. Ramamurthi KS, Lecuyer S, Stone HA, & Losick R (2009) Geometric Cue for Protein Localization in a Bacterium. *Science* 323(5919):1354-1357.
32. Ungewickell EJ & Hinrichsen L (2007) Endocytosis: clathrin-mediated membrane budding. *Curr Opin Cell Biol* 19(4):417-425.
33. Osborn MJ, Gander JE, Parisi E, & Carson J (1972) Mechanism of Assembly of Outer Membrane of Salmonella-Typhimurium - Isolation and Characterization of Cytoplasmic and Outer Membrane. *J Biol Chem* 247(12):3962-& .
34. Komeili A, Vali H, Beveridge TJ, & Newman DK (2004) Magnetosome vesicles are present before magnetite formation, and MamA is required for their activation. *Proc Natl Acad Sci U S A* 101(11):3839-3844.
35. Arai R, Ueda H, Kitayama A, Kamiya N, & Nagamune T (2001) Design of the linkers which effectively separate domains of a bifunctional fusion protein. *Protein Eng* 14(8):529-532.
36. Xue F, Gu Z, & Feng JA (2004) LINKER: a web server to generate peptide sequences with extended conformation. *Nucleic Acids Res* 32:W562-W565.

37. Taoka A, Asada R, Wu LF, & Fukumori Y (2007) Polymerization of the actin-like protein MamK, which is associated with magnetosomes. *Journal of Bacteriology* 189(23):8737-8740.

Construct	Expressed in *E.coli*	Fluoresces in *E.coli*	Localization in *E.coli*	Expressed in AMB-1	Fluoresces in AMB-1	Localization in AMB-1
GFP-HL4-GFP (3-1 to 3-5)	Y	Faint	Diffuse	Y	Y	Diffuse
GFP-HL4-mCherry (7-1 to 7-5)	Y	Both green and red	Diffuse	Y	N	N/A
GFP-1MCJ-GFP (4-1 to 4-5)	Y	Faint	Diffuse	Y	Faint	Diffuse
GFP-1MCJ-mCherry (8-1 to 8-5)	Y	Both green and red	Diffuse	Y	N	N/A

Table1: GFP constructs

HL4 linker sequence: LAEAAAKEAAAEAAAKEAAAKAAA from Arai R *et al.* (35)
1MCJ linker sequence: APTECSPSALTQPPSASGSL

Construct	Expressed in *E.coli*	Fluoresces in *E.coli*	Localization in *E.coli*	Expressed in AMB-1	Fluoresces in AMB-1	Localization in AMB-1
NGFP-1MCJ-MamB	Y	Y	Diffuse	Not full length	N	N/A
NGFP-HL4-MamB	Y	Faint	Diffuse	Low signal	N	N/A
NGFP-1MCJ-MamE (8-2)	Y Multiple bands	Y	Diffuse	Not full length Looks same in wild type and ΔMAI	Y	Diffuse
NGFP-HL4-MamT (3-2)	Y Multiple bands	Y	Diffuse and membrane	Y+degradation No full length in ΔMAI	Y	Diffuse
NGFP-HL4-MamM	Y + degradation	Y	Diffuse	N/D	N/D	N/D
NGFP-HL4-MamQ	Y + degradation	Y	Diffuse and Foci at pole	Not full length Looks same in wild type and ΔMAI	Y	Diffuse

Table 2: GFP-fusions

Construct	Expressed in *E.coli*	Correct size band in *E.coli*	Expressed in AMB-1	Correct size band in AMB-1
HA-MamT	Y	Y	N	N/A
HA-MamQ	Y	Yes, and smaller bands	Y	Y
HA-MamM	N	N/A	Y	Y
HA-Amb4179	N	N/A	N	N/A
HA-Amb3424	N	N/A	N	N/A
Amb3111-3HA	N	N/A	N	N/A

Table 3: HA-fusions

Primer Name	Primer Target	Primer Sequence
NGFP-F	GFP; adding EcoRI site	gccgaattcatgagtaaaggagaagaacttttcactcg
NGFP-HL4-R	GFP; adding HL4 linker; BamHI site; deleting STOP	ccgggatcccgctgctgctttggccgccgcttccttagccgctggctcctttggggccgcttctttagccgccgcggcctcggccagtttgtatagttcatccatgccat
MamE-F	*mamE* adding BamHi site	ggcggatccatggccatgttcaatggtgac
MamE-R	*mamE* adding SpeI site	gccactagttcaaaggacaatccagaactcttg
MamM-F	*mamM* adding BamHI site	ggcggatccatgaggaagagcggttgcac
MamM-R	*mamM* adding SpeI site	gccactagtctagttatccaccttcgacaacatga
4179-F	*amb4179* adding BamHI site	ggcggatccatgaaccgctttgtcgaggt
4179-R	*amb4179* adding SpeI site	gccactagtctattccagcgcctgccgca
3424-F	*amb3424* adding BamHI site	ggcggatccatggaccatcaaccgcgtcgt
3424-R	*amb3424* adding SpeI site	gccactagtctattcgatcttgccgggct
MamT-F	*mamT* adding BamHI site	ggcggatccatggaggcgccgcggcgcggccgt
MamT-R	*mamT* adding SpeI site	gccactagttcataattgccatctcat
MamQ-F	mamQ adding BamHI site	ggcggatccatggcattaggcgacgcgaatgttggttcggcccc
MamQ-R	mamQ adding SpeI site	gccactagttcatttcttgatgtcctgcgcatggtt
2260-F	*amb2660* adding BamHI site	ggcggatccatgctcgcccgcgtcgccgatgcccgcat
2260-R	*amb2660* adding SpeI site	gccactagttcatcgcgggttggttaggccc
cMamE-F	*mamE* adding EcoRI site	ggcgaattcatggccatgttcaatggtgac
cMamE-R	*mamE* adding BamHI site, deleting STOP	gccggatccaaggacaatccagaactcttg
cMamM-F	*mamM* adding EcoRI site	ggcgaattcatgaggaagagcggttgcacggtctgca
cMamM-R	*mamM* adding BamHI site, deleting STOP	gccggatccgttatccaccttcgacaacatga
c4179-F	*amb4179* adding EcoRI site	ggcgaattcatgaaccgctttgtcgaggt
c4179-R	*amb4179* adding BamHI	gccggatccttccagcgcctgccgca

	site, deleting STOP	
NGFP1MCJ-R	GFP, adding 1MCJ linker; BamHI Site, deleting STOP	ccgggatcccaggctgccactggcactcgggggctgggtcaggg cgctcgggctgcactcggtgggggctttgtatagttcatccatgccatgtgtaatc
c3424-F	*amb3424* adding EcoRI Site	ggcgaattcatggaccatcaaccgcgtcgt
c3424-R	*amb3424* adding BamHI site, deleting STOP	gccggatccttcgatcttgccgggctggg
cMamT-F	*mamT* adding EcoRI site	ggcgaattcatggaggcgccgcggcgcggccgtcgctgggtaag
cMamT-R	*mamT* adding BamHI site deleting STOP	gccggatcctcataattgccatctcat
cMamQ-F	*mamQ* adding EcoRI site	ggcgaattcatggcattaggcgacgcgaatgttggttcggcccc
cMamQ-R	*mamQ* adding BamHI site deleting STOP	gccggatcctttcttgatgtcctgcgcatggttgag
amb3111-F	*amb3111* adding BamHI site	ggcggatccatggcctccgctgccgagcagc
amb3111-R	*amb3111* adding SpeI site	gccactagtttaacgccgcccgcgcagccg
cAmb3111-F	*amb3111* adding EcoRI site	ggcgaattcatggcctccgctgccgagcagc
cAmb3111-R	*amb3111* adding BamHI site, deleting STOP	gccggatccacgccgcccgcgcagccg
amb4356-F	*amb4356* adding BamHI site	ggcggatccatgaacgaccagcgcaatctct
amb4356-R	*amb4356* adding SpeI site	gccactagtctatttctcctcggcgcgcttc
cAmb4356-F	*amb4356* adding EcoRI site	ggcgaattcatgaacgaccagcgcaatctct
cAmb4356-R	*amb4356* adding BamHI site deleting STOP	gccggatcctttctcctcggcgcgcttc

Table 4: Primer List

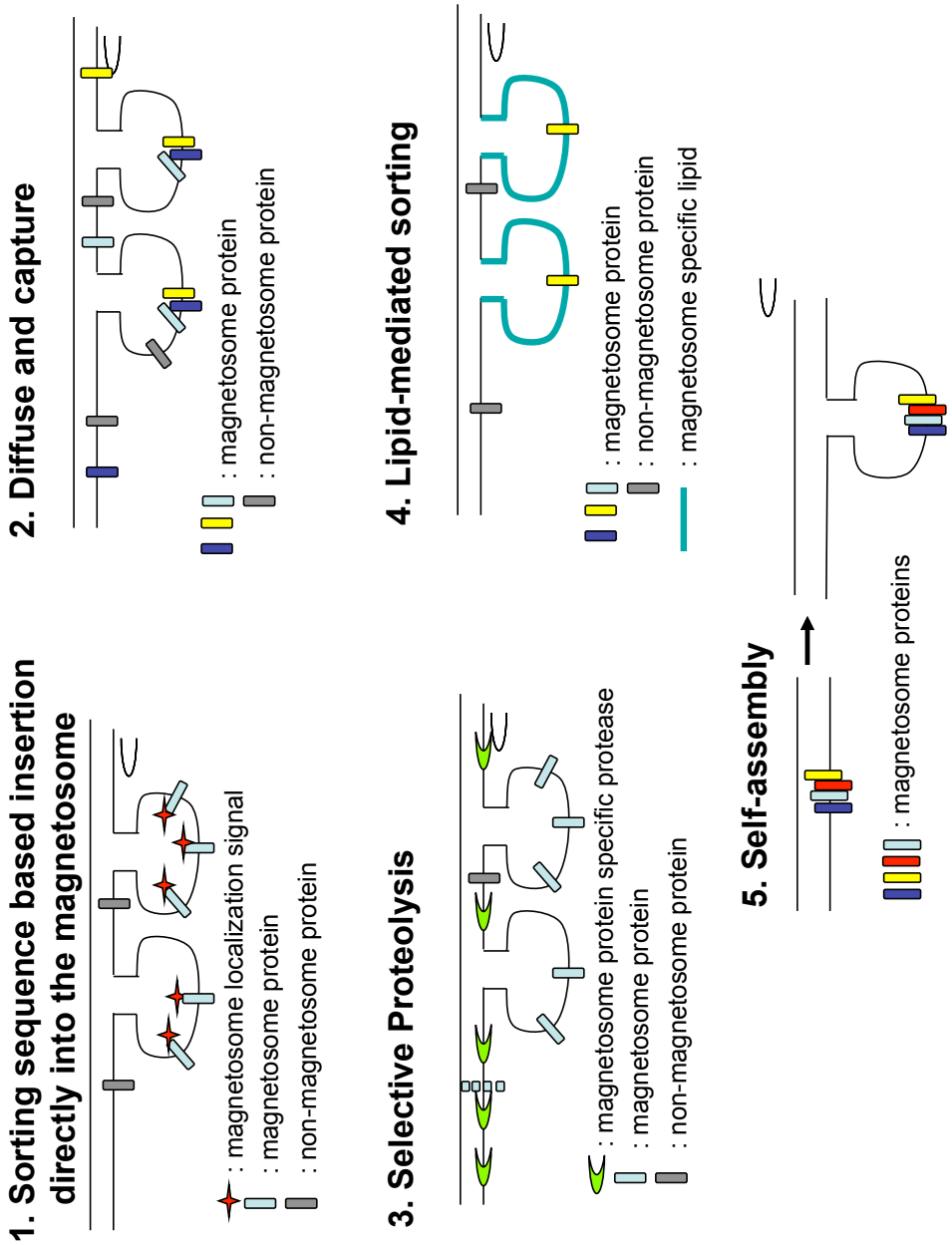

Figure 1: Possible models for magnetosome protein sorting in AMB-1. Models are not mutually exclusive.

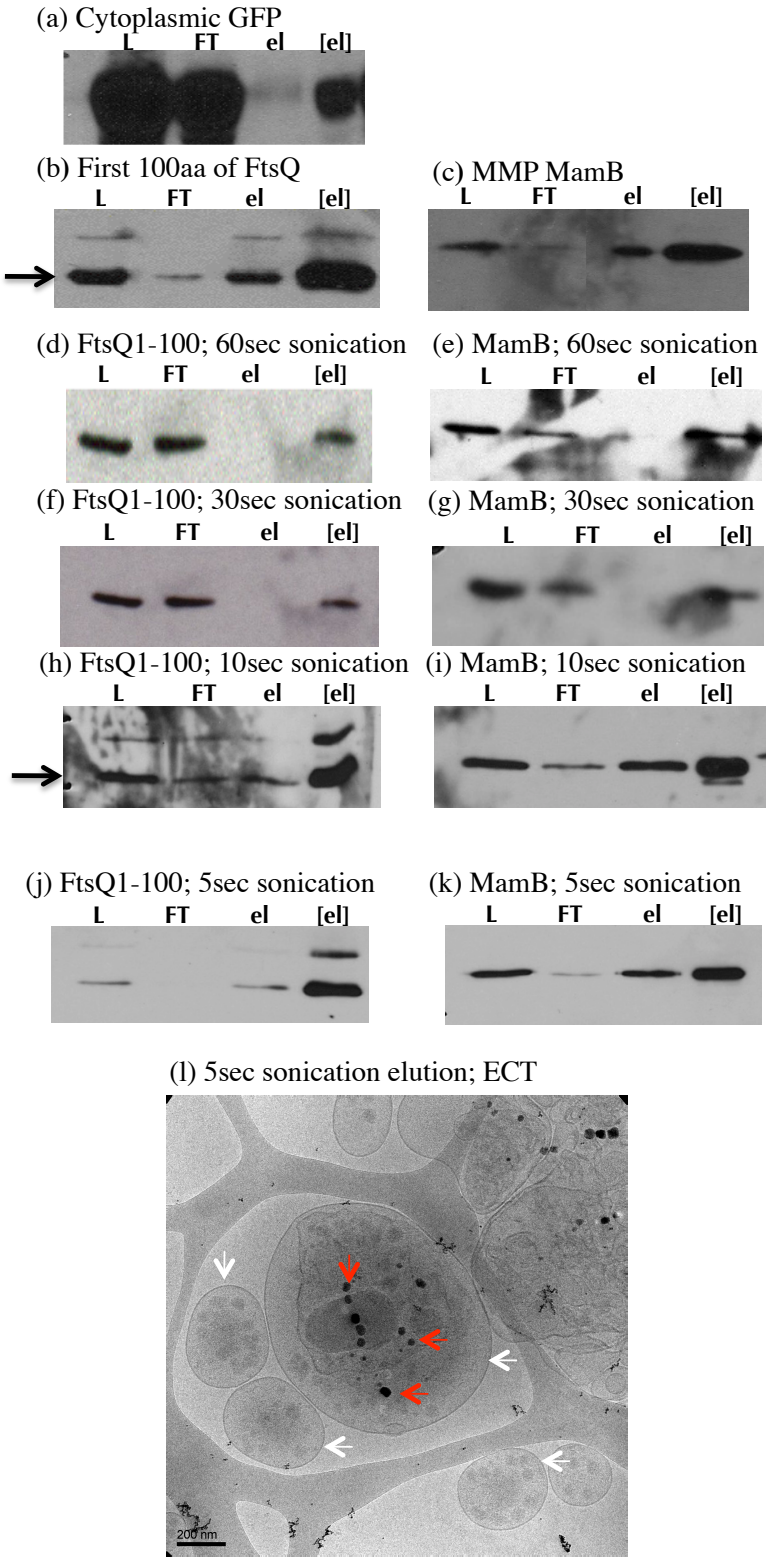

Figure 2: Effect of sonication on fractionation of the inner membrane marker FtsQ1-100 and the MMP MamB. Figure legend on next page.

Figure 2: Effect of sonication on fractionation of the inner membrane marker FtsQ1-100 and the MMP MamB. (a)-(c) traditional magnetosome protocol; (d)-(k) magnetosome protocol supplemented with indicated amount of sonication of lysate; (l) Electron cryo-tomography image of magnetosome fraction of magnetosome purification protocol with 5 seconds of sonication. Black arrows point at correct-sized FtsQ band. Red arrowheads indicate crystals of magnetite. White arrowheads indicate membranous structures.

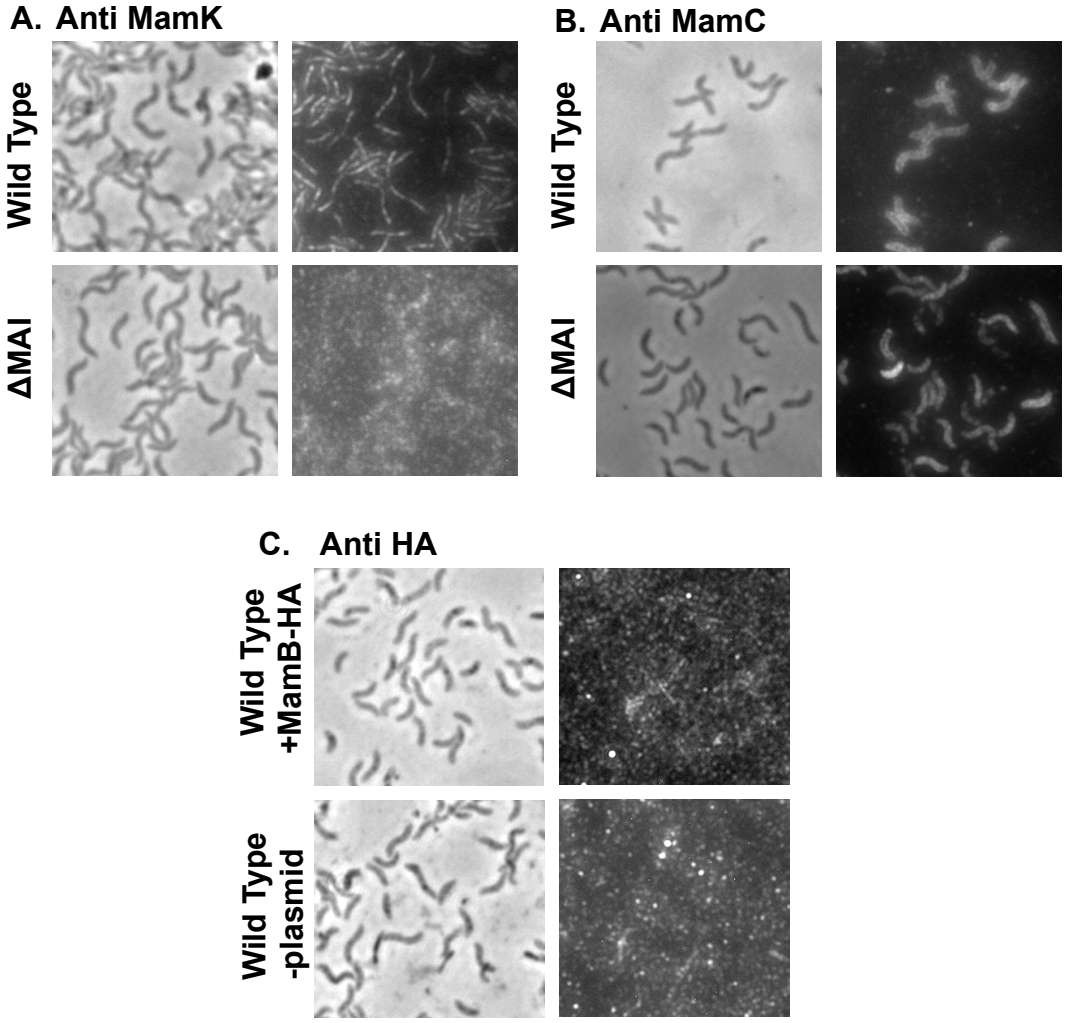

Figure 3: Immunofluorescence for MMPs. Immunofluoresence against (A) MamK and (B) MamC using antibodies supplied by the Fukumori lab. (C) Immunofluorecence using a commercially available anti-HAtag antibody to visualize MamB-HA localization in wild type AMB-1. For (A) and (B) ΔMAI serves as the negative control. For (C) a strain not carrying an HA plasmid.

Chapter 5: Conclusion

Magnetotactic bacteria (MTB) have been the focus of much interdisciplinary research. As MTB have the unique ability to biomineralize nanometer-sized single domain crystals of iron oxide or sulfide, magnetite or greigite, respectively, efforts to understand this process of biomineralization have, in part, been driven by many proposed applications for these crystals and for MTB (1). In addition, the existence of magnetosomes, bacterial organelles that synthesize the crystals, poses interesting questions about the evolutionary origin of organelles. My work was driven by the question of how bacteria form organelles and whether these processes are similar to comparable, better characterized processes in eukaryotes. With the goal of understanding how magnetosome proteins are sorted to the magnetosomes, our research has been able to implicate a specific magnetosome protein, the HtrA/DegP family protease MamE, in this process. In addition, the work presented in this dissertation has implicated the protease activities of MamE and another related protease, MamO, in the biomineralization of magnetite, adding magnetosome formation to the already long list of known functions for HtrA/DegP proteases. In AMB-1, these proteases do not appear to be involved in stress responses but are required for magnetite formation. A more detailed characterization of MamE revealed that it is a bifunctional protein and that its protease activity, although required for the formation of large single domain magnetite crystals, is not required for its role in MP sorting or for the formation of small 20nm crystals of magnetite.

Very few HtrA/DegP proteases that have domains other than the canonical transmembrane, protease and PDZ domains have been identified. The DUF81 domain of MamO and the heme-binding motifs of MamE seem to be required for magnetosome formation, though their exact functions remain unknown. It is possible that MamO's DUF81 domain is required for proper localization of MamO or that it acts as a transporter as has been proposed for homologous domains (2). In the latter case, the DUF81 domain could be required for iron import into the magnetosome. MamE's heme-binding motifs seem to be required for wild type-like biomineralization kinetics after 20nm crystals have been formed. How these domains contribute to this crystal maturation step and whether these domains bind heme remains unknown.

In addition to assigning putative functions to the various domains of MamE and MamO, this work has also added to our understanding of the process of magnetosome formation as a whole. Initiation of crystal formation does not seem to be the only rate-limiting step in magnetite formation; instead, a potential 20nm crystal size transition requires MamE protease activity and represents a possible checkpoint at which cells could control their net magnetic dipole moment and thus control whether they are trapped in the earth's magnetic field. Whether AMB-1 is capable of modulating MamE's protease activity remains to be determined.

Several decades of MTB research have given us an extensive library of candidates implicated in different aspects of magnetosome formation as well as a thorough physical characterization of these prokaryotic organelles. To further our

understanding of how the magnetosome is formed we are now beginning to dissect the mechanisms of how individual proteins, such as MamE and MamO, contribute to the different steps of magnetosome formation. Although many new tools have to be developed to answer these new questions, a mechanistic understanding of magnetosome formation is clearly within reach.

References:

1. Schuler D & Frankel RB (1999) Bacterial magnetosomes: microbiology, biomineralization and biotechnological applications. *Appl Microbiol Biotechnol* 52(4):464-473.
2. Weinitschke S, Denger K, Cook AM, & Smits THM (2007) The DUF81 protein TauE in Cupriavidus necator H16, a sulfite exporter in the metabolism of C-2 sulfonates. *Microbiol-Sgm* 153:3055-3060.